CHOLESTEROL CATABOLISM IN *MYCOBACTERIUM TUBERCULOSIS*: STUDIES IN PATHOGENESIS, REGULATION, AND METABOLIC TOXICITY

by

Kirstin Lee Brown

B.Sc. (honours), The University of British Columbia, 2012

A THESIS SUBMITTED IN PARTIAL FULFILLMENT OF

THE REQUIREMENTS FOR THE DEGREE OF

DOCTOR OF PHILOSOPHY

in

THE FACULTY OF GRADUATE AND POSTDOCTORAL STUDIES

(Microbiology and Immunology)

THE UNIVERSITY OF BRITISH COLUMBIA

(Vancouver)

December 2019

The following individuals certify that they have read, and recommend to the Faculty of Graduate and Postdoctoral Studies for acceptance, the dissertation entitled:

Cholesterol catabolism in *Mycobacterium tuberculosis*: studies in pathogenesis, regulation, and metabolic toxicity

submitted by Kirstin Lee Brown in partial fulfillment of the requirements for

the degree of Doctor of Philosophy

in Microbiology and Immunology

Examining Committee:

Dr. Lindsay Eltis, Microbiology and Immunology; Biochemistry
Supervisor

Dr. Charles Thompson, Microbiology and Immunology
Supervisory Committee Member

Dr. Yossef Av-Gay, Division of Infectious Diseases
University Examiner

Dr. Theodore Steiner, Division of Infectious Diseases
University Examiner

Additional Supervisory Committee Members:

Dr. Rachel Fernandez, Microbiology and Immunology
Supervisory Committee Member

Dr. Kenneth Harder, Microbiology and Immunology
Supervisory Committee Member

Abstract

Tuberculosis (TB), a disease caused by the airborne bacterial pathogen *Mycobacterium tuberculosis* (Mtb) claims the lives of ~1.3 million people every year. Control of Mtb has been hindered by the inefficiency of the current treatment for the disease, which involves several months on a multi-drug regimen with extensive side-effects. The ability of Mtb to enter a state of metabolic quiescence further complicates the development of antimycobacterial agents. During infection, Mtb relies on host-produced cholesterol as a source of carbon and energy. The essentiality of cholesterol catabolism for Mtb during infection has been repeatedly demonstrated and the pathway has thus emerged as a potential target for the development of new TB therapeutics. Catabolism of the cholesterol sidechain and rings A/B leads to the production of propionyl-CoA, pyruvate, and the rings C/D containing metabolite 3aα-H-4α(3'-propanoate)-7aβ-methylhexahydro-1,5-indanedione (HIP). Many of the enzymatic steps involved in the degradation of HIP yield CoA thioester metabolites, the accumulation of which have been shown to cause cholesterol-mediated toxicity in deletion mutants. The findings presented in Chapter 3.1 demonstrate that HIP catabolism is important for the pathogenesis of Mtb and that the cholesterol catabolic pathway is a valid drug target. Chapter 3.2 reveals a novel mechanism involved in the regulation of HIP catabolism in which the first enzyme in its catabolism is reversibly acetylated. In Chapter 3.3, I have shown that deletion of certain HIP catabolizing enzymes leads to the accumulation of cholesterol-derived CoA thioesters, sequestration and depletion of free CoA resulting in a toxic phenotype. These findings suggest that HIP catabolizing enzymes are intriguing candidates for the development of novel TB antibiotics. Together, these data build on previous studies and provide additional insights into cholesterol catabolism in Mtb.

Lay Summary

Tuberculosis (TB), a disease caused by the airborne bacterial pathogen *Mycobacterium tuberculosis* (Mtb) claims the lives of ~1.3 million people every year. Control of Mtb has been hindered by the inefficiency of the current treatment regimen. It is crucial to better understand the biology of Mtb and how it survives within the human body in order to develop more effective treatments. I investigated how the bacterium degrades cholesterol, a molecule produced by the human host which provides Mtb with nutrients. First, I demonstrated that cholesterol is an essential nutrient for Mtb during infection. Second, I characterized a mechanism used by Mtb to regulate the utilization of cholesterol. Finally, I established that inhibiting certain steps in the degradation of cholesterol impairs the ability of Mtb to replicate, even when other nutrients are provided. This dissertation provides insight into cholesterol utilization by Mtb which may facilitate the development of novel TB therapeutics.

Preface

Parts of the work presented in this thesis are published or drawn from manuscripts currently in preparation. Contributions by fellow scientists and collaborators were made as follows:

Chapter 3.1

Work from chapter 3.1 is published: Crowe, A.M., Casabon, I., Brown, K.L., Liu, J., Lian, J., Rogalski, J.C., Hurst, T.E., Snieckus, V., Foster, L.J., and Eltis, L.D. (2017). Catabolism of the last two steroid rings in *Mycobacterium tuberculosis* and other bacteria. *mBio*. 8(2):e00321-17. J. Liu assisted in strain construction. A.M. Crowe conducted LC-MS analysis and identified CoA thioester metabolites. I generated mutant and complemented strains, performed growth experiments and metabolite extractions, conducted GC-MS analyses, and performed infection studies. Dr. A.M. Crowe wrote the first draft of the manuscript. Dr. L.D. Eltis was the principal investigator and was involved throughout the project in concept formation.

Additional work from chapter 3.1 is included in a manuscript in preparation: Brown, K.L., Wilburn, K.M., VanderVen, B.C., Eltis, L.D., *et al*. *In preparation*. Screening of the compound library was done by scientists at GSK. I determined IC_{50} values and conducted intracellular and extracellular metabolite analyses.

Chapter 3.2

Work from chapter 3.2 is included in a manuscript in preparation: Brown, K.L., Liu, J., Eltis, L.D. Post-translational regulation of cholesterol catabolism through reversible lysine acetylation. *In preparation*. J. Liu produced mutant strains. Trypsin digestion and mass spectrometry was performed by the Core Proteomics Facility at the University of British Columbia. I constructed expression constructs, performed protein expression and purification, *in vitro* acetylation and deacetylation assays, Western blot analysis, and bacterial growth

experiments. I wrote the manuscript. Dr. L.D. Eltis was the principal investigator and was involved throughout the project in concept formation.

Chapter 3.3

Work from chapter 3.3 is included in a manuscript in preparation: Brown, K.L., Xing, S., Chorolovski, J., Liu, J., Huan, T., Liu, and Eltis, L.D. Cholesterol-mediated coenzyme A depletion in cholesterol catabolic mutants of *Mycobacterium tuberculosis* leads to toxicity. *In preparation.* I conducted bacterial growth experiments and GC-MS and HPLC analyses of metabolite production, and preparation of samples for LC-MS analysis. S. Xing conducted LC-MS analyses. I wrote the manuscript. Dr. L.D. Eltis was the principal investigator and was involved throughout the project in concept formation.

Table of Contents

List of Tables

List of Figures

List of Abbreviations

1,4-BNC-CoA	3-oxo-23,24-bisnorchola-1,4-dien-22-oic acid-CoA
3-HSA	3-hydroxy-9,10-seconandrost-1,3,5(10)-triene-9,17-dione
5-OH HIC	3a*α*-*H*-4*α*(carboxyl-CoA)-5-hydroxy-7a*β*-methylhexahydro-1-indanone-
9OHADD	9-hydroxy-androsta-1,4-diene-3,17-dione
Ab	Antibody
AC	Adenylyl cyclase
ACAD	Acyl-CoA dehydrogenase
ACP	Acyl carrier protein
AD	Androstenedione
ADD	1,4-Androstenedione
AES	Allelic exchange substrate
ATP	Adenosine triphosphate
BCG	*Mycobacterium bovis* bacillus Calmette-Guerin
cAMP	3',5'-cyclic adenosine monophosphate
CCR	Carbon catabolite repression
CFU	Colony forming units
CoA	Coenzyme A
COCHEA-CoA	(*R*)-2-(2-carboxyethyl)-3-methyl-6-oxocyclohex-1-ene-1-carboxyl-CoA
CRP	cAMP receptor protein
DAP	Diaminopimelic acid
DC	Dendritic cell
DHSA	3,4-dihydroxy-9,10-seconandrost-1,3,5(10)-triene-9,17-dione
DSHA	4,5-9,10-diseco-α3-hydroxy-5,9,17-trioxoandrosta-1(10),2-diene-4-oic
ETC	Electron transport chain
FA	Fatty acid
FAS	Fatty acid synthase
GC-MS	Gas chromatography coupled mass spectrometry
GNAT	GCN5-like protein *N*-acetyltransferases
HHD	2-hydroxy-hexa-2,4-dienoic acid
HIEC-CoA	(7aS)-7a-methyl-1,5-dioxo-2,3,5,6,7,7a-hexahydro-1*H*-indene-4-carboxyl-CoA
HIP	3aα-H-4α(3'-propanoate)-7aβ-methylhexahydro-1,5-indanedione
HIV	Human immunodeficiency virus
HPLC	High performance liquid chromatography
HPr	Histidine protein
ICDH	Isocitrate dehydrogenase
ICL	Isocitrate lyase
IFNγ	Interferon gamma

iNOS	Inducible nitric oxide synthase
IPTG	Isopropyl β-d-1-thiogalactopyranoside
LAM	Lipoarabinomannan
LC-MS	Liquid chromatography coupled mass spectrometry
MA	Mycolic acid
MB	Mycobactin
MCC	Methylcitrate cycle
MDR	Multiply drug resistant
MEZ	Malic enzyme
MHC	Major histocompatibility complex
MIC	Minimum inhibitory concentration
MOODA	4-methyl-5-oxo-octanedioc acid
Mtb	*Mycobacterium tuberculosis*
MΦ	Macrophage
NAD^+	Nicotinamide adenine dinucleotide
NK cell	Natural killer cell
NKT cell	Natural killer T cell
OADC	Oleic acid dextrose catalase
PCA	Pyruvate carboxylase
PCK	PEP carboxy kinase
PCR	Polymerase chain reaction
PDIM	Phthiocerol dimycocerosate
PEP	Phosphoenolpyruvate
PG	Peptidoglycan
PMA	Phorbol 12-myristate 13-acetate
PPDK	Pyruvate phosphate dikinase
RHA1	*Rhodococcus jostii* RHA1
RNS	Reactive nitrogen species
ROS	Reactive oxygen species
SDH	Succinate dehydrogenase
STPK	Serine-threonine protein kinases
TAG	Triacyl glyceride
TB	Tuberculosis
TCA	Tricarboxylic acid cycle
TDM	Trehalose 6,6’-dimycolate
TLC	Thin layer chromatography
TLR	Toll-like receptor
TNFα	Tumour necrosis factor alpha
WT	Wild-type
XDR	Extensively drug resistant

Acknowledgements

I would like to thank my supervisor, Prof. Lindsay D. Eltis for his insights into this work and for his patience and guidance during my time in his laboratory. I am grateful for the education and research opportunities he provided, and for allowing me to build my skill sets both in the lab and outside of it. I am grateful also to my committee members, Dr. Rachel Fernandez, Dr. Charles Thompson, and Dr. Ken Harder for providing feedback and encouragement throughout my research.

I gratefully acknowledge all of the past and present members of the Eltis lab who have provided insight, knowledge, advice and encouragement. This journey wouldn't have been possible without so many of you: Dr. Israel Casabon, Dr. Rahul Singh, Jennifer Lian, Keith Story, Jessica Chorolovski, and Linda Dumalo. I would particularly like to acknowledge Jie Liu for her constant support in the containment level 3 laboratory, and I would especially like to thank Dr. James Round, Dr. Adam Crowe, Dr. Eugene Kuatsjah, Dr. Morgan Fetherolf, and Raphael Roccor for their years of support, instruction, discussion, assistance, collaboration, and most of all, friendship. These years would have been a very different experience without you.

I was fortunate to collaborate with scientist at GlaxoSmithKline, Dr. Tao Huan (UBC), and Shipei Xing (UBC) and I am grateful for their insights and expertise.

I would like to acknowledge the financial support from the Canadian Institute of Health Research (CIHR), the BC Lung Association, and the University of British Columbia.

I would also like to thank my parents, Keith and Allison Brown for their enduring support throughout my education. Thank you for believing in me and for always encouraging me to pursue my goals. Thanks also to my grandparents, Bill and Lil Wright and for your continuous support and encouragement.

Finally, I would like to thank Robert Smith, my most important collaborator and partner in life. Thank you for being my number one cheerleader, for your unfailing support and encouragement, for your patience and understanding, and especially for your pipetting assistance with my late-night timepoints in the lab.

Chapter 1: Introduction

1.1 *Mycobacterium tuberculosis*

1.1.1 The current state of TB

Mycobacterium tuberculosis (Mtb), an airborne bacterial pathogen that causes Tuberculosis (TB), is responsible for the loss of ~1.3 million lives annually (1). The global burden of TB has reached staggering levels, now outranking HIV as the leading cause of death from an infectious disease worldwide (1). It is estimated that one third of the world's population is infected with *Mtb*, but that only 10% of infected individuals will develop TB disease (1). The remaining 90% of latently infected individuals contribute to a subclinical pool of infectious bacteria and complicate control of the disease. Antibiotics for the treatment of TB have been available since the 1950s when streptomycin, pyrazinamide and isoniazid were first used (2). However, these drugs are still used for the treatment of TB today, largely due to the lack of new TB drug development until 2012 (3, 4). Treatment of TB requires an extensive multidrug treatment regimen with severe side-effects, often leading to non-compliance and the development of multi- and extensively-drug-resistant strains (MDR and XDR, respectively) which thwart the attempts to control this global emergency. Out of the 10 million new cases of TB in 2017 alone, over 5% were caused by drug-resistant strains (1). MDR strains are resistant to rifampicin and isoniazid, and the recommended treatment is a two-year course of second-line antibiotics (1). XDR strains are resistant to the aforementioned first-line antibiotics plus streptomycin, fluoroquinone, and any injectable therapy (1). These grim statistics underscore the urgent need for novel therapeutics. Shortening the treatment regimen with more effective, less toxic antibiotics is arguably the most important factor in limiting the spread of drug-resistant strains and lowering the global burden of TB.

1.1.2 Mtb pathogenesis

An overview of the Mtb infection cycle is provided in Figure 1.1. Mtb is transmitted person-to-person via inhalation of aerosol droplets released into the environment when an infected individual coughs or sneezes. Upon inhalation, the bacterium is phagocytosed by alveolar macrophages (MΦs), which normally provide a first line of defense against invading bacteria but for Mtb, represent its primary niche for bacterial growth (5). Mtb resists killing by the MΦ and instead survives within the phagosome by arresting acidification and impairing phagosome maturation (6). In doing so, Mtb establishes an intraphagosomal environment that is conducive for its persistence. Infected MΦs then migrate from the airway to the pulmonary tissues (7-10).

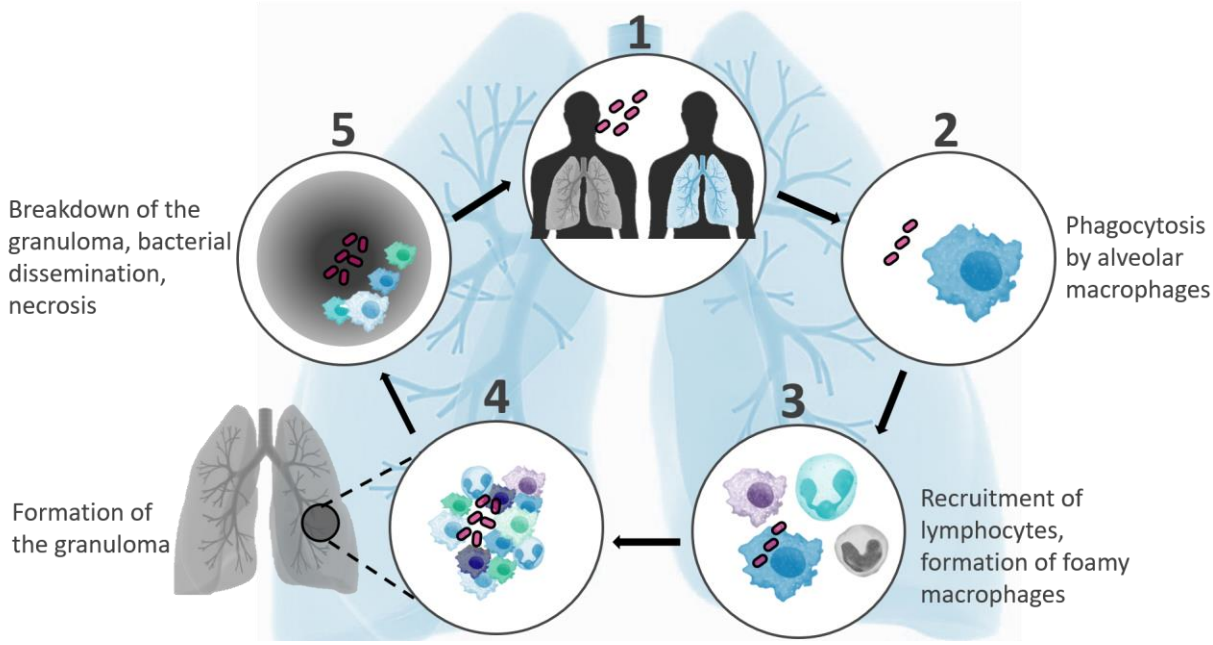

Figure 1.1 The infection cycle of Mtb

Alveolar macrophages are stimulated through Mtb-specific toll-like receptor (TLR) agonists and release pro-inflammatory cytokines and chemokines including TNFα, which recruit neutrophils, natural killer (NK) cells, $CD4^+$ and $CD8^+$ T cells, and B cells to the site of infection (10). Each newly recruited cell produces their own chemokines and cytokines, thereby amplifying immune cell recruitment (7, 8, 10, 11). The successive waves of immune cell recruitment lead to the formation of a stratified structure called a granuloma (Fig. 1.2), which is a hallmark of TB (10). The granuloma is comprised of infected and uninfected MΦs, foamy MΦs and multinucleated giant cells, surrounded by a ring of T and B lymphocytes (12). The centre of the granuloma is rich in cholesterol and other lipids and is bordered by a MΦ-rich zone containing Mtb-infected MΦs and foamy MΦs (13). As the granuloma matures, neovascularization occurs and the formation of a fibrous cuff composed of collagen and extracellular matrix components delineates the periphery (10). In 90% of cases, Mtb will remain in the solid granuloma and is controlled by the immune system at this stage. The host will show no signs of disease and the infection will not be transmitted to others.

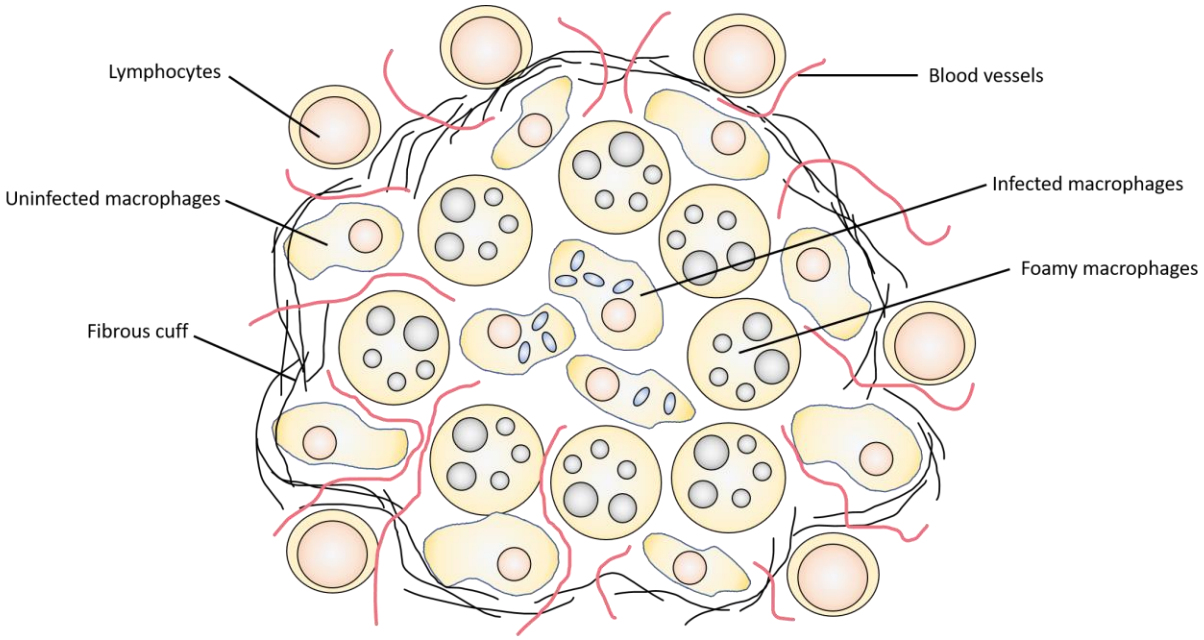

Figure 1.2 The TB granuloma

A patient who does not exhibit clinical symptoms, is non-infectious, yet harbors viable Mtb bacilli is said to have a “latent infection” (14). During latent infection, Mtb is thought to enter a state of “dormancy”, a physiological state characterized by viable, non-replicative bacteria with lesser metabolic activity (14). Mtb enters dormancy in response to stresses encountered upon infection. For example, hypoxia activates the dormancy survival (15) operon which leads to the down-regulation of central metabolism and expression of genes required for catabolism of carbon sources available to it during infection (16, 17). A latent infection is therefore a state of balance between the immune system and the bacterium which may last decades (18). These bacteria are essentially seeds of infection awaiting the breakdown of host immunological defenses which would allow for unhindered bacterial replication and dissemination. Due to the lack of animal models that accurately represent human TB disease, research aimed at understanding the nature and importance of Mtb dormancy has been challenging (14). However, because most antibiotics for the treatment of TB target metabolically active cells, understanding the physiology of dormant Mtb is imperative. This is evidenced by the formation of “persister” cells following antibiotic treatment – cells that survive treatment even though they are not inherently antibiotic-resistant (14, 19). Upon regrowth from the granuloma, these persister cells are sensitive to antibiotics even though they survived the initial onslaught of treatment during infection (20). It is thought that persister cells survive antibiotic treatment by remaining dormant and only upon resuscitation, become metabolically active and therefore sensitive to antibiotics (14). Human TB disease is likely comprised of subpopulations of bacteria in different metabolic states. During active disease, it consists of mainly metabolically active cells which are susceptible to antibiotics. However, a small population of dormant cells may persist in the face of treatment and lead to relapse with inadequate

therapy. This is in contrast to a latent infection in which the dormant population likely dominates the granuloma (14).

While the TB granuloma effectively contains the infection in the majority individuals, it will fail in about 10% of patients leading to active TB. In later stages of the infection, preceding the development symptoms, vascularization of the structure is diminished and the centre of the granuloma becomes necrotic (14). Caseation, a process in which the granuloma structure breaks down and eventually ruptures, then occurs (10). The infectious bacteria are released and disseminate throughout the lungs and to other organs allowing for transmission. The exact mechanisms that lead to the development of TB remain unclear, but the immune status of the infected individual plays an important role. TB disease is common in immunocompromised individuals as evidenced by the fact that nearly a quarter of the deaths caused by TB in 2017 were HIV-associated (1).

1.1.3 Mtb physiology

Mtb is an actinomycete with a characteristically thick cell wall composed of peptidoglycan (PG), polysaccharides, glycolipids, and fatty acids (FAs). Mtb likely began infecting humans ~10,000 years ago (21). Over time, the 4.4 mega-base pair genome of Mtb, encoding ~4000 predicted proteins, has adapted to yield a highly specialized human pathogen with extensive immunomodulatory and evasion strategies, allowing it to infect and persist within the human population.

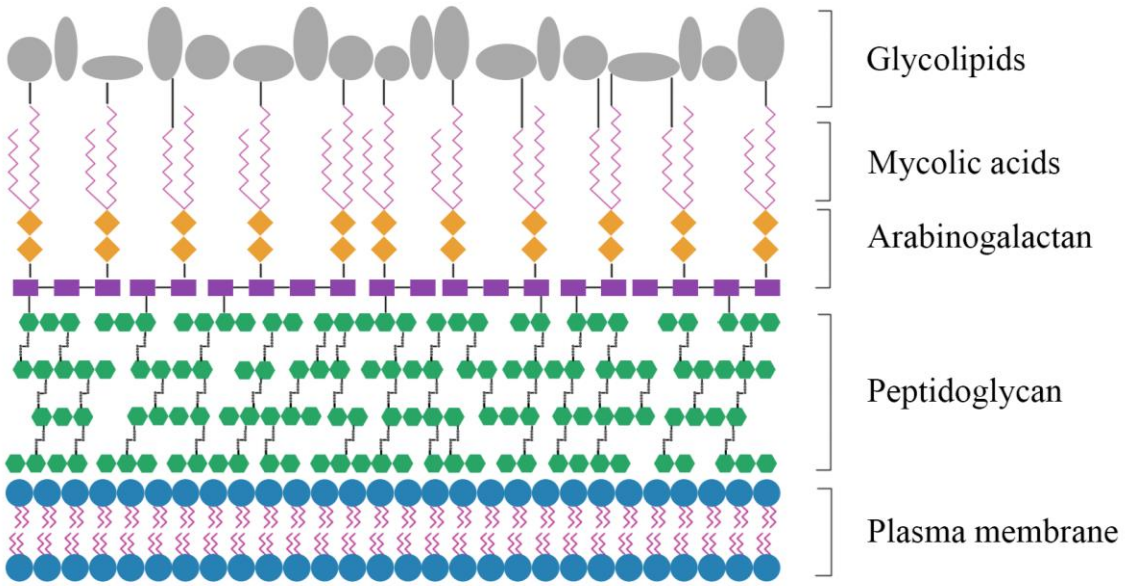

Figure 1.3 The Mtb cell wall

While Mtb is classified as a gram-positive bacterium, it does not have the prototypical gram-positive cell wall structure and does not reliably stain gram positive or negative. Gram-positive organisms have a plasma membrane surrounded by a thick layer of PG, while gram-negative bacteria have an inner plasma membrane, a thin layer of PG located in the periplasmic space, and an outer membrane. Unlike other gram-positive microorganism, Mtb has a complex cell wall structure composed of an inner and an outer layer surrounding a pseudo-periplasm (Fig. 1.3) (22). The outer layer is composed of proteins and lipids, with long- and short-chain FAs. Also associated with the outer layer are lipid-linked polysaccharides including lipoarabinomannan (23), lipomannan, phthiocerol dimycocerosate (PDIM), dimicolyl trehalose, sulfolipid, and phosphatidylinositol mannosides. Beneath the outer layer is a thick, covalently-linked layer of PG, arabinogalactan and mycolic acids (MAs) which together make up the cell wall core structure. The PG structure is similar to that of other bacteria with a few notable differences. One is that Mtb muramic acid has an *N*-glycolyl group rather than the typical *N*-acetyl group. This is a

characteristic that is unique to actinomycetes (24). Another key difference is the high percentage of peptide cross links, 25% of which are unusual in that they occur between two diaminopimelic acid (DAP) residues rather than between a DAP and an alanine residue (22). These DAP-DAP cross linkages provide increased rigidity to the PG, which may have a protective role under stress conditions (25). Arabinogalactan, a glycan chain that is approximately 30 residues in length, provides integrity to the cell wall by covalently anchoring the PG layer to the MAs. The MAs make up the outer portion of the cell wall core structure, forming a waxy barrier around the cell. They are comprised of short α-alkyl- and long β-hydroxyl-fatty acids which are 60 to 90 carbons in length and are covalently linked to the arabinogalactan. The MA layer intercalates with the outer layer of lipids and proteins.

The complexity of the Mtb cell wall is largely responsible for the pathogen's innate antibiotic resistance due to its extremely low permeability. While this impermeability may be advantageous for survival of the bacterium under stress conditions encountered during transmission and infection, it is also thought that nutrient uptake is restricted and that this may be a limiting factor in the growth rate of Mtb (22). Consistent with this, fast growing mycobacterial species express a porin that allows for rapid nutrient uptake which Mtb lacks (22).

The biochemical reactions responsible for the synthesis of MAs, encoded by many genes, have been fully defined (26-29). The precursors of MAs are mycobacterial FAs which are synthesized by two fatty acid synthases (FASs) FAS-I and FAS-II. FAS-I produces FAs with a bimodal distribution of 16-18 and 24-26 carbons in length, while FAS-II is responsible for their elongation and cannot synthesize FAs *de novo* (30). The two FASs differ in their molecular organization and substrates but the reaction sequences are the same, both of which involve an iterative series of reactions leading to the successive additions of two-carbon units from malonyl-

CoA (30). FA biosynthesis begins with acetyl-CoA carboxylase which converts acetyl-CoA to malonyl-CoA. Malonyl-CoA then feeds into FAS-I and undergoes successive additions of malonyl-CoA to generate C_{16}-C_{18} and C_{24}-C_{26} FAs (30). Malonyl-CoA is also used by the FAS-II complex to add carbon units to the FAs synthesized by FAS-I to yield C_{18}-C_{32} FAs (30). FabD, a malonyl-CoA-acyl carrier protein transacylase, exchanges the CoA for Acyl Carrier Protein (ACP) to generate malonyl-ACP (31). FA biosynthesis then proceeds through a series of elongation steps involving enzyme-bound intermediates covalently linked to ACP (30, 31).

1.1.4 Biochemical adaptations of Mtb to infection

Upon phagocytosis by alveolar MΦs, Mtb bacilli are bombarded with the immunological defenses of the host cell. In order to establish an intracellular niche conducive to bacterial survival, Mtb undergoes extensive transcriptomic and metabolic adaptations to persist in the face of host defenses. Stresses encountered by Mtb during infection include hypoxia, iron limitation, exposure to reactive oxygen and reactive nitrogen species (ROS and RNS, respectively), acidic pH, and nutrient limitation. The genetic repertoire of Mtb suggests that the pathogen is equipped with the metabolic flexibility and inherent capacity to persist despite these challenges (32). Figure 1.4 summarizes the challenges faced by Mtb while residing within the phagosome and the strategies the organism has evolved to counteract host defenses.

1.1.4.1 Hypoxia

Oxygen limitation has long been considered a host-imposed stringency encountered by Mtb during infection and is intimately linked with the latency and reactivation of the pathogen (33-36). Granulomas are thought to restrict bacterial access to oxygen thereby establishing a

hypoxic environment to limit the growth of Mtb. Numerous studies have demonstrated that the growth, metabolic, and transcriptional activity of Mtb are sensitive to variations in oxygen. One

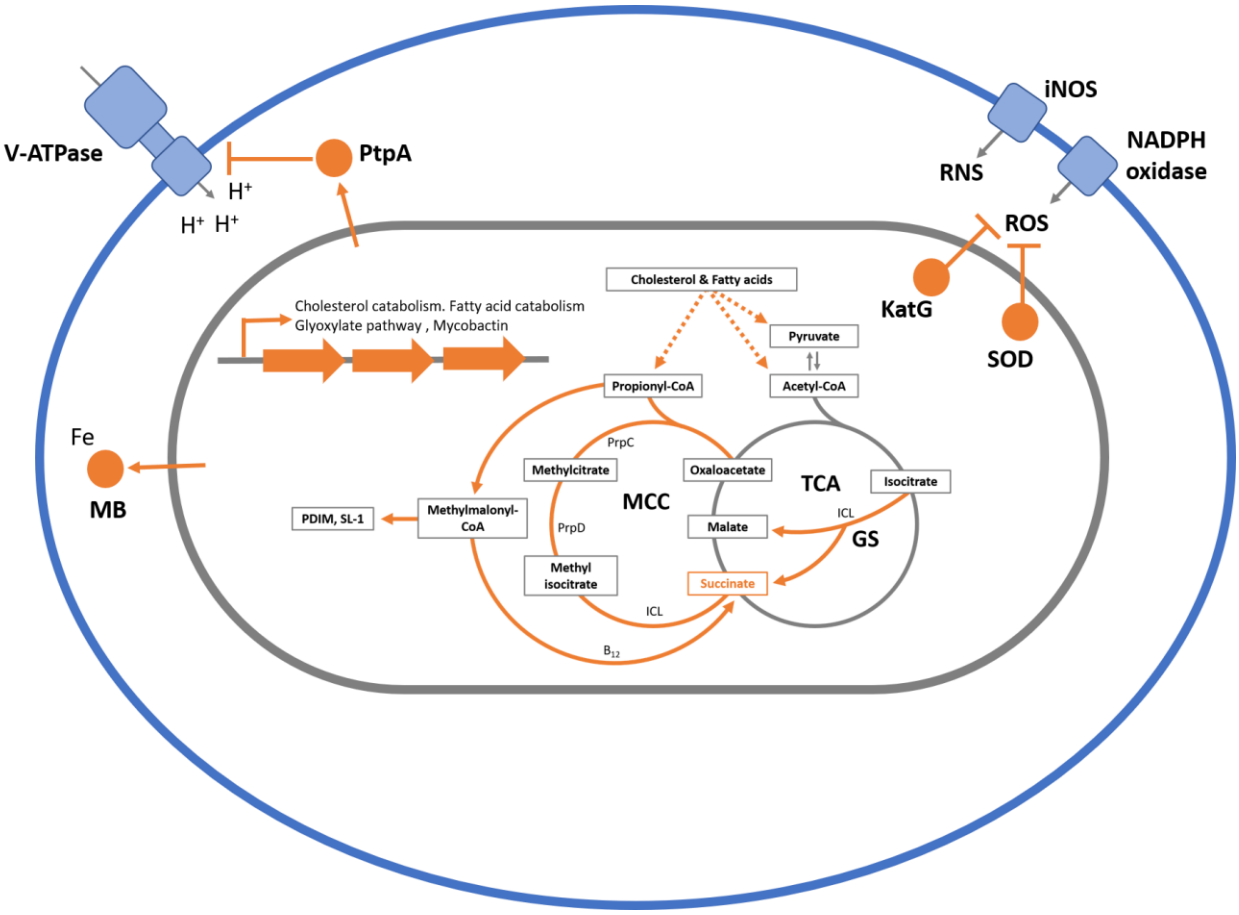

Figure 1.4 Summary of the biochemical adaptations of Mtb to infection in the phagosome. MCC, methylcitrate cycle; TCA, tricarboxylic acid cycle; GS, glyoxylate shunt; MB, mycobactin; iNOS, inducible nitric oxide synthase; SOD, superoxide dismutase.

of the most profound adaptations to hypoxia is the activation of the Dos regulon. The DosR regulator was first identified as a key regulator of the hypoxic response by Sherman *et al* (2001) and has since become one of the best characterized signal transduction systems in Mtb (37). Phosphorylation of DosR by one of two sensor kinases (DosS or DosT) leads to the induction of a

set of about 50 genes (38). Several studies have demonstrated the essentiality of the regulon in mediating the adaptation to hypoxic environments, however infection studies using Δ*dosR* mutant strains of Mtb have called into question the importance of DosR for the bacteriostasis of Mtb *in vivo* (16, 39-41). The lack of phenotype of the Δ*dosR* strain during infection led Rustad *et al.* to conclude that while the regulon is essential for the *in vitro* survival of hypoxia, a larger subset of genes known as the enduring hypoxic response is induced during infection largely independent of DosR (41).

Regardless of the regulatory mechanisms involved, hypoxia induces large-scale metabolic reprogramming. This includes the downregulation of components of the electron transport chain (ETC) leading to ATP levels approximately five times lower than aerobically growing cells (35). During hypoxia, however, Mtb still has a requirement for the sustained production of ATP, regeneration of NAD^+, and maintenance of the proton motive force to maintain viability (35). Watanabe *et al.* demonstrated that succinate accumulates in the culture supernatant of Mtb grown on glucose under oxygen limiting conditions as a result carbon flux through the reverse (reductive) TCA cycle (42). Consistent with these findings, Eoh *et al.* demonstrated that succinate accumulates under hypoxic conditions when Mtb is grown on acetate, a carbon source more relevant to infection (43). However, the mechanism of succinate production from acetate differed from that of glucose as it was found to be mediated by the glyoxylate shunt rather than a reverse TCA cycle. The authors also demonstrated the central role of succinate in maintaining membrane potential and ATP production under oxygen limiting conditions through the activity of succinate dehydrogenase (SDH), an enzyme that is involved in both the TCA cycle and the ETC. The study also revealed a previously unidentified role for the isocitrate lyase (ICL), a bifunctional enzyme involved in the glyoxylate shunt and the methylcitrate cycle (MCC), in the adaptation to hypoxia (43). As part of

the glyoxylate shunt, ICL converts isocitrate to succinate and malate. Succinate serves as a substrate for SDH, thereby donating electrons to the ETC for sustained membrane potential and production of ATP (43).

1.1.4.2 Iron limitation

Oxygen is not the only factor limiting the growth and replication of Mtb during infection. Iron sequestration is a host defense mechanism that limits the availability of iron to invading pathogens. For Mtb, iron is a cofactor for approximately 40 enzymes and is essential for its virulence (44). To survive within the host cell, Mtb has evolved mechanisms to contend with host iron sequestration. The pathogen circumvents the low iron availability by producing iron scavenging siderophores called mycobactins (MBs). The inability of strains deficient in MB biosynthesis to survive in infection models exemplifies the importance of iron acquisition during infection (47). The biosynthesis of MB is transcriptionally regulated by the iron-regulated repressor IdeR. In the presence of iron, IdeR binds and represses the MB biosynthetic gene clusters while under low iron concentrations, repression is removed allowing for the production of MBs (48).

1.1.4.3 Oxidative stress

Upon infection, alveolar MΦs produce ROS and RNS through the activity of NADPH oxidase and inducible nitric oxide synthase (iNOS) (49), respectively, as a defense mechanism against invading bacteria. The combination of nitric oxide (NO) and superoxide (O_2^-) in the phagosome lead to the production of the powerfully oxidizing peroxynitrite anion ($ONOO^-$). Together, these compounds exert their antimicrobial activity by damaging pathogen

macromolecules. To counteract this host defense mechanism, detoxification of ROS is mediated by the mycobacterial enzyme KatG which decomposes hydrogen peroxide into water and oxygen. Deletion of *katG* impaired growth of Mtb in WT and iNOS$^{-/-}$ MΦs, but they grew normally in MΦs lacking the NADPH oxidase required for the formation of ROS (50). Another enzyme important for the detoxification of ROS is superoxide dismutase (51), which catalyzes the conversion of superoxide anions to hydrogen peroxide. The genome of Mtb encodes two SODs, SodC and SodA, both of which are important for pathogenesis in infection models (52, 53). In addition to the enzymatic defenses against oxidative stress, Mtb also produces the low-molecular-weight mycothiol which serves as an antioxidant and maintains a reducing cytoplasmic environment. Mutants with reduced mycothiol levels show increased sensitivity to oxidative stress (54).

1.1.4.4 Phagosome acidification

Phagosome acidification is an antimicrobial mechanism employed by MΦs upon phagocytosis of a pathogen. The phagosomal pH is reduced through the activity of the V-ATPase complex which pumps protons into the lumen. Unsurprisingly, Mtb has evolved mechanisms to arrest phagosome maturation and acidification, stabilizing the intraphagosomal pH to 6.3-6.5 (55). The mycobacterial protein PtpA prevents the tethering of the V-ATPase to the Mtb-containing vacuole (56). Several other mycobacterial products have been shown to impair phagosome acidification including LAM and TDM (57, 58). In addition to limiting the acidification of the phagosome, Mtb is capable of resisting acid stress and remains viable at a pH as low as 4.5 (59, 60). The ability to resist acid stress is attributed in part to MarP, a membrane-associated protein which is required for survival at low pH and in mice (59). Upon exposure to low pH, Mtb responds transcriptionally through the acid-induced *phoPR* two component regulatory pathway which was

found to be essential in infection models, emphasizing that adaptation to acidic pH is relevant to the pathogenesis of Mtb (61). Baker *et al* demonstrated that upon exposure to acidic pH, Mtb exhibits growth arrest and interestingly, that the effect was carbon-source specific (62). When grown in minimal medium supplemented with glucose, glycerol, or TCA cycle intermediates, growth was completely arrested at pH 5.7. In contrast, growth was permitted at pH 5.7 when cholesterol, acetate, phosphoenolpyruvate (PEP), pyruvate, or oxaloacetate were used as sole carbon source. The authors noted that the carbon sources that permit growth of Mtb at acidic pH all feed into the anaplerotic node which includes the enzymes

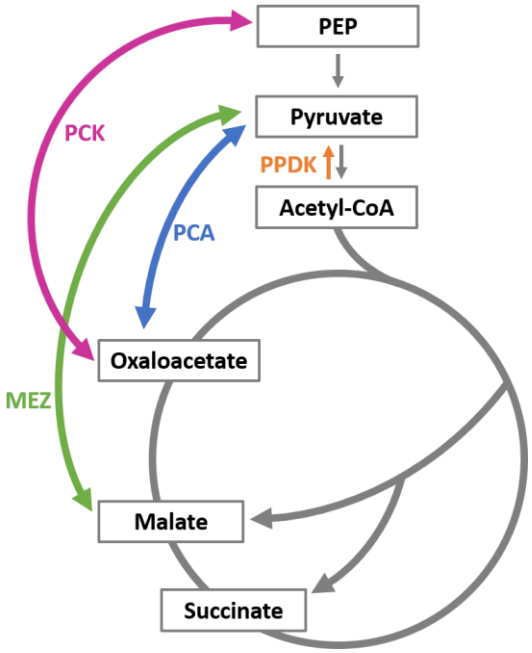

Figure 1.5 The anaplerotic node. PEP, phosphoenolpyruvate; PCK, PEP carboxylase; PCA, pyruvate carboxylase; PPDK, pyruvate phosphate dikinase; MEZ, malic enzyme.

pyruvate carboxylase (PCA), PEP carboxykinase (PCK), malic enzyme (MEZ), and pyruvate phosphate dikinase (PPDK) (Fig. 1.5). Together, these enzymes act as a key regulatory switch point between anabolism, catabolism, and energy production. Similarly, the anaplerotic node has

been associated with other conditions which slow growth including hypoxia (63). These findings suggest that the anaplerotic node is required for metabolic adaptations to acidic pH.

1.1.4.5 Carbon limitation

Intracellular pathogens rely on host cells for access to nutrients during infection. For Mtb, it must subsist on the nutrients available to it within the phagosome. However, the intraphagosomal compartment is devoid of carbohydrates which limits the availability of glycolytic substrates for Mtb consumption. As a result, the pathogen relies on alternative carbon sources during infection. Carbon sources that are abundant in the human granuloma include cholesterol, cholesteryl esters and triacylglycerol (13, 64). Upon infection with Mtb, MΦs undergo metabolic reprogramming leading to the formation of foamy MΦs filled with cholesterol- and TAG-rich lipid droplets (13, 36). It is therefore not surprising that Mtb preferentially utilizes host cholesterol and FAs for the production of energy and biosynthetic precursors during infection. The preferential use of lipid carbon sources has been inferred from the transcriptional upregulation of genes encoding FA-catabolizing enzymes (65). FAs are catabolized via β-oxidation to produce acetyl-CoA and propionyl-CoA for energy production. They can also be used in anabolic pathways to produce virulence-associated Mtb lipids or TAG. Exogenous FAs can be incorporated into the production of MAs through the FAS-II complex, or they can be donated to polyketide synthases in the form of acyl-AMP primers for the synthesis of PDIM. Host-produced FAs can also be used to produce TAG which is thought to function as a carbon storage molecule. Cholesterol catabolism (discussed further in Section 1.2) leads to the production of acetyl-CoA, propionyl-CoA, and pyruvate, and is proposed to produce succinyl-CoA, all of which feed into central metabolism.

Due to its reliance on host lipids, Mtb faces a unique metabolic consequence: a large pool of propionyl-CoA. This is problematic for Mtb as elevated concentrations of propionyl-CoA are strongly bacteriotoxic (66-68). As a result, Mtb has evolved the metabolic capacity to efficiently

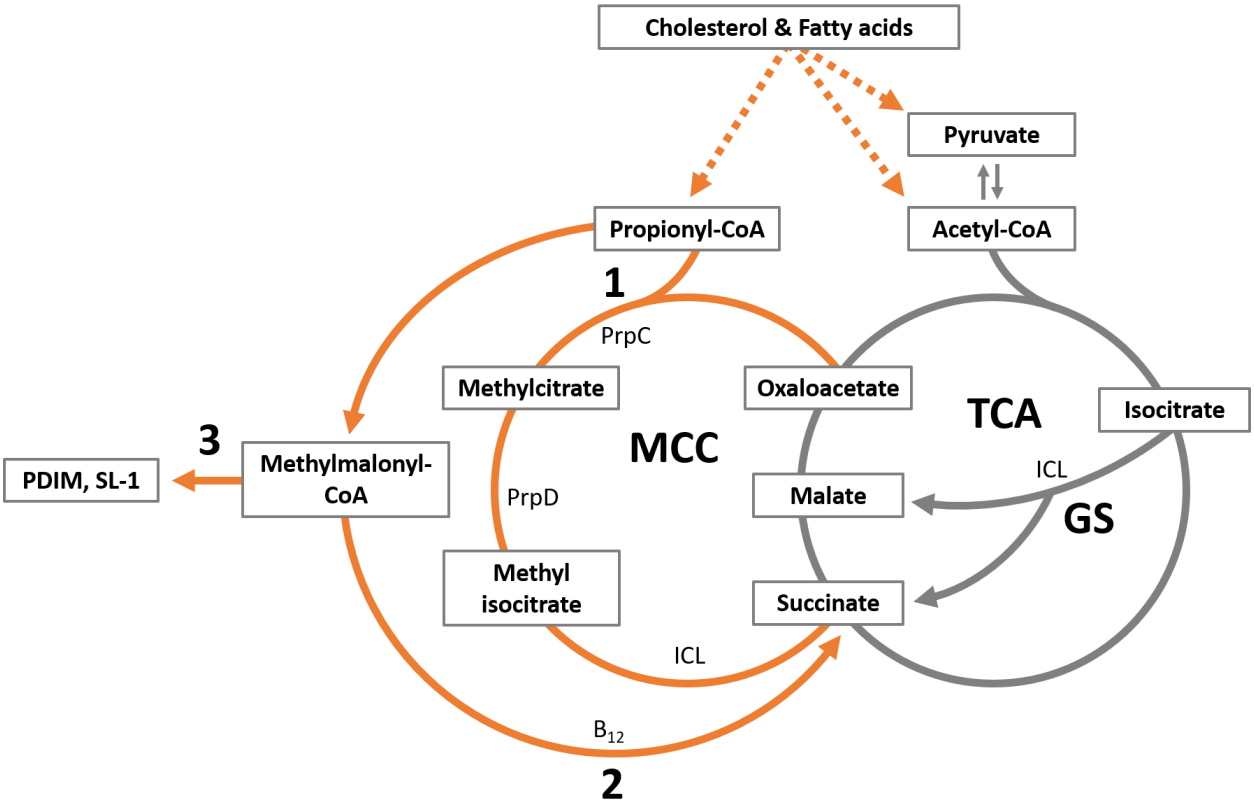

Figure 1.6 Three metabolic pathways for the detoxification and assimilation of propionyl-CoA. MCC, methylcitrate cycle; TCA, tricarboxylic acid cycle; GS, glyoxylate shunt. Pathways shown in orange are up-regulated during infection.

deal with excess propionyl-CoA using three separate pathways (Fig. 1.6). The MCC, which relies on the activity of PrpC, PrpD, and ICL, leads to the production of pyruvate and succinate which feed into the TCA cycle (66). The vitamin B_{12}-dependent methylmalonyl pathway converts propionyl-CoA into succinyl-CoA which also feeds into the TCA cycle (67). Finally, Mtb can shunt excess propionyl-CoA into the production of the methyl-branched FAs PDIM and SL-1, effectively acting as a "sink" (69, 70). Transcriptional profiling of intracellular Mtb indicates that

propionyl-CoA is predominantly processed through the MCC (71). Consistent with this, deletion of *icl1* abrogates the ability of Mtb to grow on propionate as a sole carbon source which suggests that the MCC is essential for the detoxification of propionyl-CoA (72). The addition of vitamin B_{12} to the culture media rescues growth of the Δ*icl1* mutant in the presence of propionate by increasing the flow of propionyl-CoA through the methylmalonyl pathway (72). Infection of MΦs with the Δ*icl1* mutant established the physiological significance of propionyl-CoA toxicity during infection (72). The mutant strain showed a severe defect in intracellular survival compared to the WT strain, which suggests that Mtb utilizes carbon sources that lead to the production of propionyl-CoA during infection. This was further confirmed by the rescue of intracellular growth of the Δ*icl1* strain when the MΦs were supplemented with vitamin B_{12} (72).

1.1.5 Mtb and the host immune response

1.1.5.1 Recognition and phagocytosis

Mtb gains entry into alveolar MΦs by receptor-mediated phagocytosis mediated either by complement receptors or mannose receptors. In the first mode of uptake, complement proteins bind to the mycobacterial cell surface, are then recognized by complement receptors and phagocytosis is stimulated (73). Phagocytosis can also be stimulated through the interaction of the MΦ mannose receptors with mannose residues on mycobacterial LAMs (74). While alveolar MΦs appear to be the favored host cell for Mtb, it is also capable of invading dendritic cells (DCs) and lung epithelial cells. DC uptake is mediated by DC-SIGN, a C-type lectin receptor that binds to mannose-capped LAMs (75).

1.1.5.2 Innate immunity

Following phagocytosis, infected MΦs release IL-8 which recruits the first responders to the site of infection: the neutrophils (76). The recruited neutrophils are stimulated to produce more IL-8 and TNF-α which help activate the infected alveolar MΦs and facilitate the further activation of the innate immune response (76, 77). Circulating blood monocytes arrive on the scene in response to chemokines released by infected MΦs. After extravasation, they differentiate into MΦs with the ability to ingest the infectious bacteria. NKT cells are also recruited to the site of infection and have the ability to destroy infected host cells, recognized by lipid and glycolipid antigens presented on CD1d (77). In addition to their killing functions, NKT cells activate MΦs by producing IFN-γ (77).

The complement cascade is another component of innate immunity that responds to Mtb infection. *Mycobacterium bovis* bacillus Calmette-Guerin (BCG), which shares 99.9% sequence identity with Mtb, activates the classical, lectin, and alternative complement pathways (78). Complement activation protects against pathogens through opsonization and subsequent ingestion of invading bacteria, osmotic lysis of bacterial cells through the formation of the membrane attack complex, and the recruitment of leukocytes by chemokine signaling.

1.1.5.3 Adaptive immunity

The inability of the innate immune system to clear Mtb infection leads to the activation of adaptive immunity, which includes both cell-mediated and humoral responses. $CD4^+$ T cells are activated in the lung-draining lymph node by infected DCs displaying Mtb antigen on MHC class II molecules (77). Upon recognition, T cells release IL-6, IL-21, IL-1β, IL-12p40 and TGF-β (79). Once activated, T cells undergo clonal expansion and differentiation into $CD4^+$ effector T cells.

They then migrate to the site of infection where they recognize antigen presented by infected MΦs and DCs and release IFN-γ to activate them (77). The interaction between infected MΦs and $CD4^+$ T cells is thought to be crucial for the elimination of Mtb. IFN-γ activated MΦs are stimulated to kill invading bacteria through the acidification of the phagosome, production of ROS and RNS, secretion of hydrolases into the phagosomal lumen, and phago-lysosome fusion. The importance of $CD4^+$ T cells in the immune response to Mtb infection is underlined by the increased susceptibility of $CD4^+$- and MHC class II-deficient mice (80), and in HIV^+ humans with depleted $CD4^+$ T cells (81). A balance between the T_H1 and T_H2 subsets of $CD4^+$ T cells is important for the outcome of infection (77). T_H1 cells activate MΦs by producing IFN-γ while T_H2 cells limit the damage from an excessive immune response by producing the anti-inflammatory cytokines IL-4, IL-10, and IL-13.

While the role of $CD8^+$ T cells in the immune response to Mtb remains a current area of investigation, the contribution of these cells is exemplified by the high levels of Mtb-specific $CD8^+$ T cells present in latently infected individuals (82). $CD8^+$ T cells recognize antigen presented on MHC class I molecules and CD1, both of which present cytosolic antigen. It is unclear how Mtb-specific antigen gets from the phagosome into the cytosol for MHC-I and CD1 presentation as the phagosome escape hypothesis remains a topic of debate (77).

The importance of humoral immunity in the control of Mtb infection is contentious. However, the involvement of antibody (Ab)-mediated immunity can be inferred by: (a) passive administration of pathogen-specific Abs during infection, (b) the presence and activity of Mtb-specific Abs in an infected host, and (c) an increased susceptibility of infection models lacking components of humoral immunity. Numerous passive transfer studies have shown protection against Mtb infection, which suggests that Abs can improve the immune response against Mtb

(83). Vaccination studies using mycobacterial cell wall components in mice produced high titers of Mtb-specific IgG and provided protection against Mtb infection, which suggests that host-produced Abs have a protective effect (83). Studies with B cell-deficient mice have produced inconsistent results with some studies reporting increased susceptibility of B cell-deficient mice to TB compared to control mice, while other studies reported no difference (83). However, in humans, a lack of Abs against the mycobacterial cell wall component LAM correlates significantly with disseminated TB. Moreover, patients with HIV-associated TB have lower Mtb-specific Ab titers and are more susceptible to dissemination (83). Together, these data suggest the involvement of B cells though further research is needed to definitively ascertain the role of Ab-mediated immunity in Mtb infection.

1.2 Cholesterol catabolism in Mtb

During infection, Mtb undergoes extensive metabolic reprogramming to adapt to the granuloma environment (84). This includes the up-regulation of a cluster of genes which enables the bacterium to take up and degrade host-produced cholesterol, a nutrient found in abundance within the Mtb granuloma (15, 85-88). The cholesterol catabolic pathway produces acetyl-CoA, propionyl-CoA, and pyruvate, and is proposed to produce succinyl-CoA, all of which feed into central metabolic pathways (89). Acetyl-CoA and propionyl-CoA also feed into anabolic pathways leading to the biosynthesis of MAs and methyl-branched FAs, respectively (90, 91). These are incorporated into the thick, hydrophobic cell wall that is characteristic of Mtb, and largely responsible for the intrinsic antibiotic resistance of the bacterium (92, 93). The cholesterol catabolic pathway has been shown to be essential for the virulence of Mtb in various infection models, exemplifying its potential as a novel drug target (94-98). Several transposon mutagenesis

and transcriptomics studies have led to the identification of genes involved in cholesterol catabolism, as well as those that are essential for virulence in various infection models (71, 97, 98). The findings from these studies are summarized in Table 1.1.

Table 1.1 Cholesterol catabolic genes in Mtb

Gene	Name	Upregulated on cholesterol (99)	Essential for growth on cholesterol (97)	Essential for virulence
rv1106c	*3β-HSD*			
rv1130	*prpD*	✓		✓(100)
rv1131	*prpC*	✓		✓(100)
rv1143	*MCR*			
rv3409c	*choD*			✓(101)
rv3492c	-	✓		
rv3493c	-	✓		
rv3494c	*mce4F*	✓		
rv3495c	*mce4E*	✓		
rv3496c	*mce4D*	✓		
rv3497c	*mce4C*	✓		
rv3498c	*mce4B*	✓		
rv3499c	*mce4A*	✓		
rv3500c	*yrbE4B*	✓		
rv3501c	*yrbE4A*	✓		✓(94)
rv3502c	*hsd4A*	✓	✓	
rv3503c	*fdxD*		✓	
rv3504	*fadE26*		✓	
rv3505	*fadE27*		✓	
rv3506	*fadD17*			
rv3515c	*fadD19*	✓	✓	
rv3516	*echA19*		✓	
rv3518c	*cyp142*		✓	
rv3520c	-		✓	
rv3521	-		✓	
rv3522	*ltp4*		✓	
rv3523	*ltp3*		✓	
rv3526	*kshA*	✓	✓	✓(102)
rv3534c	*hsaF*	✓	✓	
rv3535c	*hsaG*		✓	
rv3536c	*hsaE*	✓	✓	
rv3537	*kstD*	✓	✓	✓(98)
rv3538	*hsd4B*		✓	
rv3540c	*ltp2*	✓	✓	
rv3541c	*chsH1*			
rv3542c	*chsH2*	✓	✓	✓(98)

rv3543c	***chsE2***	✓	✓	
rv3544c	***chsE1***	✓	✓	✓(98)
rv3545c	***cyp125***	✓	✓	
rv3546c	***fadA5***	✓	✓	✓(99)
rv3548c	**-**	✓	✓	
rv3549c	**-**	✓	✓	
rv3550	***echA20***		✓	
rv3551	***ipdA***	✓	✓	✓(98)
rv3552	***ipdB***		✓	✓(98)
rv3553	***ipdC***	✓	✓	
rv3556c	***fadA6***		✓	✓(98)
rv3557c	***kstR2***		✓	
rv3559c	***ipdF***	✓	✓	
rv3560c	***fadE30***	✓	✓	
rv3561	***fadD3***	✓		
rv3562	***fadE31***		✓	
rv3563	***fadE32***	✓	✓	✓(98)
rv3564	***fadE33***	✓	✓	
rv3565	***aspB***		✓	
rv3567c	***hsaB***		✓	
rv3568c	***hsaC***	✓	✓	✓(95)
rv3569c	***hsaD***	✓	✓	✓(103)
rv3570c	***hsaA***	✓	✓	✓(98)
rv3571	***kshB***	✓	✓	✓(102)
rv3573c	***cshE3***	✓	✓	
rv3574	***kstR***		✓	

*deletion of the gene or disruption through transposon mutagenesis in Mtb reduced virulence in infection studies
Genes are color-coded with respect to their known or predicted functions: cholesterol uptake, red; sidechain degradation, pink; catabolism of rings A and B, green; catabolism of rings C/D, blue, transcriptional regulators, purple, and all other genes, black. Table adapted from Crowe (2018) (104)

1.2.1 Cholesterol

Steroids are a class of molecule found in all domains of life. All steroids share a core gonane structure, a 17-carbon skeleton arranged as four fused cycloalkanes (Fig. 1.7). Rings A, B, and C are cyclohexanes while ring D is a cyclopentane. Modifications to the core structure gives rise to a variety of steroid molecules with diverse biological functions. These include the solubilization of fats and fat-soluble vitamins in the digestive tract by bile acids, hormonal

signaling by the steroidal human sex hormones, and the regulation of membrane fluidity by cholesterol and ergosterol in animals and fungi, respectively.

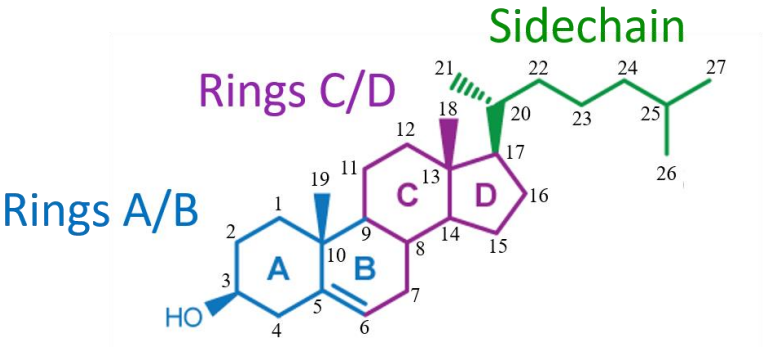

Figure 1.7 The chemical structure of cholesterol. C atoms are colored according to how they are degraded.

Cholesterol is a steroid molecule with the following modifications: a β-hydroxyl group on C3, a double bond between C5 and C6, β-methyl groups on C10 and C13, and an 8-carbon sidechain at C17 (Fig. 1.7). This 27-carbon steroid is a critical component of animal cell membranes. In mammalian cell plasma membranes, cholesterol is thought to make up more than 20% of the membrane weight (105) where it functions to regulate fluidity of the membrane in a temperature-dependent manner. At low temperatures, the presence of cholesterol in the phospholipid bilayer increases membrane fluidity by interfering with the tight packing of the phospholipid fatty acid tails while at high temperatures, it decreases membrane fluidity by limiting phospholipid motility. In addition to regulating membrane fluidity, cholesterol is a major component of membrane lipid rafts, specialized membrane microdomains which serve as organization centers on the cell surface, compartmentalizing cellular processes. Cholesterol is also

an essential component of caveolae and clathrin-coated pits which function in endocytosis, intracellular trafficking, intercellular communication and signaling, and nerve conduction (106).

Bacteria do not synthesize steroids or use cholesterol as a structural or regulatory component of their cell membranes. However, some species that interact with an animal host have evolved mechanisms to utilize the abundance of cholesterol and other steroids to their advantage. Some pathogenic bacteria, including Mtb, catabolize steroids and use them as a carbon and energy sources (94, 107). Others interact with lipid rafts, cholesterol-rich microdomains on animal cell membranes, to gain access to mammalian cells (108). For commensal bacteria residing in the human gut, bile acids serve as an electron sink during fermentative growth and the byproducts of these pathways can act as secondary bile acid hormones that affect host physiology (109). The ability of bacterial species to transform steroid molecules has been exploited for the industrial production of high-value steroidal compounds from low value steroids (110, 111).

1.2.2 The cholesterol catabolic gene cluster

In 2007, Van der Geize *et al.* conducted a transcriptomic analysis of the soil actinobacterium *Rhodococcus jostii* RHA1 (RHA1) growing on cholesterol as a sole carbon source, enabling the identification of genes that encode cholesterol-degrading enzymes (112). Bioinformatic analysis revealed that 51 of the genes specifically upregulated in RHA1 during growth on cholesterol were conserved within an ~80-gene cluster in the Mtb genome (Fig. 1.8). The ability of *M. bovis* BCG to grow on cholesterol as a sole carbon source, combined with the predicted essentiality of genes within the gene cluster (57, 98), led the authors to hypothesize that cholesterol catabolism is important for the pathogenesis of Mtb (112). These findings spurred a

multitude of studies aimed at understanding the genetics and biochemistry behind cholesterol catabolism in Mtb and its role in infection.

Figure 1.8 depicts the organization of the cholesterol catabolic gene cluster in Mtb. The gene cluster is largely comprised of two regulons, each under the control of a TetR-type transcriptional repressor (113, 114). Kendall *et al.* predicted that KstR (Rv3574) controls a subset of 74 genes, 51 of which encode the proteins required for cholesterol uptake and the catabolism of the cholesterol sidechain and rings A and B (114). KstR exerts its control by binding to a 14-nucleotide inverted repeat in the absence of its inducer molecule (113). The Mtb genome contains 16 predicted KstR binding motifs, 13 of which are located in the cholesterol catabolic gene cluster. The inducer of the KstR regulon is 3-oxo-cholest-4-en-26-oyl-CoA, a cholesterol metabolite produced during catabolism of the sidechain (115). Binding of the inducer to KstR causes its release from the DNA-binding motif, thereby permitting transcription.

A smaller subset of ~14 genes is controlled by the second transcriptional repressor, KstR2 (113). Genes within the KstR2 regulon code for enzymes involved in the catabolism of cholesterol rings C and D (89). The inducer for the KstR2 regulon was identified by Casabon *et al.* (2013) to be 3aα-H-4α(3'-propanoate)-7aβ-methylhexahydro-1,5-indanedione (HIP) -CoA, the first metabolite produced in the catabolism of cholesterol rings C and D (116). Consistent with this, RT-qPCR analysis of RHA1 grown on the rings C and D-containing metabolite HIP showed upregulation of genes in the KstR2 but not the KstR regulon (116).

1.2.3 Cholesterol import

The hydrophobic and largely impermeable MA-containing cell envelope of Mtb poses a barrier for the import of hydrophobic molecules like cholesterol and fatty acids. The transport of

these nutrients across the cell envelope requires specialized Mce proteins, which were originally associated with mammalian cell entry (117, 118). The genome of Mtb encodes four *mce* loci (*mce1-mce4*). While the functions of the proteins encoded by the *mce2* and *mce3* loci remain to be determined, the multi-subunit transporter for the import of cholesterol is encoded by the *mce4* locus (94), and the *mce1* locus codes for fatty acid transport (64). The *mce4* operon includes the genes *rv3492c-rv3501c* which encode 10 putative proteins that make up the Mce4 transporter. The complex includes predicted two-subunit integral membrane permease which transports cholesterol across the plasma membrane (119). The Mce4 complex has six cell wall proteins (Mce4A-F) which assemble to form a hetero-hexameric ring with a helical C-terminal domain that spans the cell envelope, connecting the plasma membrane to the outer layer (117). Additionally, two accessory proteins (Rv3493 and Rv3492) are encoded by the *mce4* operon and are required for cholesterol import (119). MceG is a putative ATPase which suggests that cholesterol transport is ATP-dependent. Disruption of *mce4G* decreased growth of Mtb on cholesterol, but did not completely inhibit cholesterol utilization (94). Consistent with this, deletion of the entire *mce4* operon in *M. smegmatis* did not completely inhibit the uptake of cholesterol (120). These data suggest that other mechanisms in addition to Mce4 may be involved in the transport of cholesterol into the bacterial cell. However, the *mce4* genes are essential for persistence of Mtb in infection studies which suggests that Mce4 is likely the primary transport mechanism (46, 94, 121). Nazarova *et al.* recently demonstrated that the previously uncharacterized protein LucA (Rv3723) is required for the import of both FAs and cholesterol by Mtb *in vitro* and in MΦs (64). The authors determined that LucA facilitates uptake of cholesterol and FAs by stabilizing the subunits of the Mce1 and Mce4 transporters. These data suggest that the uptake of cholesterol and FAs is coordinated and that LucA is necessary to support intracellular growth of Mtb.

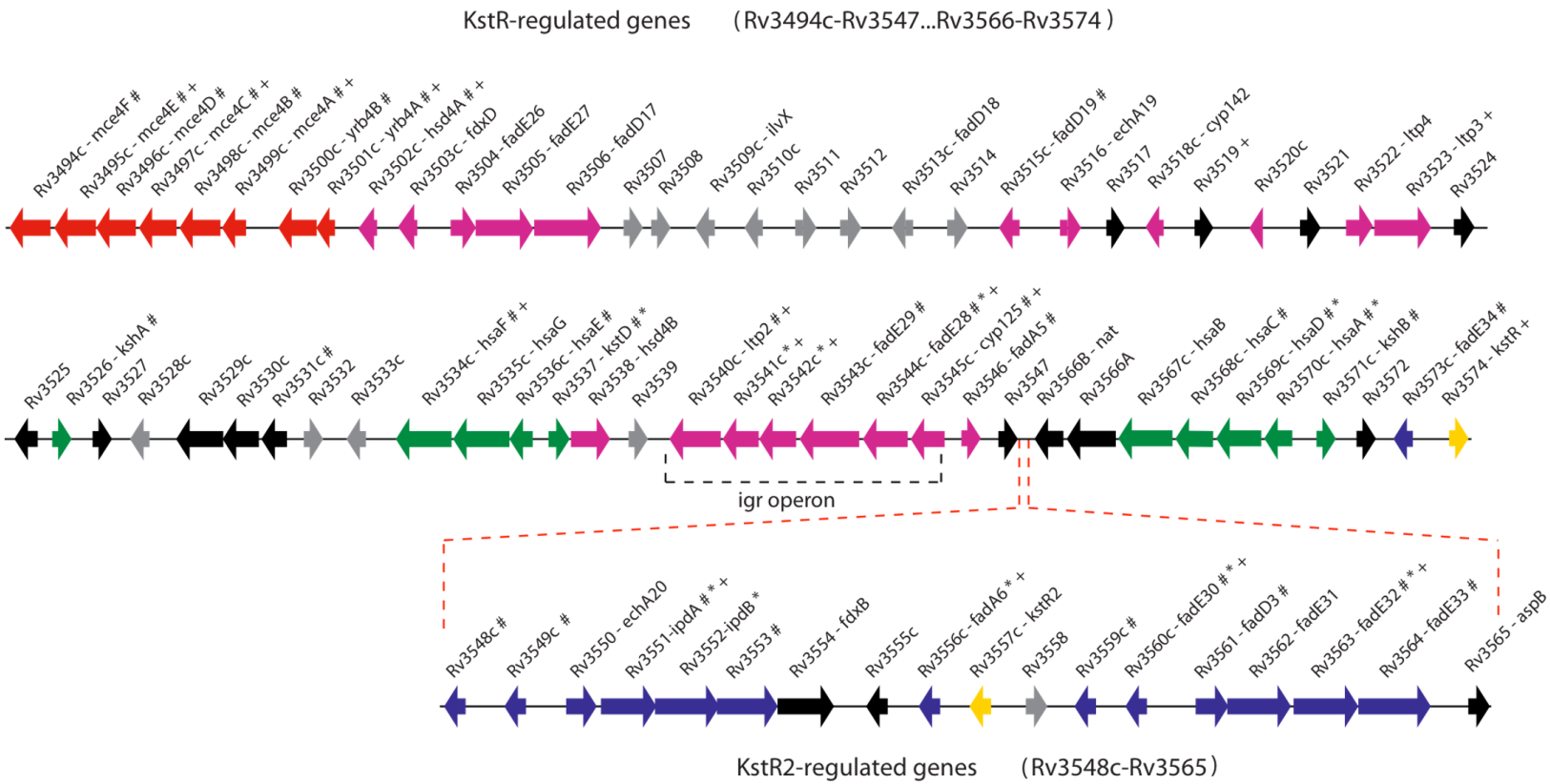

Figure 1.8 The cholesterol catabolic gene cluster in Mtb. Genes are color-coded with respect to their known or predicted functions: cholesterol uptake, red; sidechain degradation, pink; catabolism of rings A and B, green; catabolism of rings C/D, blue, and genes not involved in cholesterol catabolism, grey. Figure adapted from Capyk, J. (2012) (122)

1.2.4 Side chain catabolism

Catabolism of the cholesterol side chain proceeds via β-oxidation to yield two propionyl-CoA and one acetyl-CoA (Fig. 1.9). The first step is catalyzed by one of two cytochrome P450s in Mtb, Cyp125 or Cyp142, which oxidize the terminal C26 or C27 carbons of the cholesterol side chain, respectively to form 5-cholestene-26-oate (123, 124). KshB appears to be the reductase component that transfers reducing equivalents from NADH to Cyp125 (123, 125). FadD19 is an acyl-CoA synthetase that then catalyzes the thioesterification of the C8 alkanoate side chain to produce 3-hydroxy-cholest-5-ene-26-oyl-CoA, thereby activating the substrate for the first cycle of β-oxidation (126). Each round of β-oxidation involves four sequential steps: desaturation of the α and β carbons adjacent to the CoA by an acyl-CoA dehydrogenase (FadE), hydroxylation of the double bond at the β carbon by an enoyl-CoA hydratase (EchA), oxidation of the C_β hydroxyl by a 3-hydroxyl-acyl-CoA dehydrogenase (FadB), and finally the thiolysis of the β-keto-acyl-CoA releasing an acetyl- or a propionyl-CoA unit catalyzed by a thiolase (FadA). The first round of side chain β-oxidation is mediated by the multimeric acyl-CoA dehydrogenase complex comprised of ChsE4-ChsE5 and results in the release of propionyl-CoA (127, 128). The second round of β-oxidation releases acetyl-CoA and involves the dehydrogenase ChsE3 and the thiolase FadA5 (99, 128). The final round of side chain β-oxidation releases a second propionyl-CoA and involves the dehydrogenation of cholest-22-CoA by the multimeric complex ChsE1-ChsE2, followed by the hydroxylation of C17 of ring D catalyzed by the hydratase complex ChsH1-ChsH2 (128). Finally, the aldolase Ltp2 cleaves the carbon-carbon bond between the side chain and the D ring of cholesterol to release the propionyl-CoA (129).

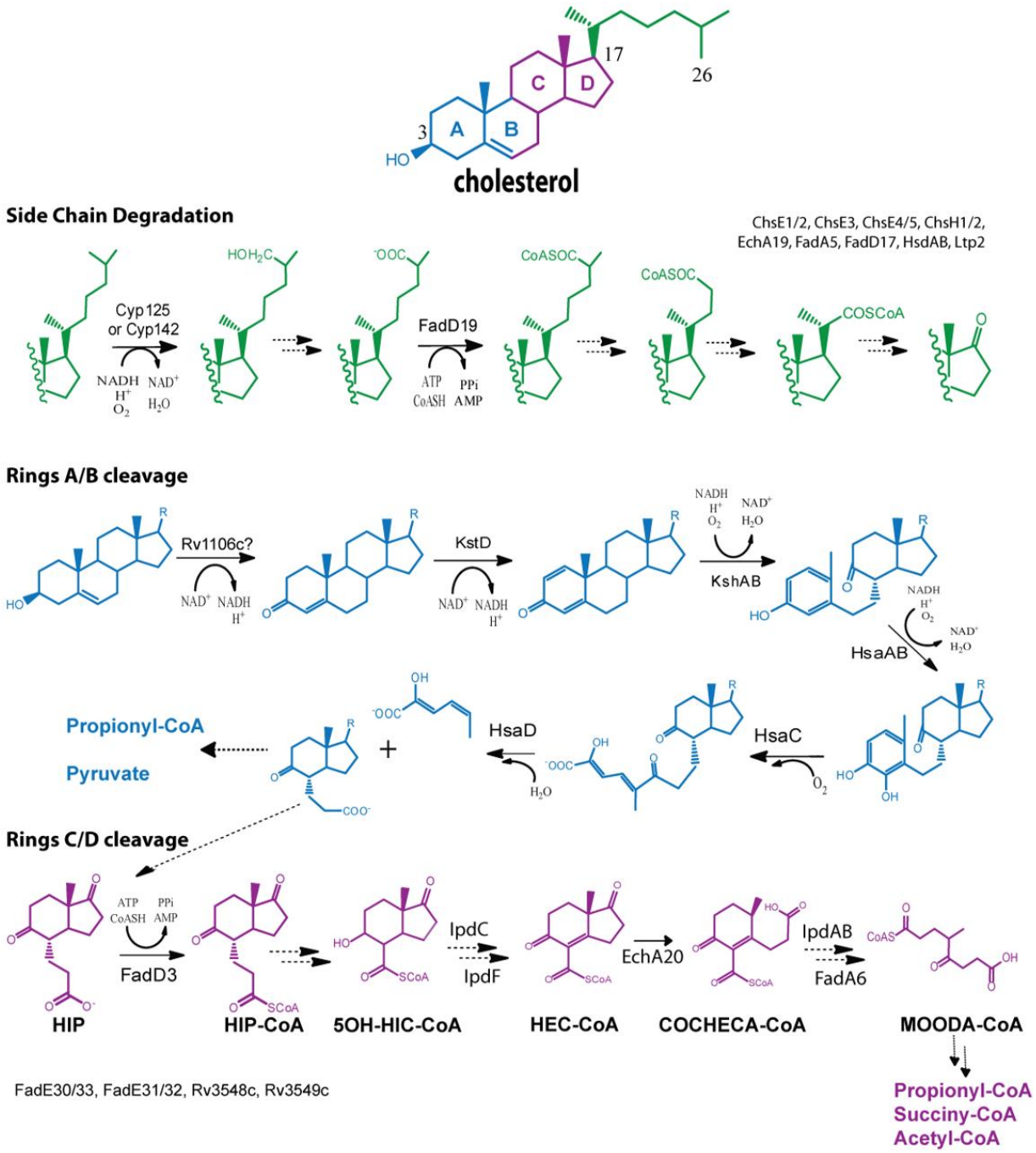

Figure 1.9 The cholesterol catabolic pathway of Mtb.

Complete side chain degradation leads to the formation of androstenedione (AD) comprised of the four steroid rings and an oxo group at C17. However, evidence suggests that side chain and rings A and B degradation occur concurrently as some cholesterol rings A and B catabolizing enzymes appear to preferentially act on substrates with partially degraded side chains. Most notably, Capyk *et al.* (2011) demonstrated that KshAB shows higher substrate specificity for the CoA-thioesterified substrate 3-oxo-23,24-bisnorchola-1,4-dien-22-oic acid-coenzyme A (1,4-BNC-CoA) compared to the non-thioesterified substrate 1,4-androstenedione (ADD), which has the same core structure but with a completely degraded sidechain (130). Similar findings were reported by Crowe (2018) for HsaD, which showed higher specificity for substrates with partially degraded side chains over those with a fully degraded side chain (104).

1.2.5 Rings A and B catabolism

Catabolism of cholesterol rings A and B yields one propionyl-CoA and one pyruvate (Fig. 1.9). The first step in the degradation of rings A and B is a dehydrogenation reaction to form 4-androstenedione (4-AD) (101, 131). Two Mtb enzymes, 3β-hydroxysteroid dehydrogenase (3β-HSD) and cholesterol oxidase (ChoD), are predicted to be able to catalyze this reaction but only 3β-HSD has been shown to catalyze the reaction *in vitro* (131). However, it appears that neither homolog is required for growth of Mtb on cholesterol, and deletion of 3β-HSD did not impair growth of Mtb in a guinea pig model (131). These data suggest that the genome of Mtb may harbor an alternative enzyme that catalyzes the first reaction in the degradation of cholesterol rings A and B. Regardless of how 4-AD is produced, desaturation of ring A is catalyzed by 3-ketosteroid Δ^1-dehydrogenase (KstD) to produce ADD (132). This is followed by the hydroxylation at the C9 position by KshA and KshB, a monooxygenase and a reductase, respectively, to produce 9-

hydroxy-androsta-1,4-diene-3,17-dione (9OHADD) (123, 130). This is followed by the non-enzymatic opening of ring B and aromatization of ring A to form 3-hydroxy-9,10-seconandrost-1,3,5(10)-triene-9,17-dione (3-HSA). 3-HSA is hydroxylated by HsaAB, a flavin-dependent monooxygenase, at the C4 position to generate the catechol 3,4-dihydroxy-9,10-seconandrost-1,3,5(10)-triene-9,17-dione (DHSA) (133). HsaC, an extradiol dioxygenase, then catalyzes the *meta*-cleavage of DHSA to produce 4,5-9,10-diseco-α3-hydroxy-5,9,17-trioxoandrosta-1(10),2-diene-4-oic acid (DSHA) (95). Finally, the MCP hydrolase HsaD catalyzes the cleavage of the carbon-carbon bond between C5 and C10 to generate 2-hydroxy-hexa-2,4-dienoic acid (HHD) and 3aα-H-4α(3′propanoyl-CoA)-7aβ-methylhexa-hydro-1,5-indanedione (HIP) (134). HHD is converted to propionyl-CoA and pyruvate by the enzymes HsaEFG while HIP feeds into cholesterol rings C and D degradation (135, 136).

1.2.6 Rings C and D catabolism

Catabolism of the last two cholesterol rings releases one acetyl-CoA and is predicted to produce one more acetyl-CoA, one propionyl-CoA and one succinyl-CoA (Fig. 1.9). The acyl-CoA synthetase FadD3 catalyzes the first step, which is the thioesterification of HIP to yield HIP-CoA (136). In Crowe *et al.* (2017), we proposed a model for the complete catabolism of HIP-CoA (89). Briefly, the propionyl side chain is first degraded via β-oxidation to yield 3a*α*-*H*-4*α*(carboxyl-CoA)-5-hydroxy-7a*β*-methylhexahydro-1-indanone (5-OH HIC-CoA). This is transformed to (7aS)-7a-methyl-1,5-dioxo-2,3,5,6,7,7a-hexahydro-1*H*-indene-4-carboxyl-CoA (HIEC-CoA) by IpdF and IpdC before undergoing two successive ring-cleavage reactions: EchA20-catalyzed hydrolysis of Ring D to produce (*R*)-2-(2-carboxyethyl)-3-methyl-6-oxocyclohex-1-ene-1-carboxyl-CoA (COCHEA-CoA), followed by IpdAB-catalyzed hydrolysis of Ring C. Thiolysis of

the Ring C-opened product, potentially by FadA6 or another thiolase, yields 4-methyl-5-oxo-octanedioc acid (MOODA-CoA) which is then oxidized to $^{2}\Delta$-MOODA-CoA by an ACAD comprised in whole or in part by FadE32. Although the fate of $^{2}\Delta$-MOODA-CoA is unclear, it has been proposed that it undergoes a final round of β-oxidation to yield 2-methyl-β-ketoadipyl-CoA (MβKA-CoA). This could then be cleaved to propionyl-CoA and succinyl-CoA in a manner analogous to the cleavage of β-ketoadipyl-CoA to succinyl-CoA and acetyl-CoA in the final step of the β-ketoadipate pathway used in the bacterial catabolism of aromatic compounds (137).

Overall, the cholesterol catabolic pathway is predicted to produce four propionyl-CoA, four acetyl-CoA, one pyruvate, and one succinyl-CoA. These products can feed into central metabolic pathways or anabolism as discussed in Section 1.1.4.5.

1.2.7 Cholesterol catabolism in Mtb virulence

Proteins involved in cholesterol uptake and catabolism of rings A and B have been shown to be essential for virulence in infection models. More specifically, disruption of genes encoding the Mce4 transporter which is required for optimal uptake of cholesterol led to a severe growth defect in mice (94). Catabolism of the cholesterol sidechain has also been implicated in pathogenesis. Deletion of genes within the *igr* locus, which encode enzymes that catalyze the removal of the final propionyl-CoA from the side chain, attenuated growth in MΦs and in mice (138). Deletion of the genes encoding the rings A and B catabolizing enzymes HsaC (95), HsaD (98, 139), FadA5 (99), and KshA (102) lead to attenuated growth in infection models. A strain lacking the genes encoding the rings C and D catabolizing enzyme IpdAB in the horse pathogen *R. equi* is avirulent and is patented as a live vaccine (140). Finally, deletion of *ipdAB* in Mtb

attenuated growth in MΦs as discussed in Section 3.1. Together, these data strongly implicate the cholesterol catabolic pathway in the pathogenesis of Mtb.

As a result of the burgeoning evidence that cholesterol is essential for the virulence of Mtb, several studies have aimed to identify compounds that inhibit growth of Mtb on cholesterol for drug development. For example, VanderVen *et al.* (2015) screened a compound library and identified compounds that inhibited growth in MΦs and on cholesterol as a sole carbon source (139). The screen yielded an inhibitor of an MCC enzyme PrpC required for the detoxification of propionyl-CoA produced from cholesterol, and an inhibitor of the rings A and B-degrading enzyme HsaA. The authors also identified a compound that appears to target the adenylyl cyclase Rv1625c discussed in Section 3.1.

1.3 Post-translational regulation of bacterial enzymes

1.3.1 Mechanisms of regulation

During infection, bacterial pathogens are required to alter their cellular processes to adapt to the host environment. Host-induced alterations to bacterial physiology and metabolism rely on the modification of enzymatic activities. For an enzyme to be produced and active in the cell, there are a series of tightly regulated processes that need to occur: transcription of the gene by RNA polymerase, translation of the resulting mRNA by ribosomes, and the folding and assembly of the active protein. Regulation of protein production occurs at each of these steps, and this regulation is vitally important for the bacterial cell to adapt to new environments. Unregulated production of proteins consumes unnecessary energy and resources and leads to aberrant enzymatic activities that may be detrimental to the cell under certain circumstances.

Transcription of bacterial genes relies on sigma factors, which are responsible for the recognition of a consensus sequence within the promoters of genes that are to be transcribed (141). Different sigma factors recognize particular consensus sequences so that the transcription of entire sets of genes can be up- or down-regulated depending on the levels of different sigma factors present in the cell. Transcriptional control is also mediated by transcription factors which bind DNA and can either repress or promote expression of specific genes. Transcription factors will bind or release DNA upon conformational changes induced by ligand binding, resulting in transcriptional regulation as a function of the ligand concentration in the cell. Translation of the resulting mRNA is also regulated in prokaryotic organisms and this is usually mediated by secondary structure within the mRNA itself, or interactions between the mRNA and mRNA-binding proteins or other RNA molecules (142). Regulation may occur at the initiation or the elongation stage of translation. Together, these processes are required to limit the wasteful production of unneeded proteins.

When the aforementioned regulatory processes allow a protein to be produced, the function of the protein product is often modulated through post-translational modifications (PTMs) which include but are not limited to phosphorylation, acetylation, methylation, pupylation, glycosylation, as well as regulated proteolysis. With the advent of mass-spectrometry-based methodologies for the analysis of PTMs, it has become clear that they are highly prevalent in bacteria, particularly by phosphorylation and acetylation (143). Analyses of the phospo- and acetyl-proteomes have been conducted in species including *E. coli*, *Bacillus subtilis*, *Streptococcus pneumoniae*, *Salmonella enterica*, *Staphylococcus aureus*, *Thermus thermophilus*, *Mycoplasma pneumoniae*, *Rhodopseudomonas palustris*, *Corynebacterium glutamicum*, and Mtb (143). These studies have demonstrated that there is a high prevalence of phosphorylation and acetylation among metabolic

enzymes. Post-translational regulation of bacterial metabolic processes by these mechanisms is discussed below.

Phosphorylation of bacterial metabolic enzymes, which involves the addition of a phosphate group onto Ser, Thr, or Tyr residues, has been identified as a key regulatory mechanism. Proteomics analyses of diverse species have identified extensive phosphate modifications on Ser, Thr, and Tyr residues. Phosphoproteomics of Mtb identified the highest number of phosphorylation events occurring on 516 sites (144). In a study of the *E. coli* phosphoproteome conducted by Hansen *et al*, 342 proteins with phosphorylation at Tyr residues were identified, including enzymes involved in glycolysis and the TCA cycle (145). Similar phosphorylation events were identified in *S. aureus* (143). Phosphorylation has also been shown to play a role in carbon catabolite repression (CCR) in various species of gram-positive and gram-negative bacteria (143). In this system, the histidine protein (HPr), which acts as a phosphocarrier in the sugar transferase system, is regulated through phosphorylation at a Ser residue. HPr phosphorylation is mediated by HPr kinase/phosphorylase in response to high fructose-1,6-bisphosphate concentrations. Phosphorylated HPr binds catabolite control protein A (CcpA), which then allows CcpA to regulate the expression of hundreds of genes for the catabolism of preferred carbon sources. The genome of Mtb encodes 11 serine-threonine protein kinases (STPKs), two of which are essential for mycobacterial growth and four of which play a role during infection (144). Phosphorylation mediated by the STPK PknG was found to regulate central metabolism through the regulatory protein GarA (146). Non-phosphorylated GarA binds and inactivates α-ketoglutarate dehydrogenase and glutamate dehydrogenase. It also binds glutamate synthase and in doing so, activates the enzyme. The result is reduced flow of carbon through the TCA cycle and

increased production of glutamate. Despite the identification of extensive protein phosphorylation in bacteria, there is still much to be learnt about the physiological roles of these modifications.

Protein *N*-acetylation involves the addition of an acetyl group to either the ε-amine of Lys or the α-amine of the *N*-terminal residue, termed N^{ε}-acetylation and N^{α}-acetylation, respectively (147). The addition of the acetyl group can result in a conformational change in the protein and alters the chemistry of the affected amines by converting them to relatively unreactive amides (Fig. 1.10). *N*-acetylation also prevents protonation of the residue leading to a charge reduction. Acetylation is mediated by GCN5-like protein *N*-acetyltransferases (GNATs), while removal of the acetyl group is catalyzed by NAD^{+}-dependent Sir2-like protein deacetylases (sirtuins). Acetylation is a prominent post-translational modification in bacteria. The most well-characterized and highly conserved acetylation system in bacteria was first described in *S. enterica* and is comprised of the *N*-acetyltransferase Pat and the sirtuin CobB. Starai *et al*. first demonstrated that Pat acetylates and negatively regulates acetyl-CoA synthetase (Acs), and that activity of Acs is restored via deacetylation catalyzed by CobB. Homologs of Pat and CobB have been identified in various bacterial species including Mtb as discussed in Section 1.3.2.

Acetylation is not the only modification that occurs on Lys residues. Enzymes of the GNAT superfamily can transfer acyl groups from succinyl-CoA, malonyl-CoA, and propionyl-CoA leading to succinylation, malonylation, and propionylation, respectively, of their protein substrates. It appears that the Pat/CobB regulatory network shows dual functionality in some bacteria, mediating both acetylation and propionylation. These modifications, though less prevalent than acetylation, are interesting in that they result in more drastic chemical changes to their protein targets (Fig. 1.10).

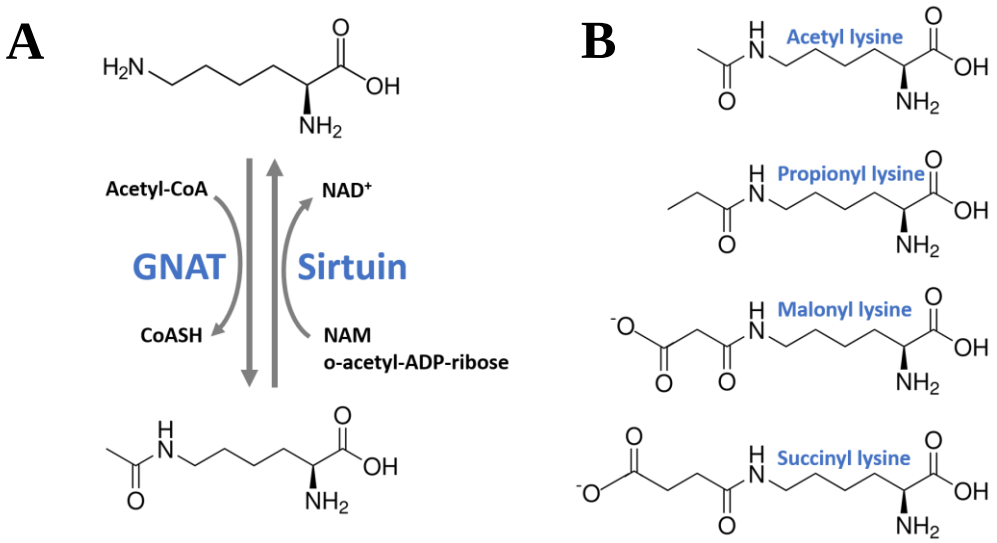

Figure 1.10 Protein lysine *N*-acetylation and deacetylation (A) and other lysine modifications (B)

1.3.2 Reversible lysine acetylation in Mtb

Figure 1.11 summarizes the central metabolic enzymes known to be regulated through acetylation in Mtb. Protein lysine acetylation in Mtb was first described by Nambi *et al* (2010) with the identification of the cAMP-dependent *N*-acetyltransferase MtPat (Rv0998) and its homolog from *M. smegmatis* MSMEG_5458 (148). Bioinformatic analysis of MtPat revealed a fusion of a cAMP binding domain to a GNAT-like *N*-acetyltransfase domain. The fusion of these two domains is unique to mycobacteria and has not been found in any other prokaryotic or eukaryotic genome to date. However, it is found in all sequenced mycobacterial genomes which suggests that the direct regulation of protein lysine acetylation by cAMP is unique to this genus (148). A pull-down assay using MSMEG_5458 revealed an interaction with the universal stress protein

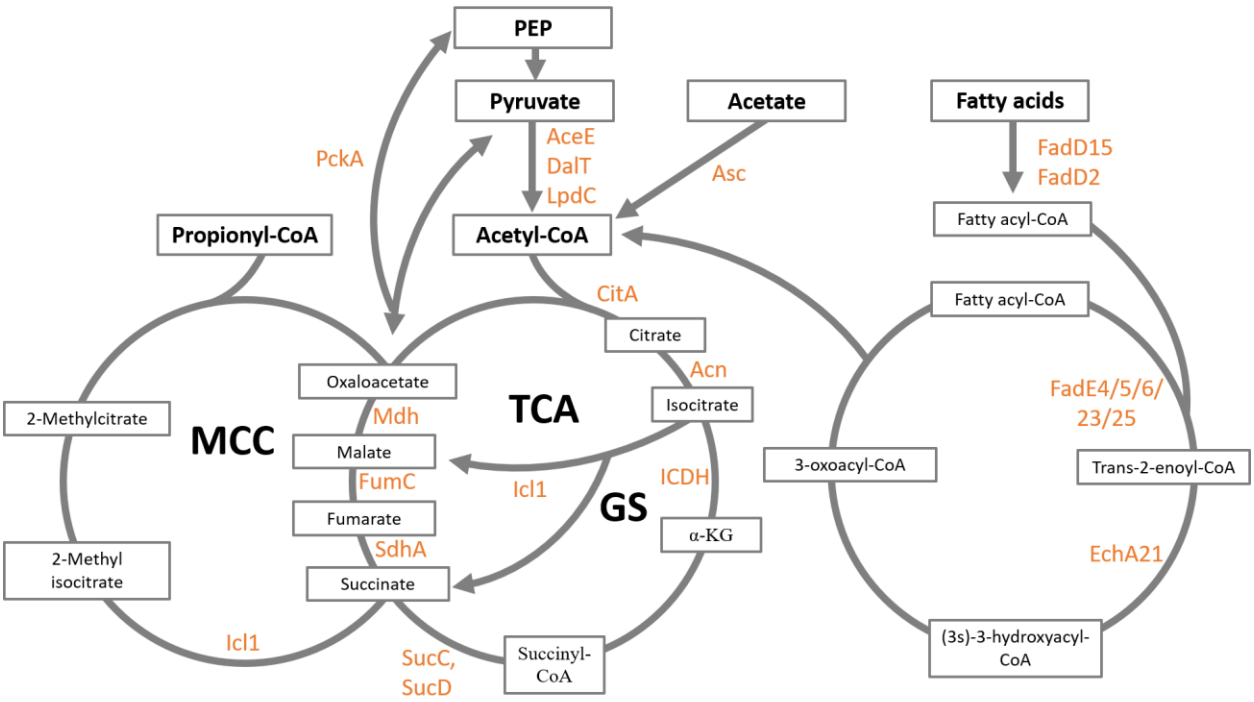

Figure 1.11 Central metabolic enzymes of Mtb that are subject to regulation by lysine acetylation. Enzymes shown in orange have been identified in acetylome analysis and/or through *in vitro* acetylation. MCC, methylcitrate cycle; TCA, tricarboxylic acid cycle; GS, glyoxylate shunt.

(USP) MSMEG_4207 which was subsequently shown to be a substrate for MSMEG_5458-mediated lysine acetylation (148). Xu *et al* (2011) identified the NAD^+-dependent deacetylase Rv1151c and showed that Acs is a substrate for the regulatory network (149). Based on bioinformatic analysis, eighteen more Mtb proteins that could serve as substrates for MtPat were identified, four of which were confirmed to be acetylated by MtPat *in vitro* and deacetylated by Rv1151c (150). All of the MtPat substrates identified in this study were FadD enzymes, which are acyl-CoA synthetases that activate lipid substrates for their catabolism. Eight more FadD enzymes were found to be acetylated by MtPat while 14 FadD enzymes were not (150). Protein sequence alignments of all of the FadD enzymes tested revealed four motifs that were conserved among MtPat substrates: GGXNX4EXE/D, E/DX7E/D, K/AXP, and PX4GK, all located in the C-terminal domains. Acetylation of FadD enzymes occurred at an active site lysine residue and was

found to inhibit the AMP-ligase activity. Deletion of the gene encoding MtPat, *rv0998*, resulted in a growth defect when growing on propionate as a sole carbon source. Propionate is converted to propionyl-CoA by Acs, a known substrate for MtPat. The growth defect can be explained by the excesses production of propionyl-CoA (which is toxic in high concentrations) in the absence of MtPat-mediated regulation of Acs (150). Together, these data suggest that acetate, propionate, and FA catabolism are regulated through reversible lysine acetylation in Mtb. Furthermore, central carbon metabolism also appears to be regulated by MtPat and Rv1151c through the acetylation of ICL1 (151).

MtPat is essential for Mtb survival under hypoxic conditions (152). Rittershaus *et al* demonstrated that the viability defect of the Δ*mtPat* mutant under hypoxic conditions was dependent on the presence of FAs in the culture medium, and that MtPat acts to prevent the formation of acetyl-CoA under these conditions (152). The lack of MtPat resulted in the continuous flux of carbon through the oxidative branch of the TCA cycle under hypoxic conditions rather than through the reductive branch as seen for the WT strain. The inability of the Δ*mtPat* strain to adapt to hypoxia by preferential use of the reductive TCA branch led to a redox imbalance. The authors suggest that MtPat acts to limit the production of acetyl-CoA from FAs under hypoxic conditions to reduce the flux of carbon through the oxidative TCA cycle.

Carbon metabolic pathways are not the only processes regulated by MtPat. Vergnolle *et al* demonstrated that the biosynthesis of the siderophore MB is regulated through reversible lysine acetylation (153). MbtA catalyzes the first reaction in MB biosynthesis, the adenylation of salicylic acid followed by the ligation of the acyl-adenylate onto the acyl carrier protein. MbtA is inhibited by MtPat-mediated cAMP-dependent acetylation at an active site lysine residue and activity is restored by Rv1151c. Finally, the *dosR* regulon appears to be regulated by acetylation as acetylated

DosR was detected in acetylome studies (151, 154). Acetylation of DosR inhibits DNA binding (155). The enzyme responsible for DosR acetylation has not been identified, but Rv1151c can deacetylate DosR *in vitro* (155).

Lee *et al* (2010) described the crystal structures of both the cAMP-activated and auto-inhibited forms of MtPat (156). The structures revealed that cAMP binds to a regulatory domain that is located over 32 Å away from the catalytic domain. In the auto-inhibited conformation, a substrate-mimicking lid covers the protein-substrate binding surface. Upon binding of cAMP, a dramatic conformational rearrangement relieves auto-inhibition by exposing the substrate binding surface.

Two other Mtb enzymes acetylate protein substrates: the enhanced intracellular survival (Eis) protein and Rv2170. Eis is a GNAT-family bacterial acetyltransferase that mediates resistance to kanamycin by acetylating and inactivating aminoglycosides. Eis also acetylates the histone-like bacterial nucleoid-associated protein HupB, which is also deacetylated by Rv1151c (51). Rv2170 is another GNAT acetyltransferase identified by Lee *et al* (2017) (157). The authors demonstrated that Rv2170 acetylates isocitrate dehydrogenase (ICDH). Deletion of *rv2170* rescues growth of the Δ*icl* mutant growing on FAs as a sole carbon source. ICL, which functions both in the MCC and the glyoxylate shunt, is required for growth on FAs. These data suggest that the lack of acetylation of ICDH in the Δ*rv2170* mutant restores growth in the Δ*icl* background by increasing carbon flow through ICDH of the TCA cycle (157).

1.4 The role of cAMP in Mtb

1.4.1 cAMP and adenylyl cyclase

3',5'-cyclic adenosine monophosphate (cAMP) is an important second messenger in many biological processes in both eukaryotes and prokaryotes. cAMP is produced from ATP by a metal-dependent adenylyl cyclase in response to stimuli and functions in intracellular signal transduction, transcriptional regulation, and regulation of enzymatic activity (Fig. 1.12A). In bacteria, the intracellular cAMP concentration influences the expression of a large number of genes through the transcription factor cAMP receptor protein (CRP), discussed in Section 1.4.3.

Adenylyl cyclase (AC) is the most polyphyletic enzyme with six evolutionarily distinct classes. Each class of AC catalyzes the same reaction but are encoded by unrelated gene families with no homology. Class I ACs were the first to be characterized and are commonly found in bacteria (158). These are large, cytosolic enzymes with a regulatory subunit that detects cytoplasmic glucose concentrations. Class II ACs are secreted by pathogenic bacteria including *Bacillus anthracis*, *Bordetella pertussis*, *Pseudomonas aeruginosa*, and *Vibrio vulnificus* (159-161). The class II AC secreted by *B. anthracis* is commonly known as anthrax toxin edema factor. Class III ACs are the most well-studied class and have implications in human health and physiology (162). Class III ACs are diverse and are subdivided into four subclasses (class IIIa-d) (162). Class IIIa ACs are integral membrane proteins allowing them to transmit signals from the extracellular environment to the cytosol. Mammalian class IIIa ACs have 12 transmembrane segments and two cytoplasmic catalytic domains (Fig. 1.12B) (162). The protein is organized with six transmembrane segments at the N terminus, followed by the C1 cytoplasmic domain, then another six transmembrane segments, and finally the C2 cytoplasmic domain at the C terminus (162). The C1 and C2 domains form an intramolecular dimer which makes up the active site. In

bacteria, class IIIa ACs are comprised of only six transmembrane domains followed by a single cytoplasmic domain, but they form homodimers to resemble the mammalian class III ACs (163). Class IV ACs are the smallest of the ACs with no known regulatory component and are found in bacteria including *Yersinia pestis* (164). Class V and VI ACs are also found in bacteria but are not well-characterized (158).

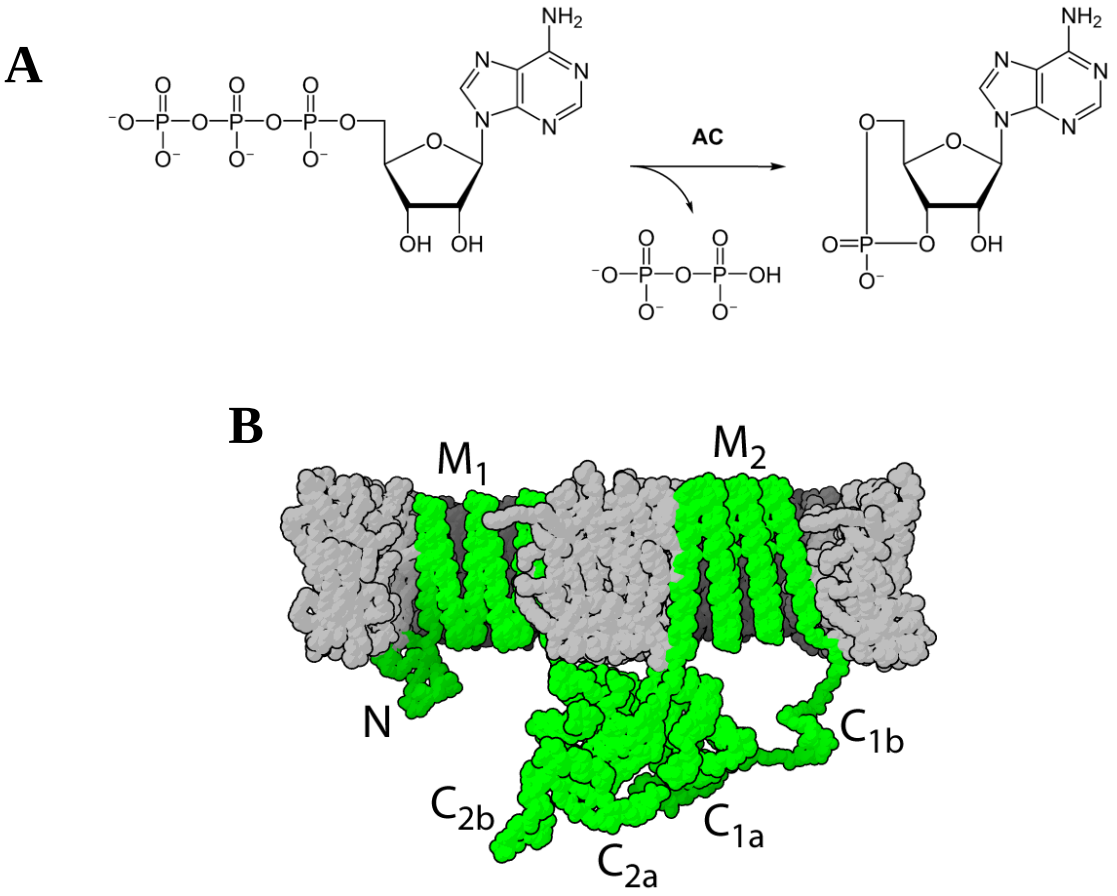

Figure 1.12 The reaction catalyzed by ACs (A) and the structure of the mammalian class IIIa AC (B)

1.4.2 Adenylyl cyclases in Mtb

The genome of Mtb H37Rv encodes 15 class III ACs, ten of which have demonstrated AC activity, and one additional AC pseudogene (163). It appears the number of ACs is not conserved across Mtb strains as one additional AC was found in Mtb CDC1551 which is thought to have evolved from the duplication of *rv1318c* (163). The unusually large number of ACs in Mtb suggests an importance for cAMP-mediated signaling for its survival and pathogenesis.

Mtb ACs include both soluble and membrane-associated enzymes, two of which (Rv1625c and Rv2435) are mammalian-like Class III ACs (165). Rv1318c, Rv1320c, Rv2435c, and Rv3645c are all membrane-associated ACs with HAMP (histidine kinases, adenylyl cyclases, methyl binding proteins, and phosphatases) domains, which are common in two-component signal transduction pathways suggesting their importance in responding to external stimuli (165). The stimuli to which each of the Mtb ACs responds to have not been fully characterized but they include host-associated factors like pH, CO_2 levels, and FAs (165). Consistent with this, the intracellular cAMP concentrations increase ~50-fold upon infection of MΦs (166).

1.4.3 cAMP signaling in Mtb

In Mtb, cAMP regulates cellular processes transcriptionally through two cAMP-responsive transcription factors CRP (Rv3676, cAMP responsive protein) and Cmr (Rv1675c, cAMP and macrophage regulator) (167). cAMP also post-translationally regulates enzymatic activity through the cAMP-dependent *N*-acetyltransferase MtPat (Rv0998) described in Section 1.3. Seven other Mtb proteins are predicted to bind cAMP but have not been characterized (167).

The cAMP-responsive transcription factor CRP is essential for pathogenesis in mice, suggesting the importance of cAMP signaling in the adaptation of Mtb to the host environment

(168). CRP, which can act as both a repressor and an activator, controls a putative regulon of over 100 genes encoding proteins involved in diverse cellular functions (167). These include respiration, nitrogen assimilation, and fatty acid and carbohydrate metabolism. In comparison, relatively little is known about Cmr in Mtb. The transcription factor has not been shown to bind cAMP directly but does appear to regulate genes in response to cAMP levels (167).

In addition to regulating its own cellular physiology and metabolism, Mtb secretes a large amount of cAMP to influence the host cell (167). The production of cAMP to modulate host cells is a common strategy employed by pathogenic bacteria, though in other species such as *B. anthracis*, *B. pertussis*, and *P. aeruginosa*, this is accomplished by secreted ACs (159, 160, 169), or in *Vibrio cholerae*, *E. coli*, and *B. pertussis*, by secreting enzymes that post-translationally modify host ACs (170, 171). The AC Rv0386 is responsible for the production of cAMP that is secreted into the MΦ, which results in TNF-α production (23). The importance of host cell cAMP intoxication was demonstrated by the deletion of *rv0386* which attenuated survival in mice (23).

1.4.4 TB drugs targeting cAMP production

VanderVen *et al* (2015) identified a novel class of molecules that stimulate the Mtb AC Rv1625c to produce excess amounts of cAMP resulting in the inhibition of the cholesterol catabolic pathway and the attenuation of growth in MΦs (139). While the link between cAMP and the cholesterol catabolic pathway has yet to be elucidated, it is clear that cAMP can impact central metabolism and other cellular processes (149, 156, 167). These findings suggest that stimulating cAMP production may be a novel mechanism for the elimination of intracellular Mtb.

1.5 Coenzyme A

CoA is an essential enzyme cofactor in all domains of life (Fig. 1.13). In fact, all genomes sequenced to date encode enzymes that require CoA and it is estimated that 9% of all identified enzyme activities use CoA or its thioesters as substrates (172). CoA participates in catalysis as an acyl group carrier and carbonyl activating group in numerous biochemical reactions that are essential for living organisms. It is required for the catalysis of many reactions central to cellular metabolism including those in the TCA cycle and FA synthesis and oxidation. It also provides the 4'-phosphopantetheine prosthetic group of acyl carrier proteins (ACPs).

Coenzyme A is synthesized from the precursor pantothenate (vitamin B_5). Humans and most other living organisms are incapable of *de novo* synthesis of pantothenate and must therefore obtain the vitamin through their diet. Pantothenate is synthesized by some bacteria and plants and it is therefore not an essential nutrient for these organisms (172).

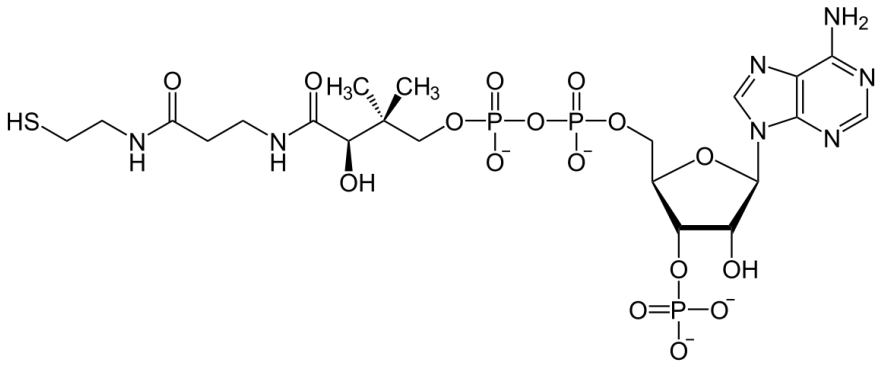

Figure 1.13 The structure of coenzyme A

1.5.1 CoA biosynthesis in Mtb

Production of CoA in Mtb first requires the biosynthesis of pantothenate, which is synthesized from β-alanine and α-ketoisovalerate, an intermediate in the biosynthesis of branched chain amino acids (Fig. 1.14A) (172). α-Ketoisovalerate is converted to ketopantoate by PanB, which is then reduced by PanE to produce pantoate. Pantoate is condensed with β-alanine by PanC to produce pantothenate (172). Sambandamurthy *et al.* demonstrated the essentiality of pantothenate biosynthesis *in vitro* and in infection models through the deletion of genes involved in pantothenate biosynthesis (173). Pantothenate supplementation was found to rescue growth of strains lacking *panC* and *panD*, establishing that Mtb is able to assimilate exogenous pantothenate (173).

Pantothenate kinase (CoaA) catalyzes the first committed step in CoA biosynthesis by phosphorylating pantothenate to produce 4'-phosphopantothenate (172). CoaA activity is tightly regulated through feedback inhibition *in vitro* and *in vivo* by free CoA (174, 175). The activity of CoaA from *E. coli* is also inhibited by thioesters, though not as strongly as free CoA (174). Similarly, the mammalian CoaA is regulated by free CoA and its thioesters (176). Crystal structures of the *E. coli* CoaA in complex with ATP, CoA, and pantothenate and ADP have been solved, shedding light on the competitive binding of free CoA and ATP to the active site (177). CoaA from Mtb has also been structurally and biochemically characterized (178, 179).

A gene encoding a pantothenate kinase that shares no sequence homology with CoaA, designated *coaX*, was identified in the genome of *B. subtilis* (172). The gene was found to be essential in a strain of *B. subtilis* lacking *coaA*, consistent with *coaX* encoding a pantothenate kinase. Like *B. subtilis*, Mtb has genes encoding both CoaA and CoaX (172). In contrast to CoaA, CoaX is not regulated by CoA or its thioesters. A possible explanation for the lack of

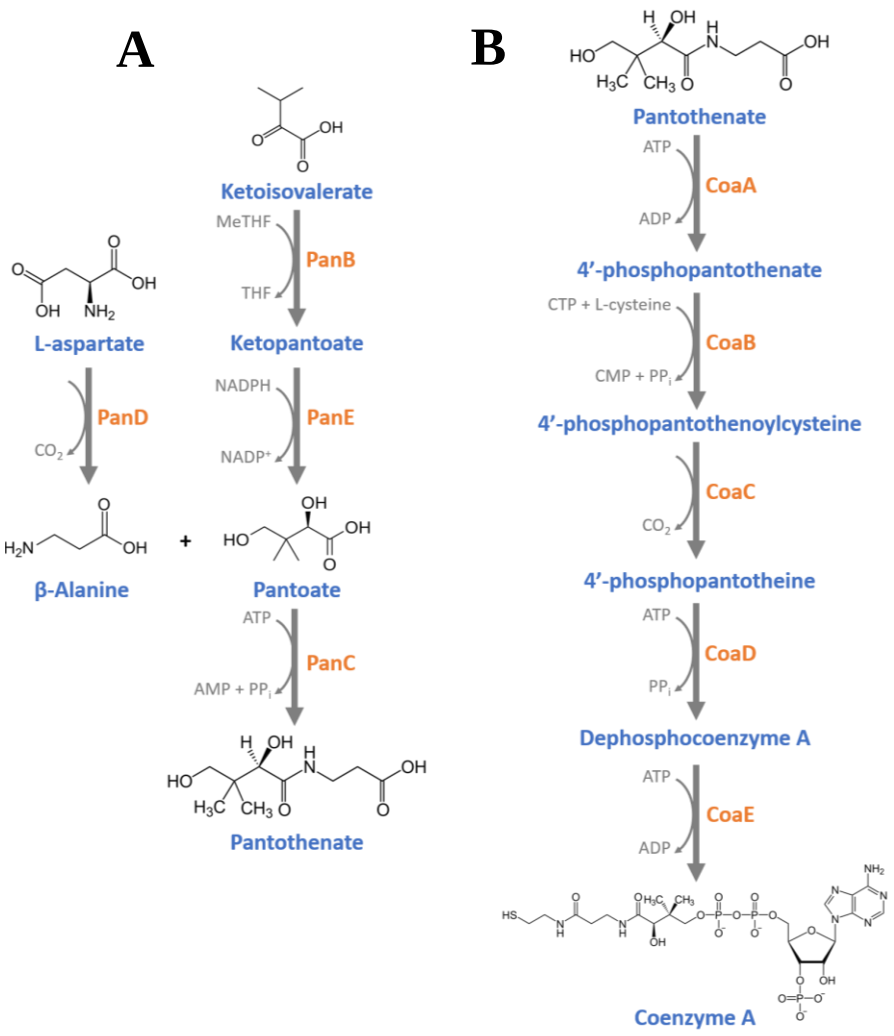

Figure 1.14 The biosynthesis of pantothenate (A) and CoA (B) in Mtb

inhibition of CoaX is the absence of a hydrophobic pocket that accommodates the thiol tail of CoA in CoaA structures (180).

The next step in CoA biosynthesis is the condensation of 4'-phosphopantothenate with a cysteine molecule catalyzed by CoaB followed by its decarboxylation by CoaC to produce 4'-phosphopantotheine (172). The conditional knockdown of CoaBC in Mtb led to a bactericidal phenotype and has thus been proposed as a promising drug target (181). CoaD catalyzes the reversible transfer of an adenylyl group from ATP to 4'-phosphopantetheine to form dephospho-

CoA (172). While CoaA is the only enzyme in the pathway known to be regulated through feedback inhibition, CoaD purified from *E. coli* was tightly bound to free CoA and the crystal structure of the *E. coli* CoaD in complex with CoA has been described (182, 183). Furthermore, 4'-phosphopantetheine accumulates in *E. coli* suggesting that the CoaD-catalyzed reaction may be another regulatory step (184). The final step in CoA biosynthesis is catalyzed by CoaE which phosphorylates the 3'-hydroxyl group of the ribose sugar moiety of dephospho-CoA (172).

The pantothenate and CoA biosynthetic pathways are both essential for Mtb viability *in vitro* and in infection models (46, 173, 181). Mtb can take up and utilize exogenously provided pantothenate and pantetheine, but the inability of auxotrophs to persist in infection models suggest that the availability of these precursors in the host is not sufficient, making the pathways an even more intriguing drug target (173, 181).

1.5.2 Effects of CoA depletion

Evans *et al* described the metabolic consequences of silencing *panB*, *panC*, *coaBC*, and *coaE*, all of which led to depletion of free CoA (181). The authors conducted an LC-MS based analysis of 69 metabolites associated with pantothenate and CoA metabolism following gene silencing. Levels of central metabolites including acetyl-CoA, phosphoenolpyruvate (PEP), α-ketoglutarate, fumarate, and malate were all depleted which suggests the impairment of the TCA cycle upon CoA depletion. Levels of various amino acids and their precursors were also dysregulated upon gene silencing, presumably as a result of TCA cycle dysfunction. Notably, malonyl-CoA, a key metabolite for FA biosynthesis, was more drastically depleted than acetyl-CoA while succinyl-CoA, unlike in *E. coli* CoA depletion, was not. These data provide a profile

for CoA starvation in Mtb and highlight the importance of the essential cofactor in the function and regulation of numerous metabolic processes.

1.6 Aims and outcomes of these studies

The aims of this study are to characterize cholesterol catabolic mutants and cholesterol-specific inhibitors in Mtb (Chapter 3.1), describe the post-translational regulatory mechanism controlling catabolism of cholesterol rings C and D (Chapter 3.2), and elucidate the mechanism of cholesterol-dependent toxicity in catabolic mutants (Chapter 3.3).

For Chapter 3.1, genes in the cholesterol catabolic cluster of Mtb were deleted and their *in vitro* growth phenotypes and metabolite accumulation were investigated. LC-MS analysis of intracellular CoA thioester metabolites was done in collaboration with Dr. Adam Crowe. The importance of cholesterol rings C and D catabolism was investigated using the THP-1 derived MΦ infection model. A cholesterol-specific inhibitor was identified in a screen conducted by GlaxoSmithKline (GSK) and characterization of this inhibitor was conducted. LC-MS analysis of cAMP production in Mtb was done in collaboration with Dr. Israel Casabon.

Chapter 3.2 describes the characterization of the reversible lysine acetylation of FadD3 catalyzed by the *N*-acetyltransferase MtPat and the deacetylase Rv1151c. FadD3 and Rv1151c from Mtb and the MtPat homolog from *M. smegmatis* were purified and the *in vitro* acetylation of FadD3 was characterized through enzyme activity assays, Western blot analysis, and protein trypsin digest followed by mass spectrometry. FadD3 was found to be acetylated and inactivated by MtPat at a catalytic lysine residue, and enzymatic activity was restored upon deacetylation by Rv1151c. Deletion of the genes encoding MtPat and Rv1151c was carried out by Jie Liu. The

MtPat mutant was found to have a growth defect in the presence of cholesterol under hypoxic conditions, indicating the importance of FadD3 regulation.

Chapter 3.3 describes a mechanism for cholesterol-dependent toxicity in catabolic mutants of Mtb and *M. smegmatis*. Gene deletions in *M. smegmatis* were carried out by Jie Liu and Dr. Adam Crowe and deletions in RHA1 were done by Dr. Hiroshi Otani. Intracellular and extracellular metabolite accumulation and CoA depletion in mutant strains growing in the presence of cholesterol were analyzed by HPLC and GC-MS. CoA was found to be depleted in mutant strains demonstrating toxicity in the presence of cholesterol. Metabolomic profiling of mutant strains upon CoA depletion was conducted by LC-MS in collaboration with Dr. Tao Huan and Shipei Xing at The University of British Columbia.

Overall, this thesis describes the importance of cholesterol catabolism for the pathogenesis of Mtb, the regulation of cholesterol rings C and D catabolism through reversible lysine acetylation of FadD3, and the mechanism of cholesterol-derived toxicity in cholesterol catabolic mutants. The work in this thesis contributes to the understanding of cholesterol catabolism in Mtb and identifies a novel mechanism for the inhibition of Mtb growth during infection.

Chapter 2: Materials and Methods

2.1 Chemicals and reagents

ATP, CoA, NADH, cholesterol (>99%), 5α-cholestane, 8-Br-cAMP, resazurin, pyruvate kinase, lactate dehydrogenase, and adenylate kinase, were purchased from Sigma-Aldrich. Restriction enzymes were purchased from Thermo Fisher Scientific Inc. T7 DNA Ligase and Gibson assembly® master mix were purchased from New England Biolabs. Oligonucleotides were ordered from Integrated DNA Technologies. Water for buffers was purified using a Barnstead Nanopure Diamond^{TM} system to a resistivity of at least 18 MΩ. Reagents were of HPLC or analytical grade

2.2 Bacterial strains and growth

2.2.1 Bacterial strains and plasmids used in this study

The bacterial strains used in this study are provided in Table 2.1. Plasmids used int his study are provided in Table 2.2.

Table 2.1 Bacterial strains used in this study

Species	Strain	Modification	Plasmid(s)	Antibiotic resistance	Reference
M. tuberculosis	Erdman	-	-	-	
M. tuberculosis	Erdman	-	PJV53	Kan	
M. tuberculosis	Erdman	Δ*ipdAB*	PJV53	Kan, Hyg	This study
M. tuberculosis	Erdman	Δ*ipdC*	PJV53	Kan, Hyg	This study
M. tuberculosis	Erdman	Δ*kshA*	PJV53	Kan, Hyg	This study
M. tuberculosis	Erdman	Δ*fadD3*	PJV53	Kan, Hyg	This study
M. tuberculosis	Erdman	Δ*mtpat*	PJV53	Kan, Hyg	This study
M. tuberculosis	Erdman	Δ*rv1151c*	PJV53	Kan, Hyg	This study
M. tuberculosis	Erdman	Δ*ipdAB*	PJV53, pMVipdAB	Kan, Hyg, Apr	This study
M. tuberculosis	Erdman	Δ*ipdC*	PJV53, pMV3550-3553	Kan, Hyg, Apr	This study
M. tuberculosis	Erdman	Δ*kshA*	PJV53, pMVkshA	Kan, Hyg, Apr	This study
M. tuberculosis	CDC1551	-	-	-	
M. tuberculosis	CDC1551	Tn*rv1625c*	-	Kan	
M. smegmatis	MC^{2}155	-	-	-	
M. smegmatis	MC^{2}155	-	pJV53	Kan	
M. smegmatis	MC^{2}155	Δ*ipdAB*	pJV53	Kan, Hyg	(89)
M. smegmatis	MC^{2}155	Δ*ipdAB*	PJV53,	Kan, Hyg, Apr	(89)

			pMVipdAB		
M. smegmatis	MC^2155	Δ*ipdF*	pJV53	Kan, Hyg	(89)
M. smegmatis	MC^2155	Δ*echA20*	pJV53	Kan, Hyg	(89)
M. smegmatis	MC^2155	Δ*fadE32*	pJV53	Kan, Hyg	(89)
M. smegmatis	MC^2155	Δ*ipdAB*	pKWcoaA	Hyg	This study
M. smegmatis	MC^2155	-	pKWcoaA	Hyg	This study
M. smegmatis	MC^2155	Δ*ipdAB*	pKWcoaX	Hyg	This study
M. smegmatis	MC^2155	-	pKWcoaX	Hyg	This study
R. jostii	RHA1	-	-	-	
R. jostii	RHA1	Δ*couO*	-	-	(185)
R. jostii	RHA1	Δ*couL*	-	-	(185)
R. jostii	RHA1	-	pTip1625c	Cam	This study
R. jostii	RHA1	-	pTipQC2	Cam	

Kan, kanamycin; Hyg, hygromycin; Apr, apramycin; Cam, chloramphenicol

Table 2.2 Plasmids used in this study

Name	Description	Reference
pYUB854	Plasmid for generating recombineering constructs. Hyg^R	(186)
pKOipdAB	Upstream and downstream regions of *rv3551* cloned on either side of the Hyg^R cassette in pYUB854 for the deletion of *rv3551* in Mtb. Hyg^R	This study
pKOipdC	Upstream and downstream regions of *rv3553* cloned on either side of the Hyg^R cassette in pYUB854 for the deletion of *rv3553* in Mtb. Hyg^R	This study
pKOkshA	Upstream and downstream regions of *rv3526* cloned on either side of the Hyg^R cassette in pYUB854 for the deletion of *rv3526* in Mtb. Hyg^R	This study
pKOfadD3	Upstream and downstream regions of *rv3561* cloned on either side of the Hyg^R cassette in pYUB854 for the deletion of *rv3561* in Mtb. Hyg^R	This study
pKO0998	Upstream and downstream regions of *rv0998* cloned on either side of the Hyg^R cassette in pYUB854 for the deletion of *rv0998* in Mtb. Hyg^R	This study
pKO1151	Upstream and downstream regions of *rv1151* cloned on either side of the Hyg^R cassette in pYUB854 for the deletion of *rv1151* in Mtb. Hyg^R	This study
pJV53	Plasmid for recombineering in Mtb, Kan^R	(186)
pMV361.apr	pMV361 modified to contain Apr^R	(187)
pMV361ipdAB	*Rv3551* cloned into pMV361.apr, $P_{hsp60,}$ Apr^R	This study
pMV361rv3550-3553	*Rv3551-3553* cloned into pMV361.apr, $P_{hsp60,}$ Apr^R	This study
pMV361kshA	*Rv3526* cloned into pMV361.apr, $P_{hsp60,}$ Apr^R	This study
pET41b(+)	Expression vector for *E. coli*, Kan^R, IPTG-inducible promoter	Novagen
pETFD3	*Rv3561* cloned into pET41b(+) with an N-terminal His-tag and a TEV^{Pro} site, Kan^R, IPTG-inducible promoter	(136)
pET5458	MSMEG_5458 cloned into pET41b(+) with an N-terminal His-tag and a TEV^{Pro} site, Kan^R, IPTG-inducible promoter	This study
pET1151c	*Rv1151c* cloned into pET28a with an N-terminal His-tag with a thrombin site, Kan^R, IPTG-inducible promoter	(149)
pETCoaA		This study
pTipQC2	Plasmid for gene expression in *R. jostii* RHA1, Thiostrepton-inducible promoter, Cam^R, Amp^R	(188)
pTip1625c	*Rv1625c* cloned into pTipQC2 with a C-terminal His-tag, Cam^R, Amp^R	This study
pKWCoaA	*Rv1092c* was cloned into pKW08-Lx under the control of the Tetracycline-inducible promoter, replacing the luciferase gene. Hyg^R	This study
pKWCoaX	*Rv1092c* was cloned into pKW08-Lx under the control of the Tetracycline-inducible promoter, replacing the luciferase gene. Hyg^R	This study

Kan, kanamycin; Hyg, hygromycin; Apr, apramycin; Cam, chloramphenicol

2.2.2 Mtb strains

Mtb strains were cultured in 7H9 medium supplemented with either 0.05% tween-80 or 0.5% tyloxapol and various added carbon sources. Strains were incubated at 37°C in roller bottles. Growth was measured by OD_{600} or by CFU/ml. Briefly, cells were serially diluted in saline containing 0.05% tween-80 and plated on 7H10 agar containing OADC and 0.2% glycerol. Mutant and complemented strains were grown in antibiotics as appropriate at the following concentrations: 50 μg/ml hygromycin, 30 μg/ml apramycin, and 20 μg/ml kanamycin.

2.2.3 *M. smegmatis* strains

M. smegmatis strains were cultured in 7H9 medium supplemented with either 0.05% tween-80 or 0.5% tyloxapol and various added carbon sources. Strains were incubated at 37°C in flasks shaking at 200 rpm. Growth was measured by OD_{600}. Mutant and complemented strains were grown in antibiotics as appropriate at the following concentrations: 50 μg/ml hygromycin, 30 μg/ml apramycin, and 20 μg/ml kanamycin. To prepare samples of LC-MS/MS analysis, *M. smegmatis* strains were grown in 7H9 containing 0.2% glycerol and 0.05% tween-80 to an OD_{600} of ~1. All strains were normalized to the same OD_{600} and then 1 ml of culture was filtered onto a 0.2 μm membrane and metabolites were extracted as described previously (189). To induce toxicity, strains were grown in 7H9 medium containing 0.2% glycerol and 0.05% tween-80 until mid-log phase. Cultures were then diluted 1:1 with 7H9 medium containing 1 mM cholesterol and 1.0% tyloxapol to give a final concentration of 0.5 mM cholesterol and 0.5% tyloxapol.

2.2.4 *R. jostii* RHA1 strains

RHA1 strains were cultured at 30°C in M9 minimal medium shaking at 200 rpm as described previously (136). Growth was measured by OD_{600}. Expression from pTipQC2-based plasmids was induced using 10 μg/ml thiostrepton. To induce toxicity, strains were grown in M9

minimal medium containing 10 mM acetate or 6.5 mM propionate to mid-log phase at which point 3 mM *p*-coumarate was added to the cultures. For strains harboring pTip1625c and pTipQC2, chloramphenicol was included in the medium at 34 μg/ml chloramphenicol.

2.2.5 *E. coli* strains

E. coli strains were cultured at 37°C shaking at 200 rpm in lysogeny broth (LB) containing the appropriate antibiotics at the following concentrations: 150 μg/ml hygromycin, 50 μg/ml kanamycin, 30 μg/ml apramycin, 20 μg/ml chloramphenicol, and 0.5 mg/ml L-arabinose.

2.3 DNA manipulation and plasmid construction

DNA was propagated, digested, and ligated using standard protocols (190). Genes were amplified using the primers and template genomic DNA listed in Table 2.2. Amplicons were digested with the enzymes indicated in the descriptions of the oligonucleotides. The nucleotide sequence of all constructs was verified prior to their use.

2.3.1 Oligonucleotides

Oligonucleotides were purchased from Integrated DNA Technologies (San Diego, CA) through the Nucleic Acid Protein Service Unit (NAPS) at the University of British Columbia. A list of oligonucleotides used to construct plasmids used in this thesis is provided in Table 2.2.

Table 2.2 Oligonucleotides used in this study

Name	Description	Sequence
Rv3551up-F	For deletion of *rv3551-3552* to generate *Mtb ΔipdAB*. *Afl*II site added at 5'; in combination with the Rv3551up-R primer, generates an amplicon upstream of *rv3551* with *Afl*II and *Xba*I ends	TGTCTTAAGTAGGTAGCGAA CCCGCAGGAGTGC
Rv3551up-R	Deletion of *rv3551-3552* to generate *Mtb ΔipdAB. Xba*I site added at 5'; in combination with the Rv3551up-F primer, generates an amplicon upstream of *rv3551* with *Afl*II and *Xba*I ends	GATCTAGAGGTTCGTTTATC GGGCACTATGACTTC
Rv3551down-F	Deletion of *rv3551-3552* to generate *Mtb ΔipdAB*. *Xho*I site added at 5'; in combination with the Rv3551down-R primer, generates an amplicon downstream of *rv3552* with *Xho*I and *Bgl*II ends	CCTCTCGAGCACCGACGAC GAACTGCACCTG
Rv3551down-R	Deletion of *rv3551-3552* to generate *Mtb ΔipdAB*. *Bgl*II site added at 5'; in combination with the Rv3551down-F primer, generates an amplicon downstream of *rv3552* with *Xho*I and *Bgl*II ends	GTAGATCTCGGCAACAGCA GCGTGGTGG
Rv3553up-F	Deletion of *rv3553* to generate *Mtb ΔipdC*. *Afl*II site added at 5'; in combination with the Rv3553up-R primer, generates an amplicon upstream of *rv3553* with *Afl*II and *Xba*I ends	TTACTTAAGGAGGCTCAGCT GCTCGCGGACAC
Rv3553up-R	Deletion of *rv3553* to generate *Mtb ΔipdC*. *Xba*I site added at 5'; in combination with the Rv3553up-F primer, generates an amplicon upstream of *rv3553* with *Afl*II and *Xba*I ends	GGTCTAGATCTGCACCACCG GGTGCTCGATG
Rv3553down-F	Deletion of *rv3553* to generate *Mtb ΔipdC*. *Nhe*I site added at 5'; in combination with the Rv3553down-R primer, generates an amplicon downstream of *rv3553* with *Nhe*I and *Bgl*II ends	ACTGCTAGCGCATTCTTGAC GACCTACCGTCGTG
Rv3553down-R	Deletion of *rv3553* to generate *Mtb ΔipdC*. *Bgl*II site added at 5'; in combination with the Rv3553down-F primer, generates an amplicon downstream of *rv3553* with *Xho*I and *Bgl*II ends.	GTAGATCTCAGGGTCATCAT CACCAGCGTCTCG
pMV361ipdAB-F	Amplification of *rv3551-3552* for complementation of *Mtb* Δ*ipdAB*. *Eco*RI and ribosome binding site (RBS) added to 5'. Adds stop codon TAA in front of the RBS to stop the potential expression of the fusion protein from pMV361.	ACGGAATTCTAAAAGGAGA TCACTCATGCCCGATAAACG AACCGCTCTTG
pMV361ipdAB-R	Amplification of *rv3551-3552* for complementation of *Mtb* Δ*ipdAB*. *Hin*dIII cut site added at 5'. In combination with pMV361ipdAB-F primer, generates an amplicon from *rv3551* to 62 bp downstream of *rv3552* with *Eco*RI and *Hin*dIII ends.	TTTAAGCTTCTTGCAGGGGA CGAAGCGATG
pMV361rv3550-3553-F	Amplification of *rv3550-3553* for complementation of *Mtb* Δ*ipdC*. *Eco*RI and ribosome binding site (RBS) added to 5'. Adds stop codon TAA in front of the RBS to stop the potential expression of the fusion protein from pMV361.	ACGGAATTCTAAAAGGAGA TCACTCATGCCGATCACCTC CA
pMV361rv3550-3553-R	Amplification of *rv3550-3553* for complementation of *Mtb* Δ*ipdC*. *Hin*dIII cut site added at 5'. In combination with pMV361rv3550-3553-F primer, generates an amplicon from *rv3550* to 181 bp downstream of *rv3553* with *Eco*RI and *Hin*dIII ends.	TTTAAGCTTGTCGTAGAACC GACGA
Rv3526up-F	For deletion of *rv3526* to generate *Mtb ΔkshA*. *Nco*I site added at 5'; in combination with the Rv3526up-R primer, generates an amplicon upstream of *rv3526* with *Nco*I and *Spe*I ends	CATGCCATGGTCTGGAATGC CGAGGTAGAGAAG
Rv3526up-R	For deletion of *rv3526* to generate *Mtb ΔkshA*. *Spe*I site added at 5'; in combination with the Rv3526up-F primer, generates an amplicon upstream of *rv3526* with *Nco*I and *Spe*I ends	GGACTAGTGAGGCTTCATA GGAAGCTCAGTCC
Rv3526down-F	For deletion of *rv3526* to generate *Mtb ΔkshA*. *Kpn*I site added at 5'; in combination with the Rv3526down-R primer, generates an amplicon downstream of *rv3526* with *Kpn*I and *Xba*I ends	GGGGTACCCAATCGGTCCCT TCACCTTG
Rv3526down-R	For deletion of *rv3526* to generate *Mtb ΔkshA*. *Xba*I site added at 5'; in combination with the Rv3526down-F primer, generates an amplicon downstream of *rv3526* with *Kpn*I and *Xba*I ends	GCTCTAGAGCTTCCCTTCCA AATAGTCCTTCG
pMV361kshA-F	Amplification of *rv3526* for complementation of *Mtb* Δ*kshA*. *Eco*RI and ribosome binding site (RBS) added to 5'. Adds stop codon TAA in front of the RBS to stop the potential expression of the fusion protein from pMV361.	ACGGAATTCTAAAAGGAGA TCACTCGTGAGTACCGACAC GAGTGG
pMV361kshA-R	Amplification of *rv3526* for complementation of *Mtb* Δ*kshA*. *Hin*dIII cut site added at 5'. In combination with pMV361kshA-F primer, generates an amplicon from *rv3526* to 80 bp downstream of *rv3526* with *Eco*RI and *Hin*dIII ends	TTTAAGCTTGATGATCACCG TGCAGCAGTAG
Rv0998up-F	For deletion of *rv0998* to generation *Mtb* Δ*mtpat*. *Hin*dIII cut site added at the 5'. In combination with Rv0998up-R primer, generates an amplicon upstream of *rv0998*.	AAAGCTTCACGTGGTCGAC GGATCCGTTGGTAGCGCGA CTCGTTCGC
Rv0998up-R	For deletion of *rv0998* to generation *Mtb* Δ*mtpat*. In combination with Rv0998up-F primer, generates an amplicon upstream of *rv0998*.	CGCCAATGACACCAGACCC TCG

Rv0998down-F	For deletion of *rv0998* to generation *Mtb* Δ*mtpat*. In combination with Rv0998down-R primer, generates an amplicon downstream of *rv0998*.	CGAGGGTCTGGTGTCATTGG CGACCATGATCGATGTGCCG GGTC
Rv0998down-R	For deletion of *rv0998* to generation *Mtb* Δ*mtpat*. In combination with Rv0998down-F primer, generates an amplicon downstream of *rv0998*.	TGACACTATAGAATACATA GGATCCGCGTCAGATGTAC GACCGGGTG
Rv3561up-F	For deletion of *rv3561* to generation *Mtb* Δ*fadD3*. *Pst*I site added at 5'; in combination with the Rv3561up-R primer, generates an amplicon upstream of *rv3561* with *Nco*I and *Spe*I ends	TGTCTGCAGTAGCCGCTGCC ACTCGTCGAAC
Rv3561up-R	For deletion of *rv3561* to generate *Mtb Δ*fadD3*. Xba*I site added at 5'; in combination with the Rv3561down-F primer, generates an amplicon downstream of *rv3561* with *Pst*I and *Hin*dIII ends	GGAAGCTTCAGCTCGGTCG ACGTGAAACGC
Rv3561down-F	For deletion of *rv3561* to generate *Mtb Δ fadD3*. *Hin*dIII site added at 5'; in combination with the Rv3561down-R primer, generates an amplicon downstream of *rv3561* with *Hin*dIII and *Kpn*I ends	TCTAAGCTTTCGGTGCGGTT CGTCGACGTAC
Rv3561down-R	For deletion of *rv3561* to generate *Mtb Δ fadD3*. *Kpn*I site added at 5'; in combination with the Rv3561down-F primer, generates an amplicon downstream of *rv3561* with *Hin*dIII and *Kpn*I ends	TTTGGTACCCAGGTTGGCCA ACTGCTGCCAC
Rv1151up-F	For deletion of *rv1151c* to generation *Mtb* Δ *rv1151c*. *Hin*dIII site added at 5'; in combination with the Rv1151up-R primer, generates an amplicon upstream of *rv1151c*.	GTGATAAACTACCGCATTAA AGCTTCAACCTGCGCACGCT GGCTAAG
Rv1151up-R	For deletion of *rv1151c* to generate *Mtb Δ rv1151c*. In combination with the Rv1151up-F primer, generates an amplicon upstream of *rv1151c*.	GTCGAATCGGGCCCACAAT CC
Rv1151down-F	For deletion of *rv1151c* to generate *Mtb Δrv1151c*. In combination with the Rv1151down-R primer, generates an amplicon downstream of *rv1151c*	GGATTGTGGGCCCGATTCGA CAATCCCGAGCCCACGCCGT TG
Rv1151down-R	For deletion of *rv1151c* to generate *Mtb Δrv1151c*. *Hin*dIII site added at 5'; in combination with the Rv1151down-F primer, generates an amplicon downstream of *rv1151c*.	CTCACTATAGGGAGACCGG AAGCTTGCGTGTCCGACCTC ATGCCTC
MSMEG5458-F	Amplification of *MSMEG5458* to generate pET5458. *Nde*I site added at 5'; in combination with MSMG5458-R generates amplicon for cloning into pET41b with N terminal His tag and a TEV cleavage site.	GCTGAACCATATGGCTACTA GTCATCACCATCACCATCAC GGCAGCTCTGAGAACCTGT ACTTCCAGTCGGCGGAACTG ACCGAG
MSMEG5458-R	Amplification of *MSMEG5458* to generate pET5458. *Eco*RI cut site added at 5'; in combination with MSMG5458-R generates amplicon for cloning into pET41b with N terminal His tag and a TEV cleavage site.	GGAATTCGTCTGCATCTCGC TG
Rv1625c-F	Amplification of *rv1625c* to generate pTip1625c. *Nde*I site added at 5'; in combination with the Rv1625c-R primer, generates an amplicon of *rv1625c* with *Nde*I and *Eco*RI ends	GCTGAACCATATGGCGGCA AGAAAATGCGGC
Rv1625c-R	Amplification of *rv1625c* to generate pTip1625c. *Eco*RI site added at 3'; in combination with the Rv1625c-F primer, generates an amplicon of *rv1625c* with *Nde*I and *Eco*RI ends.	GGAATTCGTGATGGTGATG GTGATGACTAGTAGCGACC CCTGCCGTGCGGGGTTCGAC CCCTGCCGTGCGGGG
pKWRv1092c-F	Amplification of *rv1092c* to generate pKWCoaA	CGCGGATCCGGAGGAAATG TTATGTCGCGGCTTAGCGAG CC
pKWRv1092c-R	Amplification of *rv1092c* to generate pKWCoaA	CCCAAGCTTTTACAGCTTGC GCAGCCGCA
pKWRv3600c-F	Amplification of *rv1092c* to generate pKWCoaX	TCATCGTGGAATCCTGACAG GATCCGGAGGAAATGTTGT GCTGCTGGCGATTGAC
pKWRv3600c-R	Amplification of *rv1092c* to generate pKWCoaX	CCAATTAATTAGCTAAAGCT TTCAGCGCGCCGTCTTGAG

2.3.2 Gene knockout constructs

Mtb genes were deleted using homologous recombination (186). Allelic exchange substrate (AES) constructs were generated using the oligonucleotides listed in Table 2.2 to amplify the up- and downstream regions of the genes to be deleted and cloning them on either side of the

hyg^{R} cassette in pYUB854. The linearized AES was electroporated into Mtb harboring pJV53. Hygromycin resistant colonies were screened for the absence of the gene of interest and the presence of the *hyg*^{R} cassette by PCR. The orientation of the cassette within the genome was determined using screening primers that anneal outside the AES.

2.4 Thin layer chromatography

WT and mutant strains of Mtb were grown in 7H9 medium supplemented with 0.05% tween-80 and 0.2% glycerol at 37°C in roller bottles. After 7 days, cells were harvested by centrifugation at 4000 x g for 15 min at room temperature. Cell pellets were washed 1x with dH_2O before they were autoclaved for removal from containment level 3. Autoclaved pellets were resuspended in 5 ml dH_2O and lyophilized. Dried material was weighed out and 1.6 ml methanol:0.3% NaCl (100:1) and 800 µl petroleum ether was added to 30 mg in a glass screw cap tube. Samples were rotated for 15 min, and the upper organic layer was collected. The bottom layer was extracted again with 800 µl petroleum ether. The combined organic layer was dried under nitrogen and then suspended in 150 µl dichloromethane. Two dimensional TLC was done with petroleum ether:ethyl acetate (98:2) in the first dimension three times, and once in the second dimension using petroleum ether:acetone (98:2). TLC plates were soaked in 5% phosphomolybdic acid hydrate (in 100% ethanol) and placed in an oven at 100°C.

2.5 Macrophage infections

THP-1 cells (American Type Culture Collection, TIB-202), were cultured in GIBCO® RPMI 1640 (Thermo Fisher Scientific) supplemented with 10% fetal bovine serum, 2 mM L-glutamine, and 1 mM sodium pyruvate and were maintained between 2 and 5 x 10^5 cells ml^{-1}. *Mtb* strains were

grown to late log phase in Middlebrook 7H9 supplemented with OADC, aliquots were frozen at -80°C, and CFU ml^{-1} was enumerated. THP-1 cells were seeded in 24-well flat-bottom tissue culture plates and allowed to adhere in the presence of 50 ng ml^{-1} PMA for 48 hours at 37°C in a humidified, 5% CO_2 atmosphere. Cells were washed to remove PMA and incubated for a further 48 hours prior to infection. Bacteria were added to THP-1 cells at a multiplicity of infection (MOI) of 1:1 for 6 hours. Cells were washed three times to remove extracellular bacteria and were then incubated for 7 days. At each time point, THP-1 cells were washed 2x with fresh RPMI to remove extracellular bacteria and were then lysed by adding 0.06% SDS. Bacteria were then serially diluted in saline containing 0.05% tween-80, and plated on Middlebrook 7H10 with OADC for enumeration.

2.6 Inhibitor studies

2.6.1 Determination of MIC

WT and mutant Mtb Erdman and CDC1551 were grown in 7H9 medium containing 0.5% tyloxapol supplemented with various carbon sources in 150 µl in 96-well plates at 37°C with increasing concentrations of GSK286A or DMSO alone, with each concentration in triplicate. Strains were incubated for 5-7 days. For WT Mtb Erdman harboring pCherry3, growth was measured by fluorescence at 570 nm excitation and 620 nm emission. For WT Mtb CDC1551 and mutant strains, growth was measured by adding 50 µM resazurin, incubating for 24 hours at 37°C, and measuring fluorescence at 530 nm excitation and 590 nm emission. Data were analyzed by GraphPad Prism to generate a non-linear regression model to fit the normalized results of the dose response curves and IC50.

2.6.2 Analysis of cAMP

For WT Mtb Erdman, WT Mtb CDC1551, and Tn*1625c* Mtb CDC1551, strains were grown in 200 ml 7H9 medium containing 0.5 mM cholesterol to an OD_{600} of 0.4. GSK286A was added at a concentration of 5 μM and strains were incubated for 16 h at 37°C. Cells were harvested by centrifugation at 4000 x *g* for 10 min at room temperature, suspended in 4 ml acetonitrile:methanol:water (2:2:1 v:v:v). 1.5 μM 8-Br-cAMP was added to samples to be analyzed by LC-MS. Cells were lysed by bead beating (3 cycles at 6 m/s for 30 seconds each with 5 min on ice between each run). Lysates were cleared by centrifugation at 16,000 x *g* for 10 min at 4°C. Samples were filtered through a 0.2 μm filter and removed from containment level 3 and then dried under nitrogen. For LC-MS analysis the dried extracts were suspended in 100 mM ammonium acetate pH 4.5. Samples were analyzed on an Agilent 6460 Triple Quadrupole LC-MS operated in positive ion mode at the Proteomics Core Facility at the University of British Columbia, connected to an 80 x 0.25 mm Luna 3 μm PFP(2) analytical column (prepared in house). For HPLC analysis samples were suspended in 100 mM ammonium acetate pH 4.5. Samples were analyzed using a Waters 2695 Separations HPLC module (Milford, MA) equipped with a Waters 2996 photodiode array detector and a Luna 3 μm PFP(2) 50 × 4.6 mm column (Phenomenex, Torrance, CA). The column was equilibrated with 0.1 M ammonium acetate, pH 4.5. CoA thioesters were eluted using a 20 min linear gradient of 0 to 90% methanol in 0.1 M ammonium acetate, pH 4.5. The eluate was monitored at 258 nm.

2.7 Protein production and purification

2.7.1 Production and purification of FadD3

FadD3 was purified as described previously (136). Briefly, *fadD3* (*rv3561*) from Mtb was cloned into pET41b(+) and transformed into *E. coli* BL21(DE3). The strain was grown in LB at 37°C shaking at 200 rpm to an OD_{600} of 0.6 and induced with 0.5 mM IPTG. Following induction, cultures were incubated at 16°C for 20 h and were then harvested by centrifugation at 4°C at 4000 x *g* for 10 min. Pellets were suspended in 10 mM sodium phosphate, pH 8.0 containing 10% glycerol, 50 mg/ml DNase I and the Complete Mini Protease Inhibitor cocktail (Roche, Laval, QC). Cells were subjected to five rounds of 25 s bead beating using a MP Biomedicals FastPrep-24 bead beater (Solon, OH) set to 5.0 with 5 min incubation on ice between rounds. Cell debris was removed by centrifugation at 17,000 x *g* for 20 min at 4°C and the supernatant was further clarified by ultracentrifugation at 255 000 x *g* for 2 h at 4°C. The cytoplasmic extract was recovered, supplemented with 10 mM imidazole and loaded onto 5 ml Ni-Sepharose 6 Fast Flow resin (GE Healthcare). The tagged protein was eluted in 20 mM sodium phosphate, pH 8.0 containing 50 mM NaCl and 500 mM imidazole. The recovered protein was dialyzed overnight at 4°C against 2 L of 25 mM HEPES, pH7.5, 50 mM KCl, then digested with TEV^{pro}. Briefly, 50 mg of polyHis-tagged FadD3 was incubated at 22°C for 22 h in presence of 1 mg TEV^{pro} in a total volume of 10 ml containing 50 mM Tris-HCl, pH 8.0, 0.5 mM EDTA and 1 mM DTT. Cleaved FadD3 was separated from cleaved tag and the TEV^{pro} by passing the mixture on a 0.4 ml Ni-Sepharose column equilibrated with 20 mM sodium phosphate, pH 8.0, 300 mM NaCl, 10 mM imidazole. The protein was recovered in the flow-through and dialyzed overnight at 4°C against 2 L of 25 mM HEPES, pH 7.5, 50 mM KCl. Protein was concentrated at 4°C by centrifugation in an Ultracel 10 K (EMD Millipore) and flash-frozen as beads in liquid nitrogen and stored at -80°C.

2.7.2 Production and purification of MsPat

The gene encoding MsPat (MSMEG_5458) from *M. smegmatis* was cloned into pET41b(+) and transformed into *E. coli* BL21(DE3). The strain was grown in LB containing 50 µg/ml kanamycin at 37°C shaking at 200 rpm to an OD_{600} of 0.6 and induced with 0.5 mM IPTG. Following induction, cultures were incubated at 30°C for 20 h and were then harvested by centrifugation at 4°C at 4000 x *g* for 10 min. Pellets were suspended in 10 mM sodium phosphate, pH 8.0 containing 10% glycerol, 50 mg/ml DNase I and the Complete Mini Protease Inhibitor cocktail (Roche, Laval, QC). Cells were subjected to five rounds of 25 s bead beating using a MP Biomedicals FastPrep-24 bead beater (Solon, OH) set to 5.0 with 5 min incubation on ice between rounds. Cell debris was removed by centrifugation at 17,000 x *g* for 20 min at 4°C and the supernatant was further clarified by ultracentrifugation at 255 000 x *g* for 2 h at 4°C. The cytoplasmic extract was recovered, supplemented with 10 mM imidazole and loaded onto 5 ml Ni-Sepharose 6 Fast Flow resin (GE Healthcare). The tagged protein was eluted in 20 mM sodium phosphate, pH 8.0 containing 50 mM NaCl and 500 mM imidazole. The recovered protein was dialyzed overnight at 4°C against 2 L of 25 mM HEPES, pH7.5, 50 mM KCl, then digested with TEV^{pro}. Briefly, 50 mg of polyHis-tagged MsPat was incubated at 22°C for 22 h in presence of 1 mg TEV^{pro} in a total volume of 10 ml containing 50 mM Tris-HCl, pH 8.0, 0.5 mM EDTA and 1 mM DTT. Cleaved MsPat was separated from cleaved tag and the TEV^{pro} by passing the mixture on a 0.4 ml Ni-Sepharose column equilibrated with 20 mM sodium phosphate, pH 8.0, 300 mM NaCl, 10 mM imidazole. The protein was recovered in the flow-through and dialyzed overnight at 4°C against 2 L of 50 mM Tris-HCl, pH 7.5, 150 mM NaCl, 10% glycerol. Protein was concentrated at 4°C by centrifugation in an Ultracel 10 K (EMD Millipore) and flash-frozen as beads in liquid nitrogen and stored at -80°C.

2.7.3 Production and purification of Rv1151c

The gene encoding Rv1151c (*rv1151c*) from Mtb was cloned into pET41b(+) and transformed into *E. coli* BL21(DE3) along with pGro7 (Takara Bio Inc.). The strain was grown in LB containing 50 μg/ml kanamycin, 20 μg/ml chloramphenicol, and 0.5 mg/ml L-arabinose at 37°C shaking at 200 rpm to an OD_{600} of 0.6 and induced with 0.5 mM IPTG. Following induction, cultures were incubated at 30°C for 20 h and were then harvested by centrifugation at 4°C at 4000 x *g* for 10 min. Pellets were suspended in 10 mM sodium phosphate, pH 8.0 containing 10% glycerol, 50 mg/ml DNase I and the Complete Mini Protease Inhibitor cocktail (Roche, Laval, QC). Cells were subjected to five rounds of 25 s bead beating using a MP Biomedicals FastPrep-24 bead beater (Solon, OH) set to 5.0 with 5 min incubation on ice between rounds. Cell debris was removed by centrifugation at 17,000 x *g* for 20 min at 4°C and the supernatant was further clarified by ultracentrifugation at 255 000 x *g* for 2 h at 4°C. The cytoplasmic extract was recovered, supplemented with 10 mM imidazole and loaded onto 5 ml Ni-Sepharose 6 Fast Flow resin (GE Healthcare). The tagged protein was eluted in 20 mM sodium phosphate, pH 8.0 containing 50 mM NaCl and 500 mM imidazole. The recovered protein was dialyzed overnight at 4°C against 2 L of 50 mM HEPES, pH 7.5, 150 mM NaCl, 10% glycerol. Protein was concentrated at 4°C by centrifugation in an Ultracel 10 K (EMD Millipore) and flash-frozen as beads in liquid nitrogen and stored at -80°C.

2.8 Enzymatic activity assays

2.8.1 FadD3 coupled activity assay

The activity of FadD3 was measured as described previously (136). a spectrophotometric assay that couples AMP formation to NADH oxidation was used. Reactions were performed in a

total volume of 0.25 ml of 0.1 M HEPES, pH 7.3 containing 1 mM CoASH, 2 mM ATP, 2 mM PEP, 5 units pyruvate kinase, 5 units adenylate kinase, 20 units lactate dehydrogenase, 100 mM NADH, 5 mM $MgCl_2$ and 25 μM HIP. The mixture was incubated 5 min at 22°C and the reaction was initiated by adding 10 nM FadD3. Initial velocity was recorded at 340 nm over 1 min.

2.8.2 FadD3 HPLC activity assay

Reactions were performed in 0.25 ml of 0.1 M HEPES, pH 7.3 containing 5 mM $MgCl_2$, 2 mM ATP, 1 mM CoASH, 2 μM FadD3 and 1 mM HIP. Reactions also contained 1 mM cAMP, 100 μM acetyl-CoA, with or without 0.5 μM MtPat. Reaction mixtures were incubated for 1 h at 22°C, then stopped by adding an equal volume of methanol and incubated on ice for 10 min. Methanol was evaporated at room temperature under low pressure and the mixture was centrifuged (16,000 x *g* 10 min, 4°C). The supernatant was recovered, passed through a 0.2 mm filter and stored on ice. Reaction products were analysed using a Waters 2695 Separations HPLC module (Milford, MA) equipped with a Waters 2996 photodiode array detector and a Luna 3 mm PFP(2) 50 x 4.6 mm column (Phenomenex), using a linear gradient of 0 to 90% methanol in 0.1 M ammonium acetate, pH 4.5 over 20 min at 1 ml/min. The eluate was monitored at 258 nm.

2.8.3 Acetylation of FadD3 by MsPat

Reactions were typically performed in 25 μl of 50 mM HEPES, pH 7.5 containing 150 mM NaCl, 1 mM cAMP, 100 μM acetyl-CoA, 40 μM FadD3, and 20 μM MtPat. Reactions were incubated at 37°C. At several timepoints, 10 nM of FadD3 was used to measure activity using the spectrophotometric assay described above.

2.8.4 Trypsin digest and mass spectrometry analysis of acetylated FadD3

The protein was trypsin-digested and subjected to nanoscale liquid chromatography on a C18 column eluted with water:acetonitrile:formic acid gradients. The eluant was sent to the nano-

electrospray ionization source of an LC-MS/MS Q-ToF mass spectrometer operated in positive ion mode. The MS was scanned over an *m*/*z* range of 360-2000 amu. To determine the amino acid sequence, the MS was operated in an information-dependent acquisition MS/MS mode. A survey scan was first done from 300 to 1500 *m*/*z*. The three most intense doubly or triply charged ions were selected for MS/MS fragmentation in scans from 50 to 2000 *m*/*z*. Raw data were extracted using the Mascot.dll script in the Analyst control software, and searched on a local server harboring Mascot and updated UniProt databases

2.8.5 Deacetylation of FadD3 by Rv1151c

Following acetylation by MtPat (Section 2.7.3), FadD3 was incubated in 50 mM HEPES, pH 7.5 containing 150 mM NaCl, 2 mM NAD^+, 10% glycerol, and 5 μM Rv1151c for 30 minutes at 25°C.

2.8.6 Western blots

Following acetylation and deacetylation reactions, proteins were subjected to SDS-PAGE and were then transferred to a nitrocellulose membrane. Membranes were blocked for one hour in blocking buffer (Tris buffered saline with Tween-20 (TBST) and 5% w/v nonfat dry milk) and were then incubated with the primary antibody (rabbit anti-acetyl lysine #9441, Cell Signaling Technologies) diluted 1:1000 in blocking buffer at 4°C overnight. Secondary antibody (anti-rabbit IgG HRP-linked #7074, Cell Signaling Technologies) was diluted 1:2000 in TBST and used for one hour at room temperature. Membranes were incubated with 1X SignalFire™ ECL reagent (Cell Signaling Technologies) for 1 minute and were then exposed to an X-ray film and developed.

2.9 Analysis of metabolite accumulation and CoA depletion

2.9.1 Analysis of intracellular metabolite accumulation and CoA depletion by HPLC

Cells were normalized by OD_{600} and pelleted by centrifugation at 4000 x *g* for 10 minutes at 4°C. Pellets were stored at -80°C until use. Cells were suspended in 1 ml chloroform:methanol:water (2.6:1.3:1) and an internal standard (feruloyl-CoA) was added. Phases were separated by centrifugation at 4000 x *g* for 10 minutes. The upper phase containing CoA and CoA-thioesters was transferred to new tubes. The lower phase was extracted 2 more times with 400 mM ammonium acetate in 80% (vol/vol) methanol. The extracts were combined, and the methanol was evaporated under nitrogen gas. Sample volumes were normalized and were filtered through a 0.2 μm PTFE membrane. Samples were analyzed using a Waters 2695 Separations HPLC module (Milford, MA) equipped with a Waters 2996 photodiode array detector and a Luna 3 μm PFP(2) 50 × 4.6 mm column (Phenomenex, Torrance, CA). The column was equilibrated with 0.1 M ammonium acetate, pH 4.5. CoA thioesters were eluted using a 20 min linear gradient of 0 to 90% methanol in 0.1 M ammonium acetate, pH 4.5. The eluate was monitored at 258 nm.

2.9.2 Analysis of extracellular metabolite production by GC-MS

At several timepoints, 300 μl of culture supernatant was removed for metabolite extraction. The supernatant was acidified with 10 μl glacial acetic acid, and 10 μl of a 10 mM solution of 5α-cholestane was added as an internal standard. Metabolites were extracted with 300 μl ethyl acetate. Samples were vortexed, and the phases were separated by centrifugation at 16,000 x *g* for 1 minute. The upper phase was dried under nitrogen gas and then suspended in 50 μl pyridine and 50 μl bis(trimethylsilyl)-trifluoroacetamide/trimethylchlorosilane and analyzed by GC-MS on an Agilent 6890 series GC equipped with an HP-5ms 30 m x 250 μm capillary column (Hewlett-

Packard, Palo Alto, CA) and an HP 5973 mass-selective detector as described previously (136). Abundance was normalized to that of the internal standard.

2.9.3 Analysis of metabolomes by LC-MS/MS

Targeted analysis of intracellular metabolites at different timepoints was performed on an Agilent 1290 Infinity II UHPLC system (Agilent Technologies, Santa Clara, CA, USA) connected to a Bruker Impact II QTOF mass spectrometer (Bruker Daltonics, Bremen, Germany). Two columns were used for LC separation: a) Acclaim™ Polar Advantage II C18 column (3.0 × 100 mm, 3 µm, Thermo Fisher Scientific, Rockford, IL) for CoA thioester analysis and b) SeQuant ZIC-pHILIC column (2.1 × 150 mm, 5 µm, Merck KGaA, Darmstadt, Germany) for common metabolites. Both ESI positive and ESI negative modes were carried out separately using data-dependent acquisition (DDA) mode. Mobile phases used for ESI (+) were water/acetonitrile (95/5, v/v, pH = 4.8) as phase A and water/acetonitrile (5/95, v/v, pH = 4.8) as phase B, both containing 10 mM ammonium acetate as buffer. Mobile phases used for ESI (−) were water/acetonitrile (95/5, v/v, pH = 9.8) as phase A containing 10 mM ammonium acetate and water/acetonitrile (5/95, v/v, pH = 9.8) as phase B. For CoA thioester analysis, an 18-min gradient was set as follows: 0 min, 100% B; 2.5 min, 100% B; 7 min, 0% B; 10 min, 0% B; 10.01 min, 100% B; 18min, 100% B. For other metabolites, a 23-min linear gradient from 95% B to 5% B was used for elution and another 8 min at 95% B for column equilibrium. For mass spectrometer parameter setting, the capillary voltage was set at 4.5 kV for ESI (+) and 3 kV for ESI (−); the nebulizer gas was set at 1.5 bar for CoA thioester analysis and 1.0 bar for other metabolites; drying gas flow rate was 6 L/min and source temperature was 220 °C. Mass calibration was performed on sodium acetate clusters.

Raw LC-MS data was processed on Bruker Data Analysis software. All the metabolites were confirmed by accurate mass-to-charge (*m/z*) ratios and retention times compared to the

metabolite standards within the mass tolerance of 0.005 Da and retention time tolerance of 0.1 min.

Chapter 3: Results

3.1 Cholesterol catabolism in *Mtb* pathogenesis

3.1.1 Introduction

Proteins involved in cholesterol uptake and catabolism of rings A and B have been shown to be essential for virulence in infection models. More specifically, disruption of genes encoding the Mce4 transporter, which takes up cholesterol, led to a severe growth defect in mice (94). Catabolism of the cholesterol sidechain has also been implicated in pathogenesis: deletion of genes within the *igr* locus, which encode enzymes that catalyze the removal of the final propionyl-CoA from the sidechain, attenuated growth in MΦs and in mice (138). Deletion of the genes encoding the rings A and B catabolizing enzymes HsaC (95), HsaD (98, 139), FadA5 (99), and KshA (102) also lead to attenuated growth in infection models. Furthermore, in a screen to identify compounds that inhibit intracellular growth of Mtb, two hit compounds were found to specifically target the rings A and B catabolizing enzyme HsaAB (139). A strain lacking the genes encoding the rings C and D catabolizing enzyme IpdAB in the horse pathogen *R. equi* is avirulent and is patented as a live vaccine (140). While transposon mutagenesis and transcriptomic studies implicate catabolism of cholesterol rings C and D in the pathogenesis of Mtb, it has not yet been explicitly demonstrated.

Herein, we characterized the *in vitro* growth and metabolite accumulation in cholesterol catabolic mutants of Mtb. Deletion of the genes encoding the rings C and D degrading enzymes IpdAB and IpdC aided in determining the order of reactions in the pathway (89). Furthermore, we demonstrated the importance of rings C and D catabolism in THP-1 derived MΦs. Finally, we characterized the mode of action of a cholesterol-specific inhibitor that attenuates intracellular growth of Mtb.

3.1.2 *In vitro* growth phenotypes of cholesterol catabolic mutants in Mtb

The *in vitro* growth phenotypes were determined for the Δ*kshA*, Δ*fadD3*, Δ*ipdAB*, and Δ*ipdC* mutants. Strains were grown on cholesterol or glycerol and growth was measured by CFU/ml or OD_{600}. Deletion of *kshA* impaired growth on cholesterol while complementation restored growth to that of the WT strain (Fig. 3.1A). Despite the lack of growth, the mutant depleted cholesterol from the culture supernatant, though at a slower rate compare to WT Mtb Erdman. These data suggest KshA is essential for growth on cholesterol as a sole carbon source and are consistent with the findings reported by Hu *et al* (102). The inability of the Δ*kshA* mutant to grow on cholesterol was surprising given that the mutant strain should theoretically be able to derive one acetyl-CoA and two propionyl-CoA molecules from the cholesterol sidechain.

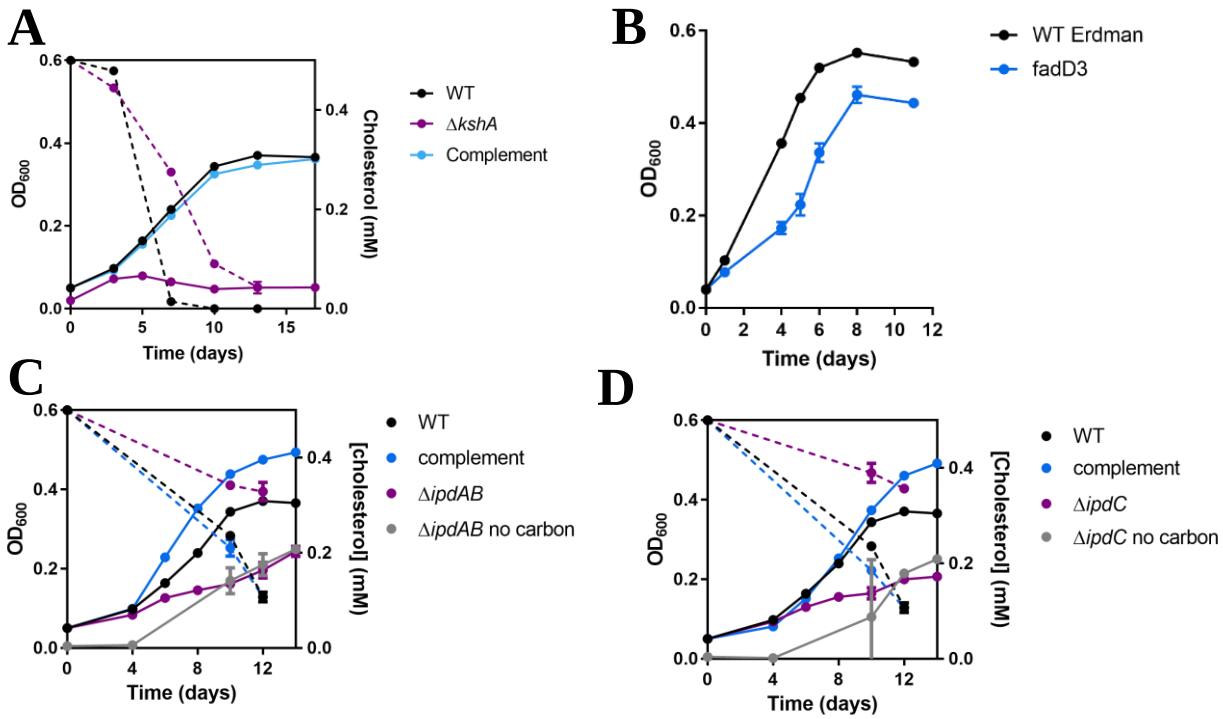

Figure 3.1 Growth of WT and mutant strains of Mtb Erdman on cholesterol. Strains were grown in roller bottles in 7H9 minimal medium supplemented with 0.5 mM cholesterol at 37°C**.** Growth and substrate depletion were monitored by OD_{600} and GC-MS, respectively. Data represent the mean of biological triplicates, error bars are the standard error of the mean.

Deletion of *fadD3* in Mtb Erdman led to growth on cholesterol that is consistent with the catabolism of the cholesterol sidechain and rings A and B (Fig. 3.1B). The Δ*fadD3* mutant should obtain one acetyl-CoA, three propionyl-CoA, and one pyruvate molecule from the catabolism of 14 of cholesterol's 27 C atoms, while WT Mtb is proposed to obtain an additional three acetyl-CoA, one propionyl-CoA, and one succinyl-CoA from the catabolism of cholesterol rings C and D (89). The mutant strain grew at a similar rate to WT Mtb Erdman on cholesterol as a sole carbon source and reached a final OD_{600} of 0.47 compared to the WT strain which reached a final OD_{600} of 0.56. These data are consistent with the deletion of *fadD3* in RHA1 (136).

Deletion of *ipdAB* and *ipdC*, both of which encode enzymes that act in the catabolism of cholesterol rings C and D, inhibited growth on cholesterol (Fig. 3.1C-D). Both mutant strains depleted significantly less cholesterol from the culture supernatant compared to WT by Day 12. The Δ*ipdAB* and Δ*ipdC* mutants should theoretically be able to derive two acetyl-CoA, three propionyl-CoA and one pyruvate from the breakdown of the cholesterol sidechain and rings A and B. Their inability to utilize cholesterol as a sole carbon source is discussed further in Section 3.3.

3.1.3 Metabolite accumulation in cholesterol catabolic mutants

The Δ*kshA* mutant depleted cholesterol and accumulated ADD in the culture supernatant by day 7 of incubation, although not in stoichiometric amounts: ~0.4 mM cholesterol was consumed and only ~0.2 mM ADD was produced based on standard curves (Fig. 3.2A). Capyk *et al* (2011) demonstrated that KshAB has higher substrate specificity for the CoA-thioesterified substrate 1,4-BNC-CoA compared to the non-thioesterified substrate ADD, which has the same core structure but with a completely degraded sidechain (130). Based on the level of ADD accumulation in the culture supernatant, we postulate that the remaining cholesterol was converted

to CoA thioesterified metabolites, such as 1,4-BNC-CoA, which would not be secreted into the culture supernatant, although analysis of intracellular metabolite accumulation is needed to confirm this hypothesis. The corresponding carboxylates of such metabolites (*e.g.*, 1,4-BNC) were not observed in the culture supernatant.

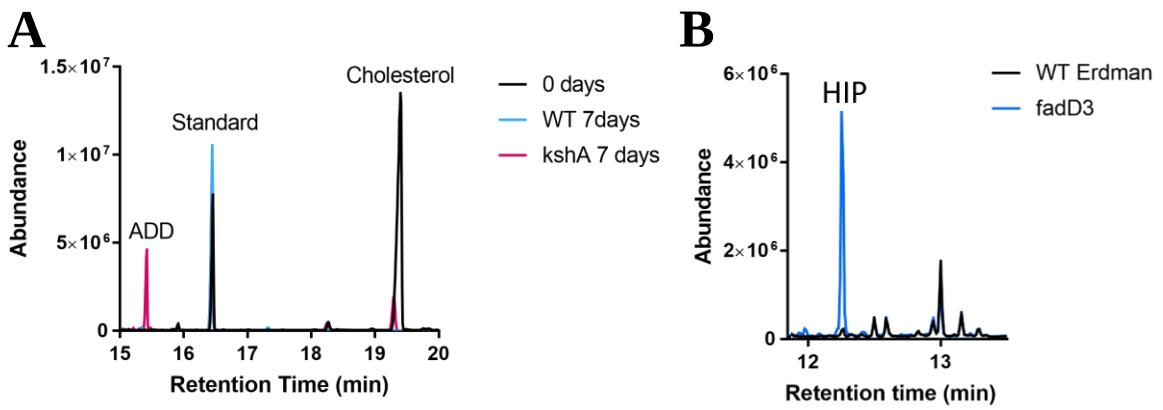

Figure 3.2 Extracellular metabolite accumulation. WT, Δ*kshA* (A), and Δ*fadD3* (B) Mtb Erdman strains were incubated in 7H9 medium supplemented with 0.5 mM cholesterol for 7 days. Metabolite accumulation in the culture supernatant was analyzed by GC-MS. Chromatograms represent the mean of biological triplicates.

The Δ*fadD3* mutant depleted cholesterol from the medium and accumulated the rings C and D-containing metabolite HIP, the substrate for FadD3, in the culture supernatant (Fig. 3.2B) (136). In contrast, no cholesterol-derived metabolites were detected in the supernatants of Δ*ipdAB* and Δ*ipdC* cultures (data not shown). We hypothesized that the failure to detect metabolites in these supernatants was due to the accumulation of intracellular, CoA thioesterified metabolites in Δ*ipdC* and Δ*ipdAB* mutants that are not readily excreted.

To test this hypothesis, we extracted metabolites from mutant and WT cells. LC-MS analysis revealed the accumulation of cholesterol-derived metabolites which were identified as CoA thioesters based on the characteristic $[M+H]^+$ -507 and 428 *m/z* fragments as described in Crowe *et al.* (2017) (89). When incubated in the presence of cholesterol, the *ipd* mutants accumulated CoA thioesters that were not detected either in the wild-type strains or in *ipd* mutants

incubated with glycerol or pyruvate. More specifically, cholesterol-incubated cells of Δ*ipdC* Mtb contained significant amounts of two CoA thioesters with *m*/*z* values of 962, one of which was more abundant than the other (Fig. 3.3A). The main CoA thioester that accumulated in cholesterol-incubated cells of Δ*ipdAB* Mtb eluted with a R_t of 22.7 min and had an *m*/*z* value of 976 (Fig. 3.3B). The metabolites were purified and their structures were determined by NMR as described in Crowe *et al* (89). The 962 *m*/*z* compounds that accumulated in the Δ*ipdC* mutant were identified as the 5α and 5β isomers of 5-OH-HIC-CoA. The 976 *m*/*z* metabolite that accumulated in the Δ*ipdAB* mutant was identified as (*R*)-2-(2-carboxyethyl)-3-methyl-6-oxocyclohex-1-ene-1-carboxyl-CoA (COCHEA-CoA). These data were used to identify the substrates of IpdC and IpdAB and helped determine the order of reactions of cholesterol rings C and D degradation (89).

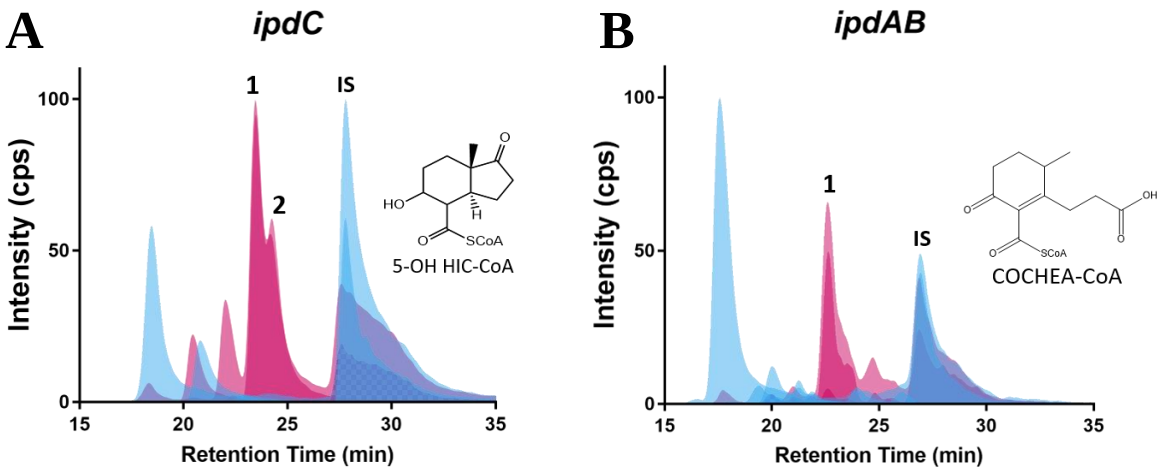

Figure 3.3 Cholesterol-derived intracellular metabolite accumulation in Mtb Δ*ipdC* (A) and Δ*ipdAB* (B). Strains were grown to mid-log phase on 7H9 medium supplemented with 0.2% glycerol and then concentrated and incubated in 7H9 medium supplemented with 0.5 mM cholesterol and incubated for 2 days at 27°C. Cells were harvested and cell lysates were analyzed by LC-MS. (A) peak 1 and 2 correspond to the 5α and 5β isomers of 5-OH-HIC-CoA, respectively. (B) peak 1 corresponds to COCHEA-CoA. IS = internal standard.

3.1.4 Intracellular growth of cholesterol catabolic mutants

Transposon mutagenesis studies suggest that *ipdA* is essential for Mtb survival in MΦs (98). Moreover, the gene is essential for survival of *R. equi* in foals (140). We therefore tested the growth of Δ*ipdAB* Mtb in PMA-differentiated THP-1 cells (Fig. 3.4). WT Mtb increased >350-fold over 7 days, corresponding to a doubling time of 19.6 hours. The mutant increased ~10-fold over this time, corresponding to a doubling time of 46.5 hours, while complementation restored intracellular replication to 131-fold. These results are consistent with Mtb catabolizing cholesterol, and more specifically rings C and D, during intracellular growth (139).

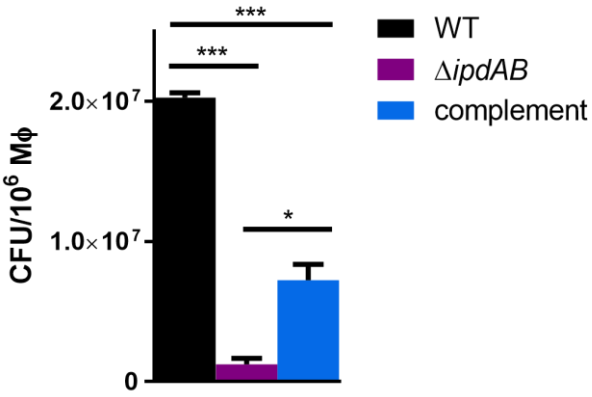

Figure 3.4 Growth of the Δ*ipdAB* mutant in THP-1 derived MΦs. WT, Δ*ipdAB*, and the complemented strain of Mtb Erdman were used to infect PMA-differentiated THP-1 cells at a MOI of 0.5:1. Intracellular CFU were enumerated 7 days post-infection. Data represent the mean of biological triplicates and is representative of two independent experiments, error bars are the standard error of the mean. ****p*< 0.001, **p*< 0.01 (One way ANOVA followed by Turkey's multiple comparisons test)

Spontaneous loss of PDIM, a cell wall lipid and virulence factor, has been observed in strains of Mtb following extended periods of *in vitro* growth (191). These findings have implications in virulence studies as the generation of mutant and complemented strains involves several rounds of transformation and passage. Loss of PDIM results in attenuation in infection models (192-194). To ensure that the loss of virulence and lack of complete complementation of the Δ*ipdAB* mutant in the THP-1 infection model was not due to loss of PDIM, we analyzed PDIM

content in the WT and complemented strain by thin layer chromatography (Fig. 3.5). PDIM was present in both strains, which indicates there was no loss of PDIM in the generation of the mutant and complemented strains. The lack of complete complementation of the Δ*ipdAB* mutant in THP-1 macrophages may be a result of insufficient expression of *ipdAB*, which is under the control of the *hsp60* promoter in the complemented strain. Alternatively, the site of integration of the complementation cassette may result in insufficient enzymatic activity to completely restore intracellular growth.

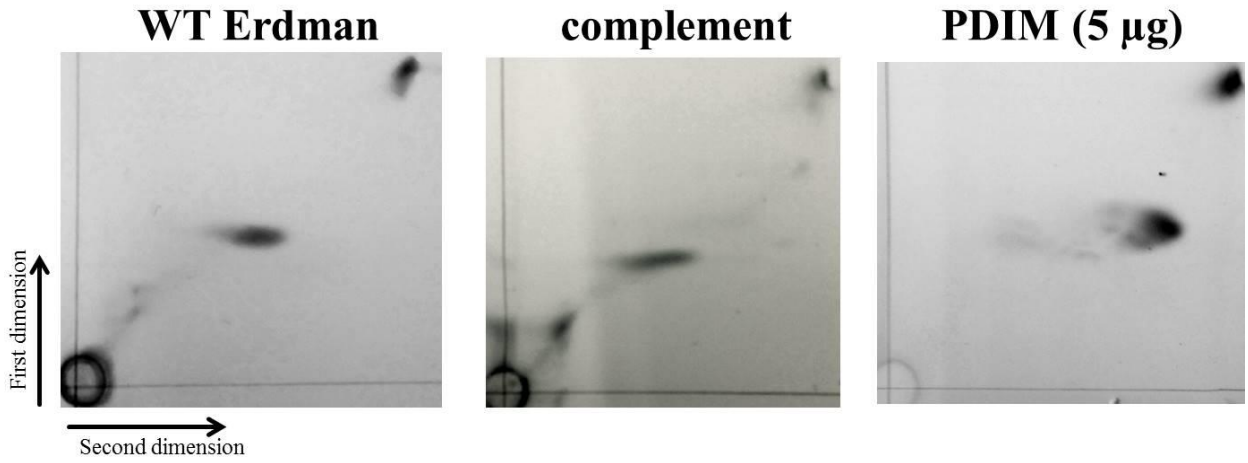

Figure 3.5 Two-dimensional thin layer chromatography of cell wall lipids of WT and the Δ*ipdAB* complemented strains of Mtb Erdman.

3.1.5 Chemical inhibition of cholesterol catabolism by GSK286A

The importance of cholesterol catabolism for Mtb pathogenesis has been further exemplified by the identification of inhibitors of intracellular Mtb growth, which were subsequently found to specifically inhibit growth on cholesterol (139). In a screen conducted by GSK, a compound library was screened for activity against intracellularly replicating bacteria (Fig. 3.6). Hits from this screen were further tested for their ability to inhibit growth of Mtb on

cholesterol as a sole carbon source. The combination of these two screens led to the identification of a cholesterol-specific inhibitor, GSK286A, capable of inhibiting growth of intracellular Mtb.

We tested the *in vitro* activity of GSK286A against Mtb Erdman growing on single carbon sources. The compound specifically inhibited growth on cholesterol with an IC_{50} of 0.34 μM (Fig. 3.7). It did not inhibit growth of Mtb on glycerol, acetate, or propionate alone but did inhibit growth on these carbon sources in the presence of cholesterol. When grown in the presence of cholesterol, the IC_{50} on alternative carbon sources was lowest for glycerol (4.0 μM), followed by propionate (15 μM) and then acetate (72 μM). These data suggest that GSK286A specifically inhibits cholesterol catabolism and in doing so, leads to the production of cholesterol-derived toxicity that inhibits growth on alternative carbon sources.

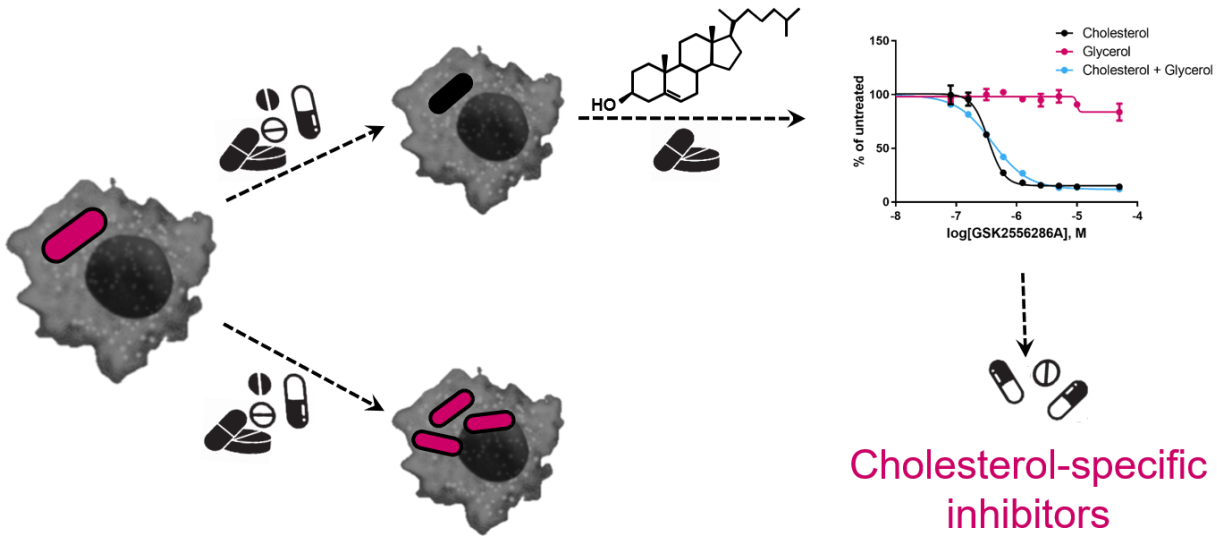

Figure 3.6 Compound library screen conducted by GSK to identify cholesterol-specific Mtb inhibitors

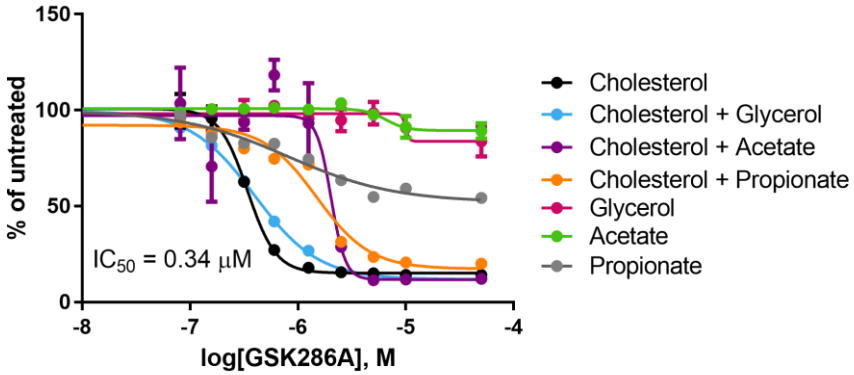

Figure 3.7 *In vitro* activity of GSK286A against Mtb Erdman grown on different carbon sources. Mtb Erdman expressing mCherry from the plasmid pCherry3 was grown in 7H9 medium supplemented with various carbon sources in a 96-well plate with increasing concentrations of GSK286A. Fluorescence was measured after 5 days of incubation at 570 nm excitation and 620 nm emission. Data represent the mean of biological triplicates, error bars are the standard error of the mean.

To determine if GSK286A inhibits upstream or downstream of KshA in the cholesterol catabolic pathway, we analyzed the ability of the Δ*kshA* mutant to transform cholesterol in the presence and absence of the compound. When treated with 10 µM GSK286A, the Δ*kshA* mutant of Mtb depleted cholesterol at the same rate as the untreated control and accumulated comparable amounts of ADD (Fig. 3.8). These data suggest that GSK286A does not inhibit cholesterol catabolism upstream of KshA as this would inhibit the production of ADD by the mutant strain. Furthermore, it suggests that cholesterol uptake and expression of the KstR regulon are not affected by GSK286A.

To determine which step of the cholesterol catabolic pathway is inhibited by GSK286A, we analyzed the extracellular and intracellular metabolite production by WT Mtb Erdman treated with the compound in the presence of cholesterol. The strain was initially grown in 7H9 medium supplemented with cholesterol to mid-log phase and was then concentrated and incubated in 7H9 medium supplemented with cholesterol in the presence or absence of GSK286A. Cells were harvested following two days of incubation. The culture supernatant was analyzed for

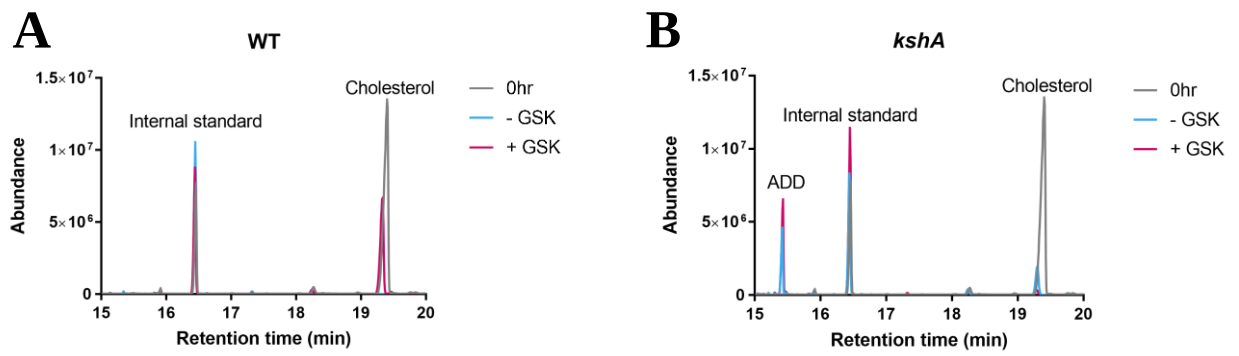

Figure 3.8 GC-MS analysis of extracellular metabolite accumulation of WT (A) and Δ*kshA* (B) Mtb Erdman grown in the presence of cholesterol. Strains were grown in 7H9 medium supplemented with 0.2% glycerol to mid-log phase and then concentrated and incubated in 7H9 medium supplemented with 0.5m cholesterol ± 10 μM GSK286A. Culture supernatant was analyzed by GS-MS. Chromatograms represent the mean of biological duplicates.

extracellular metabolite production by GS-MS and the cell lysate was analyzed for intracellular metabolite accumulation by LC-MS. However, we did not detect any intracellular or extracellular cholesterol-derived metabolites accumulating in cells treated with GSK286A (data not shown). This is in contrast to the metabolite accumulation observed for gene knockout mutants described above. These data suggest that GSK286A does not inhibit cholesterol catabolism by targeting a specific enzymatic step and that it may inhibit growth of Mtb on cholesterol through another mechanism.

3.1.6 GSK286A-mediated production of cAMP

To identify the target of GSK286A, spontaneous resistant mutants were isolated by GSK. Whole genome sequencing of the resistant mutants revealed mutations in *rv1625c*, a gene encoding a class IIIa membrane-anchored adenylyl cyclase (163). To investigate the involvement of Rv1625c in the mode of action of GSK286A, WT Mtb Erdman was grown on cholesterol or glycerol to mid-log phase and then treated with the compound or DMSO for 24 hours. The

intracellular cAMP levels, analyzed by LC-MS, were approximately 50-fold higher in treated vs. untreated cells (Fig. 3.9). These data suggest that the mode of action of GSK286A involves the over-production of cAMP mediated by Rv1625c. Consistent with this, cAMP production was not induced in an *rv1625c* transposon mutant of Mtb CDC1551, which suggests that the compound-induced cAMP is produced solely by Rv1625c and not one of the other 16 adenylyl cyclases encoded by the Mtb genome (Fig. 3.10A). Moreover, GSK286A did not inhibit the ability of the transposon mutant to grow on cholesterol (Fig. 3.10B). Finally, when *rv1625c* was expressed in *R. jostii* RHA1, an actinobacterium with a cholesterol catabolic pathway but no homolog of Rv1625c, cAMP production was induced when treated with GSK286A only when Rv1625c was expressed (Fig. 3.10C). These data indicate that Rv1625c is the target of GSK286A.

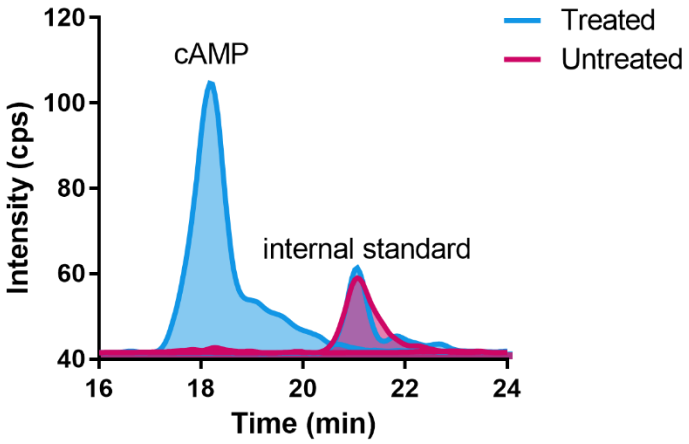

Figure 3.9 GSK286A-mediated production of cAMP by Mtb Erdman. Mtb Erdman was grown in 7H9 medium supplemented with 0.2% glycerol and then concentrated and incubated in 7H9 medium supplemented with 0.5 mM cholesterol ± 10 μM GSK286A. Cells were harvested after 24 hours and cell lysates were analyzed by LC-MS. Internal standard = 8-Br-cAMP. Data are representative of three biological replicates.

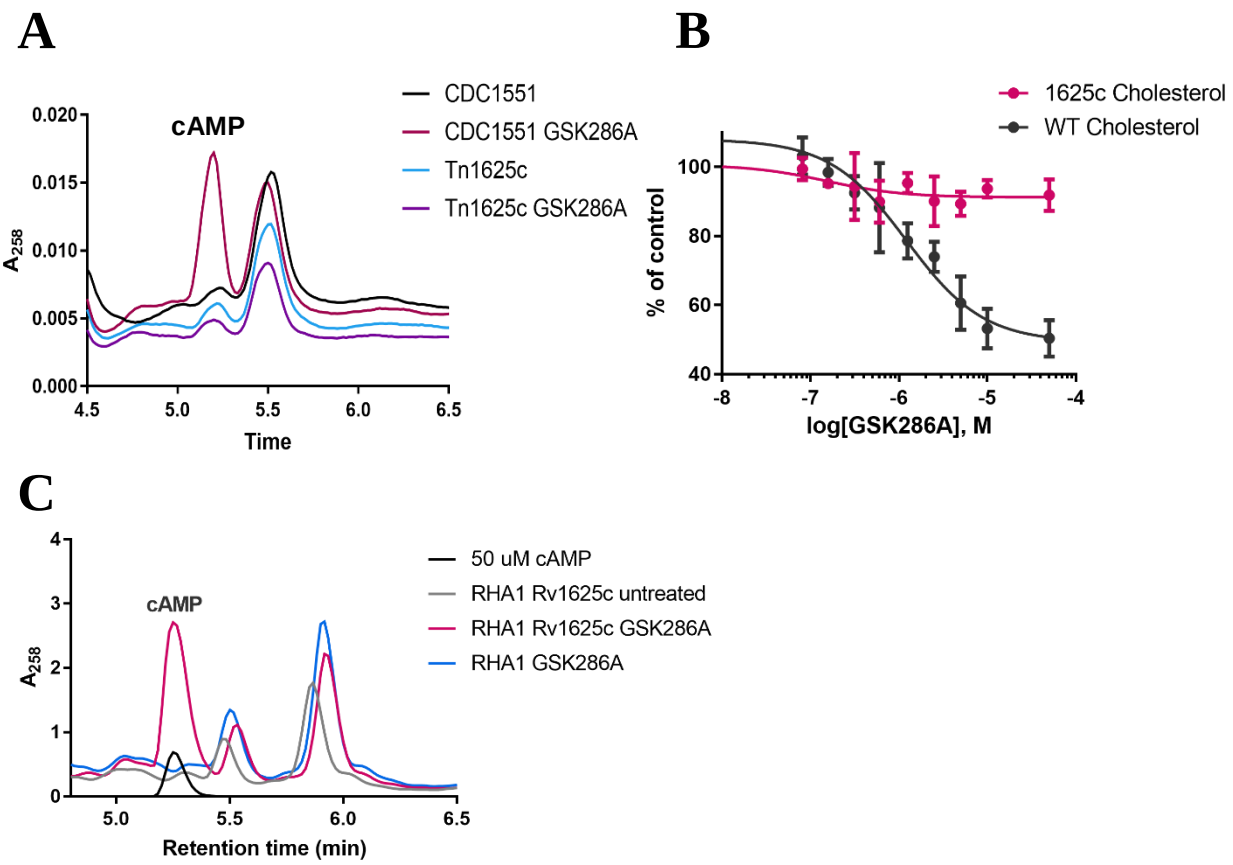

Figure 3.10 Rv1625c-dependent cAMP production and inhibition of growth. (A) WT and an *rv1625c* transposon mutant of Mtb CDC1551 was grown in 7H9 medium supplemented with 0.2% glycerol and then concentrated and incubated in 7H9 medium supplemented with 0.5 mM cholesterol ± 10 μM GSK286A. Cells were harvested after 24 hours and cell lysates were analyzed by HPLC. (B) WT Mtb CDC1551 and the *rv1625c* transposon were grown in 7H9 medium supplemented with 0.5 mM cholesterol in a 96-well plate with increasing concentrations of GSK286A. Growth was measured after 5 days using a Resazurin assay. (C) WT *R. jostii* RHA1 carrying pTipRv1625c or empty pTip plasmid was grown in M9 minimal medium supplemented with 0.5 mM cholesterol ± 10 μM GSK286A. Cell lysates were analyzed by HPLC. Data represent the mean of three biological replicates.

3.1.7 The GSK286A mechanism of action does not involve MtPat mediated acetylation

cAMP has been shown to regulate metabolic pathways by binding to the *N*-acetyltransferase MtPat, which in turn acetylates and inactivates enzymes (148-150). As a case in point, Section 3.2 of this thesis describes the regulation of cholesterol catabolism by the cAMP-dependent MtPat. We therefore hypothesized that the increase in intracellular cAMP in Mtb upon

treatment with GSK286A may lead to MtPat activation and acetylation of cholesterol catabolic enzymes. To test this, we deleted the gene encoding MtPat (*rv0998*) and the deacetylase *rv1151c* and tested the sensitivity of these strains to GSK286A. As shown in Figure 3.11, the Δ*mtpat* and the Δ*rv1151c* strains are both sensitive to GSK286A. These findings suggest that the primary mechanism of action of GSK286A does not involve the MtPat-mediated acetylation of cholesterol catabolic enzymes.

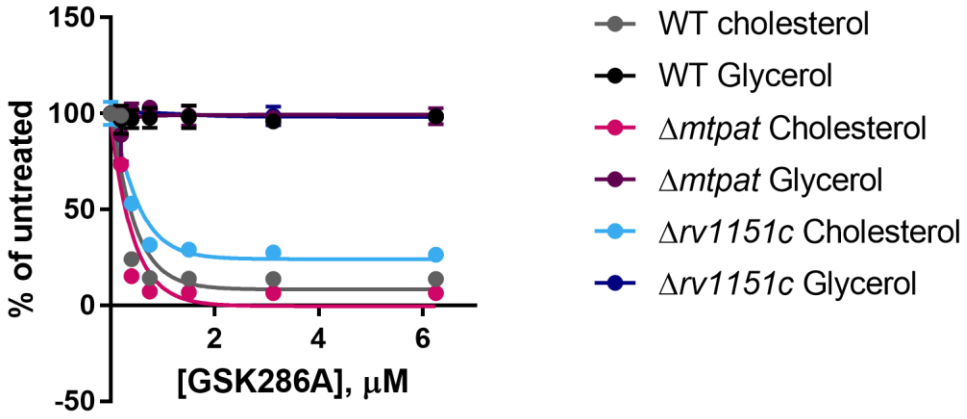

Figure 3.11 Sensitivity of Δ*mtpat* and Δ*rv1151c* Mtb Erdman to GSK286A. WT and mutant strains were grown in 7H9 medium supplemented with 0.2% glycerol or 0.5 mM cholesterol in 96-well plates with increasing concentrations of GSK286A or DMSO alone. Cell were incubated for 7 days at 37°C, and then the resazurin assay was performed. Data represent the mean of biological triplicates, error bars are the standard error of the mean.

Together, these data demonstrate the importance of cholesterol catabolism for the pathogenesis of Mtb. Deletion of cholesterol catabolic genes inhibit growth of Mtb on cholesterol to varying degrees. Deletion of genes encoding the rings C and D catabolizing enzymes IpdAB inhibit growth on cholesterol *in vitro* and in THP-1-derived MΦs confirming that rings C and D are catabolized during infection. The ability of GSK286A, a cholesterol-specific inhibitor, to prevent growth of intracellular Mtb further exemplifies the importance of cholesterol catabolism

for its survival during infection. We identified the target of the GSK286A compound to be the membrane-anchored adenylyl cyclase Rv1625c and demonstrated that the mode of action of GSK286A is through the stimulation of the enzyme to produce excess amounts of cAMP (Fig. 3.12. The compound appears to act in the same manner as the orphan inhibitors identified by VanderVen *et al* (2015) (139). How cAMP inhibits the cholesterol catabolic pathway remains to be elucidated.

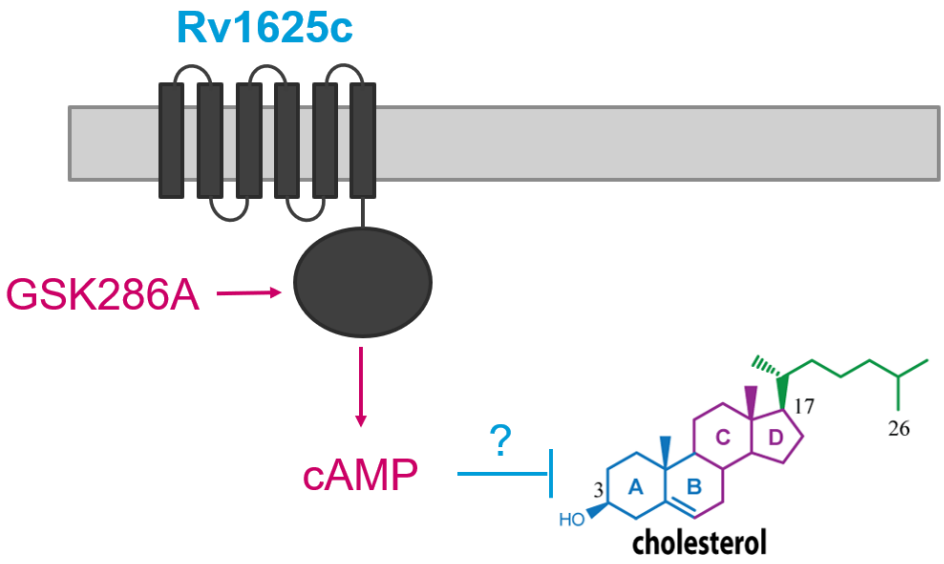

Figure 3.12 The mode of action of GSK286A. The compound stimulates the membrane-bound adenylyl cyclase Rv1625c to produce cAMP. How excess cAMP inhibits cholesterol catabolism remains to be determined.

3.2 Regulation of cholesterol catabolism through reversible lysine acetylation

3.2.1 Introduction

CoA thioesters are metabolites that are formed by acyl-CoA synthetases. For fatty acid and lipid substrates, CoA thioesterification activate them for catabolism. The accumulation of CoA thioesters has been shown to be bacteriotoxic (72, 89, 195) and possibly as a result of this, acyl-CoA synthetases, FadDs, are often subject to post-translational regulatory mechanisms (149, 150, 196-199). In Mtb, FadDs are regulated through reversible lysine acetylation mediated by the cAMP-dependent *N*-acetyltransferase MtPat and the NAD^+-dependent deacetylase Rv1151c (150). FadD3 is an acyl-CoA synthetase in Mtb which is the first enzyme to act in the catabolism of cholesterol rings C and D. It thioesterifies the rings C and D-containing metabolite HIP to produce HIP-CoA (136). Once produced, HIP-CoA binds to the KstR2 repressor, thereby relieving repression and allowing for the expression of the genes required for the catabolism of rings C and D (116). Many of the metabolites of the HIP catabolic pathway are CoA thioesters that would cause toxicity if they accumulate (89). Because FadD3 is the first enzyme to act in the catabolism of HIP, and because it produces the inducer for a regulon with the potential to generate toxicity, we hypothesized that FadD3 is a likely regulatory step. We therefore investigated the regulation of FadD3 by reversible acetylation.

Herein, we characterized the post-translational regulation of FadD3. We demonstrated that the enzyme is acetylated and inactivated by the MtPat homolog from *M. smegmatis* MsPat, and that the acetylation occurs on an active site lysine residue. Furthermore, we showed that Rv1151c deacetylates FadD3 and restores enzymatic activity. Finally, we deleted MtPat and Rv1151c in Mtb and characterized the growth phenotypes of the mutant strains under cAMP-inducing conditions in the presence of cholesterol. A growth defect was observed for the MtPat mutant

which suggests that FadD3 acetylation is important for the survival of hypoxia in the presence of cholesterol.

3.2.2 FadD3 shares conserved motifs for regulation through lysine acetylation

Nambi *et al*. (2013) identified multiple fatty acyl-CoA synthetases as substrates for the *N*-acetyltransferase MtPat (150). By analyzing the amino acid sequences of FadDs that are substrates for MtPat and those that are not, the authors identifed the motifs and residues required for MtPat-mediated acetylation. The following four conserved motifs were identified in the C-terminal domains of MtPat substrates: GGXNX$_4$EXE/D, E/DX$_7$E/D, K/AXP, and PX$_4$GK. To determine if FadD3 could be a substrate for MtPat, we aligned the enzyme's amino acid sequence with other FadDs. As shown in figure 3.13, FadD3 contains all four of the conserved motifs predicted to be required for acetylation by MtPat which suggests that it is likely regulated by post-translation lysine acetylation.

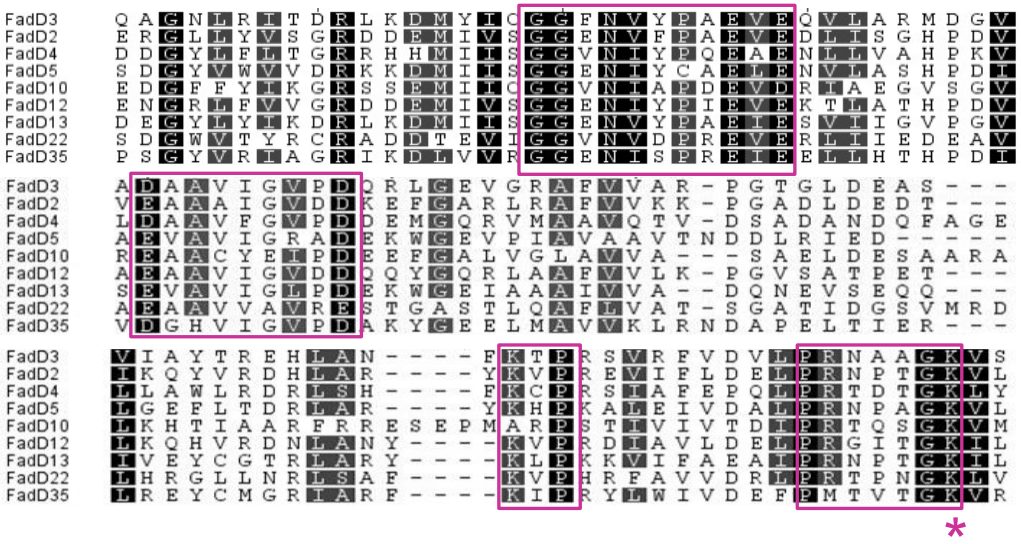

Figure 3.13 Amino acid sequence alignment of FadD enzymes from Mtb.

3.2.3 Acetylation and inactivation of FadD3 by MtPat

To investigate the post-translational regulation of FadD3 by MtPat and Rv1151c, we cloned, expressed, and purified the three enzymes to >95% homogeneity (Fig. 3.14, Methods section 2.7). It has been observed by us and others that purified MtPat is often inactive (149), while the homolog from *M. smegmatis*, which shares ~60% amino acid sequence identity, displays activity. For this reason, the gene encoding MsPat was cloned and the protein was purified.

To determine if MsPat could acetylate and inactivate FadD3, the enzyme was incubated with MsPat, cAMP, and acetyl-CoA at 30°C for 50 minutes. Following incubation, the activity of FadD3 was measured using the coupled spectrophotometric assay outlined in Figure 3.15. (136).

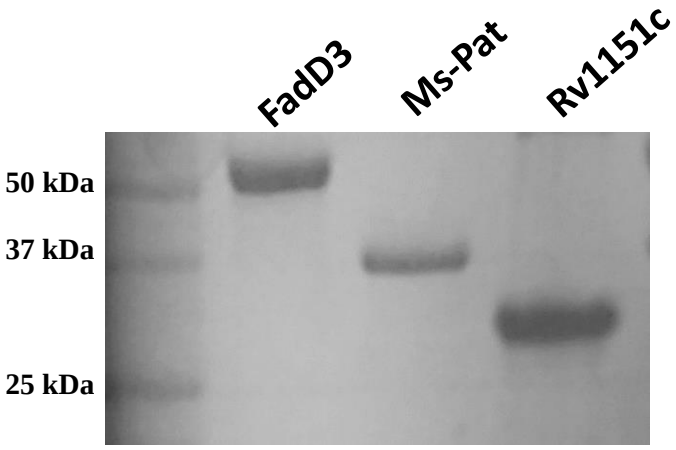

Figure 3.14 SDS-PAGE of recombinantly expressed and purified FadD3, MsPat, and Rv1151c.

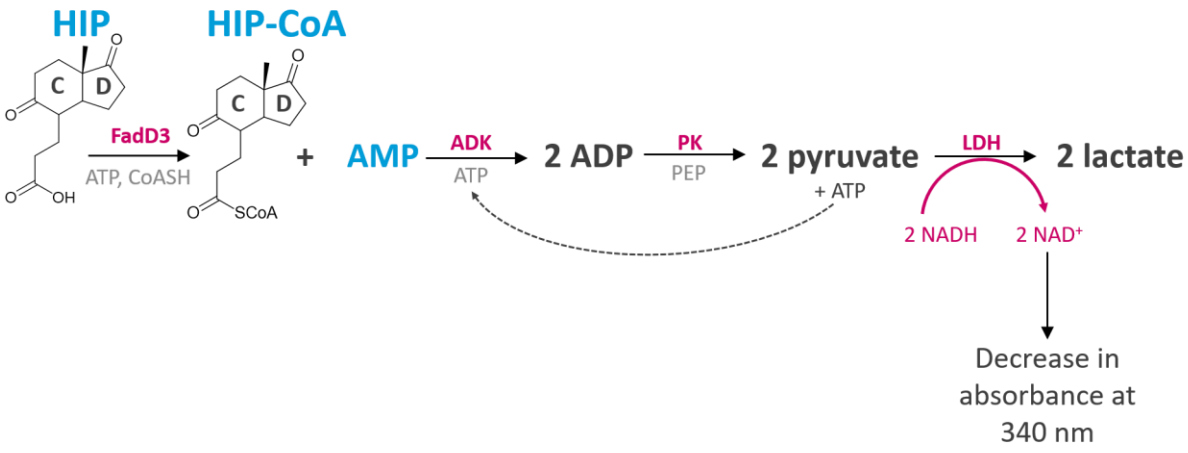

Figure 3.15 Coupled spectrophotometric assay for measuring FadD3 activity following incubation with MsPat and Rv1151c. Adenylate kinase, ADK; pyruvate kinase, PK; lactate dehydrogenase, LDH.

The activity of FadD3 was measured at 10-minute intervals throughout the incubation with MsPat. We observed a time-dependent decrease in FadD3 activity upon incubation with MsPat, while the activity FadD3 incubated without MsPat was unchanged (Fig. 3.16A). Activity of the inactivated FadD3 was also measured by HPLC (Fig. 3.16B). Active and inactive FadD3 were incubated with HIP and acetyl-CoA at room temperature for 30 minutes. HIP-CoA was produced following incubation of the active FadD3 with its substrates, while minimal product formation was observed for the MsPat-treated FadD3.

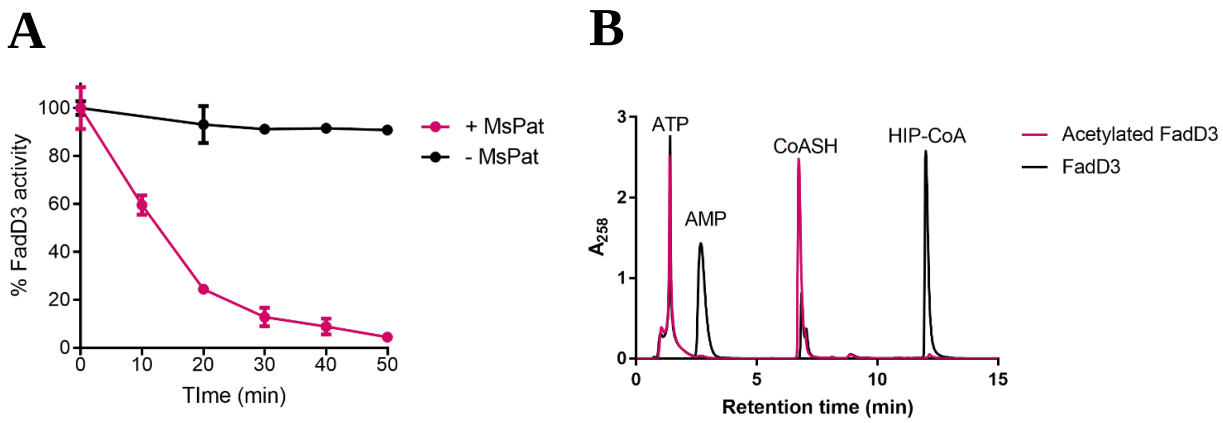

Figure 3.16 Inactivation of FadD3 by MsPat. (A) Time-dependent inactivation of FadD3 upon incubation with MsPat. Each reaction was performed in triplicate and at every time point, enzyme activities were measured in duplicate. (B) Product formation by active and inactive FadD3 measured by HPLC. Data represent the mean of three replicates, error bars are the standard error of the mean.

To confirm that the MsPat-inactivated FadD3 was acetylated, we used trypsin digest followed by LC-MS analysis to identify post-translational modifications. As summarized in figure 3.16, an acetyl group was detected on Lys497. The acetyl group was detected by the presence of the diagnostic peak at *m/z* 126.1. Acetylation at the active site lysine residue also results in a missed trypsin cleavage site. The identification of the peptide shown in figure 3.17 confirms the missed cut site and the acetylation of Lys497. This active site lysine corresponds to the residue that is acetylated by MtPat in other FadDs (150).

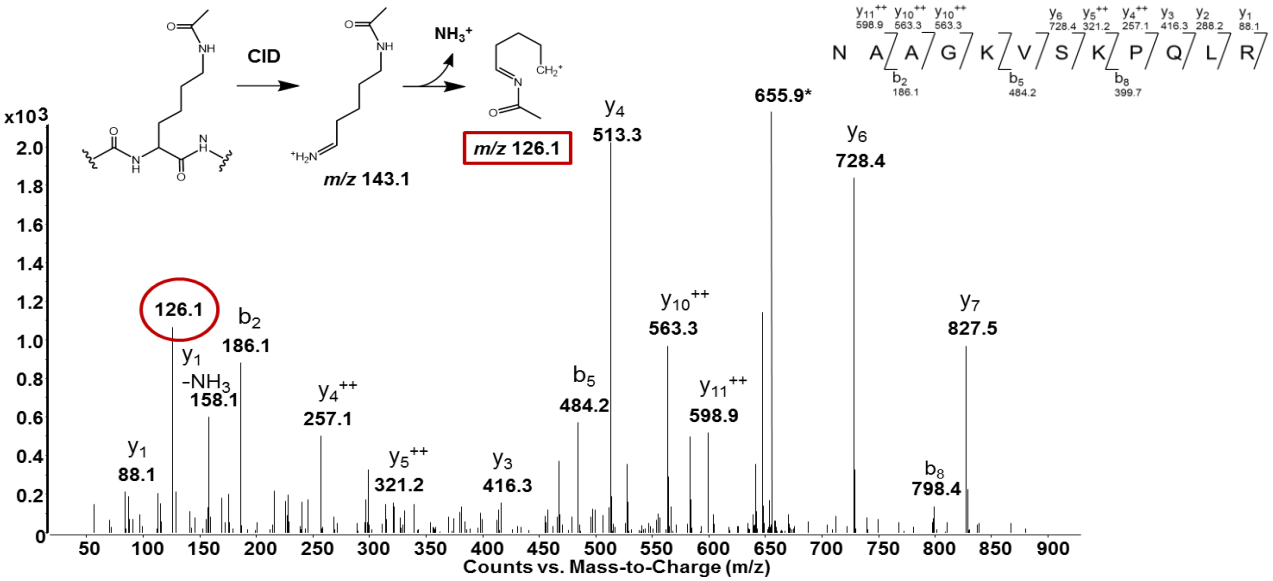

Figure 3.17 Trypsin digest followed by LC-MS/MS analysis of MsPat-inactivated FadD3. MS/MS spectrum of the acetylated tryptic peptide NAAGKVSKPQLR of FadD3. The observed fragment ions (b and y ions) are marked on the spectrum and summarized schematically

3.2.4 Deacetylation of FadD3 by Rv1151c

To determine if the activity of the acetylated FadD3 could be restored through deacetylation by the NAD^+-dependent deacetylase Rv1151c, we incubated the acetylated FadD3 with Rv1151c (Fig. 3.18A). The specific activity of FadD3 prior to acetylation was 3.5 ± 0.1 µmol

min^{-1} mg^{-1}. Following incubation with MsPat for 10 minutes at 37°C the specific activity was 0.69 ± 0.05 μmol min^{-1} mg^{-1}. The acetylated FadD3 was then incubated with Rv1151c with or without NAD^+ at 30°C for 30 minutes. The specific activity was 0.53 ± 0.03 μmol min^{-1} mg^{-1} and 2.10 ± 0.03 μmol min^{-1} mg^{-1} following incubation in the absence and in the presence of NAD^+, respectively. These data suggest that Rv1151c restores activity of acetylated FadD3 through NAD^+-dependent deacetylation.

Western blot analysis with an anti-acetyl lysine antibody was used to probe the acetylation state of FadD3 following incubation with Rv1151c (Fig. 3.18B). The acetyl-lysine was detected when FadD3 was incubated with MsPat but not in the -MsPat control as shown in lanes 1 and 2, respectively. Incubation of the acetylated FadD3 with Rv1151c and NAD^+ removed the acetyl-lysine, while incubation in the absence of NAD^+ did not. These data confirm that the restoration of activity by Rv1151c by treatment with Rv1151c is due to the deacetylation of FadD3.

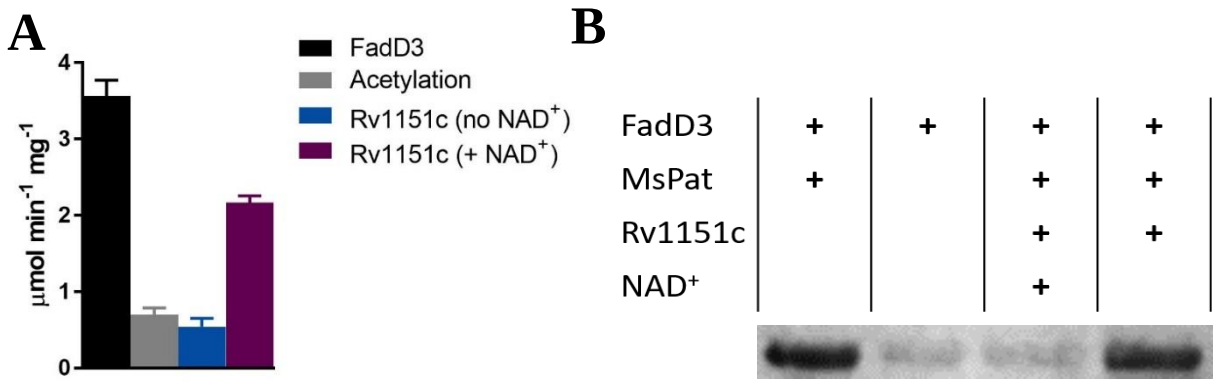

Figure 3.18 NAD^+-dependent restoration of activity of acetylated FadD3 by Rv1151c. (A) Activity of FadD3 measured before and after acetylation by MsPat (black and grey bars, respectively), and the activity of the acetylated FadD3 following incubation with Rv1151c in the absence and presence of NAD^+ (blue and purple bars, respectively). Each reaction was performed in triplicate and the enzyme activity for each was measured in triplicate, error bars are the standard error of the mean. (B) Western blot analysis using an anti-acetyl lyine antibody.

3.2.5 Growth of Δ*mtpat* and Δ*rv1151c* in the presence of cholesterol

MtPat is essential for Mtb survival under hypoxic conditions (152). Rittershaus *et al* demonstrated that the viability defect of the Δ*mtPat* mutant under hypoxic conditions depends on the presence of fatty acids in the culture medium, and that MtPat functions to prevent the formation of acetyl-CoA under these conditions (152). The lack of MtPat resulted in the continuous flux of carbon through the oxidative branch of the TCA cycle under hypoxic conditions rather than through the reductive branch as seen for the WT strain. The inability of the Δ*mtPat* strain to adapt to hypoxia by preferential use of the reductive TCA branch led to a redox imbalance. The authors suggest that MtPat acts to limit the production of acetyl-CoA from fatty acids under hypoxic conditions to reduce the flux of carbon through the oxidative TCA cycle.

Like fatty acid catabolism, cholesterol catabolism results in the production of acetyl-CoA. Most of the cholesterol-derived acetyl-CoA is produced from the breakdown of cholesterol rings C and D (89). To determine if cholesterol catabolism is regulated through acetylation during hypoxia, we grew the Δ*mtPat* and Δ*rv1151c* strains in the presence of cholesterol and glucose under hypoxic conditions (Fig. 3.19). The Δ*mtPat* mutant showed a significant reduction in CFU/ml after 15 days compared to the WT and Δ*rv1151c* strains. These data are consistent with the loss of viability of the Δ*mtPat* strain during hypoxia in the presence of fatty acid (152).

Together, these data indicate that catabolism of cholesterol rings C and D may be regulated through the reversible lysine acetylation of FadD3, and that this regulation may be important under hypoxic conditions by maintaining the flow of carbon through the reductive branch of the TCA cycle. It may also function to limit the production of cholesterol-derived CoA thioesters and propionyl-CoA which are toxic if allowed to accumulate (discussed in Section 3.3).

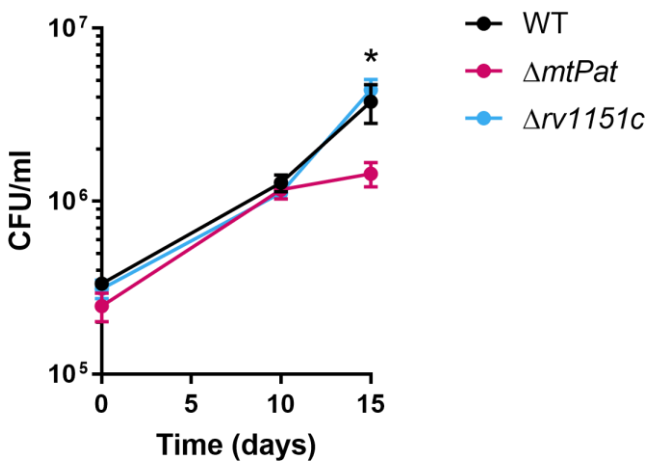

Figure 3.19 Growth of WT, Δ*mtPat*, and Δ*rv1151c* Mtb Erdman in the presence of cholesterol under hypoxic conditions. Strain were grown aerobically in 7H9 + glucose + 0.5 mM cholesterol to an OD_{600} of 0.3 and were then transferred to hypoxic conditions. Data represent the mean of biological triplicate, error bars are the standard error of the mean. *p = 0.001 (Two way ANOVA with Dunnett's multiple comparisons test)

3.3 Coenzyme A depletion in cholesterol catabolic mutants

3.3.1 Introduction

In Crowe *et al*., we demonstrated that deletion of genes within the KstR2-regulon leads to the accumulation of cholesterol-derived CoA thioesters and, interestingly, that accumulation of these metabolites appears to be toxic to Mtb and related actinobacteria (89). Cholesterol-derived toxicity in catabolic mutants was hypothesized to be due to the sequestration of free CoA. That is, the large accumulation of CoA-thioesters limits the availability of CoA for other cellular processes. Consistent with this hypothesis, metabolomic analysis revealed depleted CoA levels in KstR2-regulon mutants during biotransformation of cholesterol, a method which involves concentrating and incubating bacteria with a substrate in order to generate large amounts of a desired metabolite (89). While intriguing, the depleted CoA levels may have been an artifact of the biotransformation protocol used to produce excess amounts of cholesterol-derived CoA-thioesters.

CoA is an essential cofactor involved in a myriad of cellular processes. It plays a particularly important role in the biosynthesis of Mtb-specific lipids, some of which are virulence factors for Mtb pathogenesis (72). The importance of CoA for the survival of Mtb *in vivo* was demonstrated by Evans *et al*. through the conditional knockdown of CoA-biosynthetic genes during infection (181). CoA depletion led to bacteriostatic and bactericidal phenotypes and abrogated the ability of knockdown strains to grow and persist in mice. Furthermore, the TB drug pyrazinamide, which has very poor *in vitro* but good *in vivo* activity, appears to target CoA biosynthesis and leads to depletion of free CoA (200, 201). As a result, the CoA biosynthetic pathway has been proposed as a promising drug target for the treatment of TB and other bacterial infections (172).

Herein, we set out to confirm the mechanism of cholesterol-dependent toxicity in KstR2-regulon knockout mutants. We utilized mutants in Mtb and the related actinobacterium *M. smegmatis* to show that the deletion of genes within the KstR2-regulon leads to the accumulation of cholesterol-derived CoA-thioesters, depletion of free CoA, and subsequent toxicity in the presence of cholesterol. Hydrolysis of cholesterol-derived CoA-thioesters and export of the corresponding carboxylate was found to diminish the toxic phenotype and restore CoA levels. We used LC-MS/MS analysis to characterize the metabolic profile of cholesterol-dependent CoA depletion, which led to the dysregulation of central metabolic pathways and was consistent with previously characterized CoA-depletion models (181). Finally, we used mutant strains deficient in *p*-coumarate catabolism in the actinobacterium *R. jostii* RHA1 to demonstrate that CoA-thioester accumulation and CoA depletion is not limited to the cholesterol catabolic pathway. These data suggest that targeting catabolic enzymes that act on CoA-thioester substrates for the development of novel therapeutics may both inhibit the catabolism of important carbon sources during infection and simultaneously deplete the essential cofactor CoA.

3.3.2 Cholesterol-dependent toxicity in catabolic mutants

Deletion of genes within the KstR2-regulon produces strains with the ability to catabolize the cholesterol side chain and Rings A/B, theoretically obtaining about half of the carbon and energy stored in the cholesterol molecule. Consistent with this prediction, deletion of *fadD3*, which encodes the first enzyme to act in Rings C/D catabolism, resulted in a decreased final growth yield on cholesterol compared to WT Mtb Erdman, and the accumulation of the Rings C/D containing metabolite HIP in the culture supernatant (Section 3.1, Fig. 3.1B and 3.2B). These data are consistent with the deletion of FadD3 in *R. jostii* RHA1 (136).

Mutants harbouring deletions of *ipdAB* and *ipdC*, both of which encode enzymes that act downstream of FadD3 (89), were unable to utilize cholesterol as a sole carbon source despite the fact that they should be able to liberate one more acetyl-CoA from cholesterol than the Δ*fadD3* mutant (Fig. 3.20). Growth on cholesterol was restored by complementation with *ipdAB* or *ipdC* on an integrative plasmid. Interestingly, the presence of cholesterol in the medium abrogated growth of the Δ*ipdAB* and Δ*ipdC* strains on glycerol, suggesting the accumulation of a toxic, cholesterol-derived metabolite (Fig. 3.20). Complementation restored growth on glycerol in the presence of cholesterol.

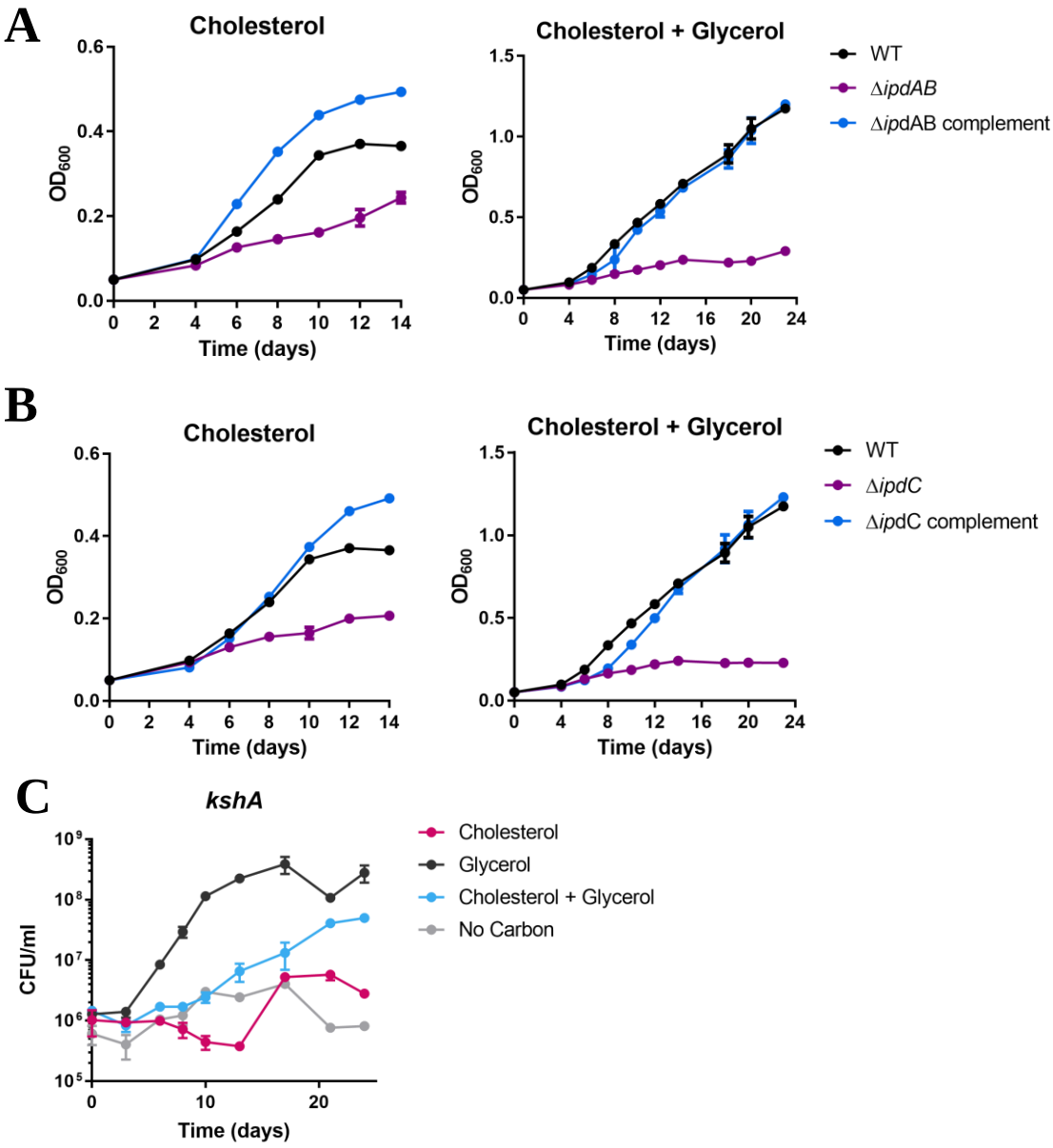

Figure 3.20 Cholesterol-derived toxicity in Δ*ipdAB* (A), Δ*ipdC* (B), and Δ*kshA* (C) Mtb Erdman. WT, Δ*ipdAB*, and Δ*ipdC Mtb* Erdman were grown in 7H9 containing 0.5 mM cholesterol, 0.5% tyloxapol, ± 0.2% glycerol at 37°C. Cholesterol growth in panels A and B are the same data presented in Figure 3.1. Data represent the mean of biological triplicates, error bars represent the standard error of the mean.

Deletion of *ipdAB* in *M. smegmatis* similarly inhibited growth on cholesterol and led to a toxic phenotype in the presence of the CoA-dependent carbon sources acetate and propionate, while showing reduced toxicity when glycerol and glucose were used as alternative carbon sources (Fig. 3.21). The inability of the mutant strain to utilize acetate and propionate in the presence of cholesterol is consistent with the hypothesis that CoA thioester accumulation leads to depletion of free CoA as both carbon sources require CoA for the first step in their catabolism.

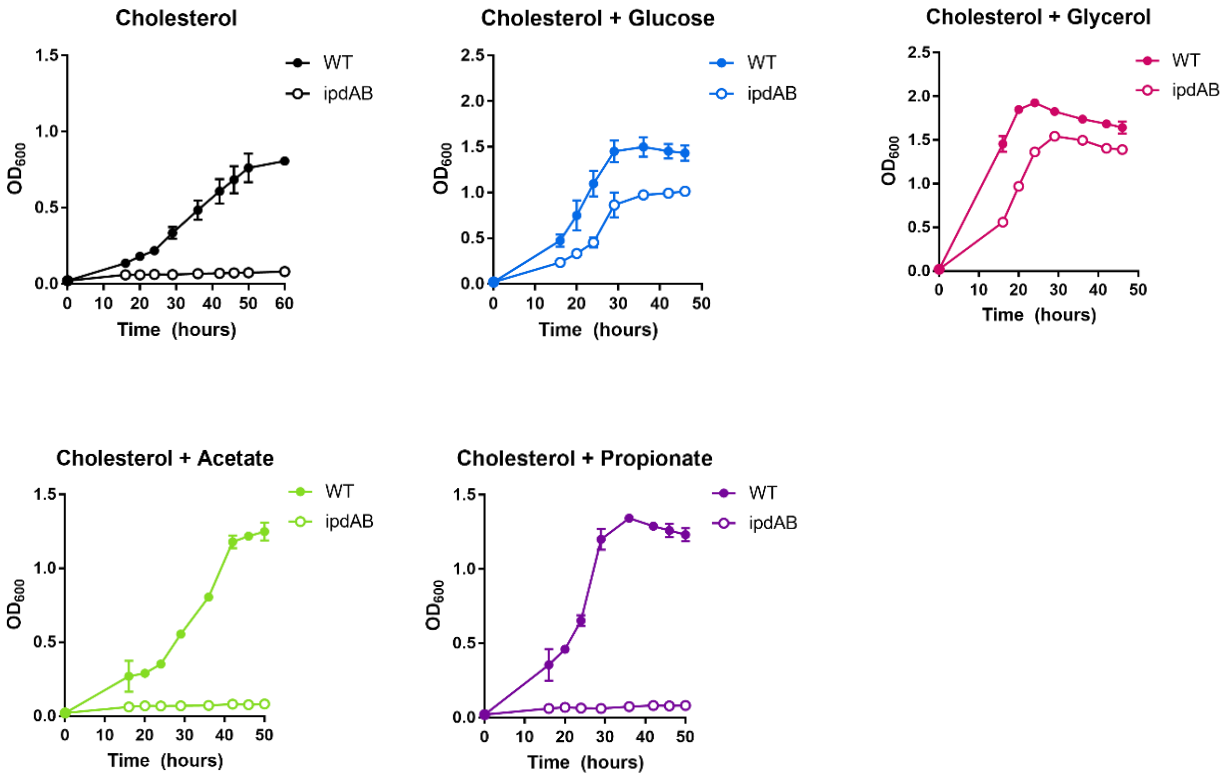

Figure 3.21 Cholesterol-derived toxicity in Δ*ipdAB M. smegmatis* is carbon source-dependent. WT and Δ*ipdAB M. smegmatis* were grown in 7H9 containing 0.5 mM cholesterol and 0.5% tyloxapol ± 2.25 mM glucose, 4.5 mM glycerol, 6.75 mM acetate, or 4.5 mM propionate at 37°C. Data represent the mean of biological triplicates, error bars represent the standard error of the mean.

Cholesterol-dependent toxicity in the Δ*ipdAB M. smegmatis* strain was dose-dependent and showed complete inhibition of growth in the presence of 0.1 mM cholesterol and slight growth at 0.05 mM cholesterol (Fig. 3.22). Deletion of *ipdF*, *echA20*, and *fadE32*, all of which encode enzymes involved in catabolizing Rings C and D and that act on CoA thioester substrates, also led to dose-dependent toxicity in the presence of cholesterol, although to different extents (Fig. 3.22). The Δ*ipdAB* mutant was the most sensitive to the presence of cholesterol showing slowed growth at a cholesterol concentration as low as 0.02 mM (Fig. 3.22). Deletion of *ipdF* also lead to strong toxicity, showing slightly more growth at a cholesterol concentration of 0.05 mM compared to the Δ*ipdAB* strain (Fig. 3.22). Deletion of *echA20* resulted in slowed growth in a dose-dependent manner and a strong toxic phenotype in the presence of 0.5 mM cholesterol (Fig. 3.22). In contrast, deletion of *fadE32* resulted in minimal cholesterol-dependent toxicity (Fig. 3.22). When grown in the presence of cholesterol, the Δ*ipdF*, Δ*echA20*, and Δ*fadE32* strains all accumulate cholesterol-derived metabolites in the culture supernatant, while the Δ*ipdAB* strain does not (89). The Δ*ipdF* and Δ*echA20* strains both produced 5OH-HIC in the culture supernatant (89). This metabolite is the carboxylate of the CoA thioester substrate that accumulates in both of these strains (89). The Δ*fadE32* strain accumulates the carboxylate of MOODA-CoA in the culture supernatant (89). These findings suggest that these strains are able to hydrolyze the accumulating CoA thioesters and export the resulting carboxylate. In doing so, the sequestered CoA may be liberated thereby reducing the toxicity of cholesterol.

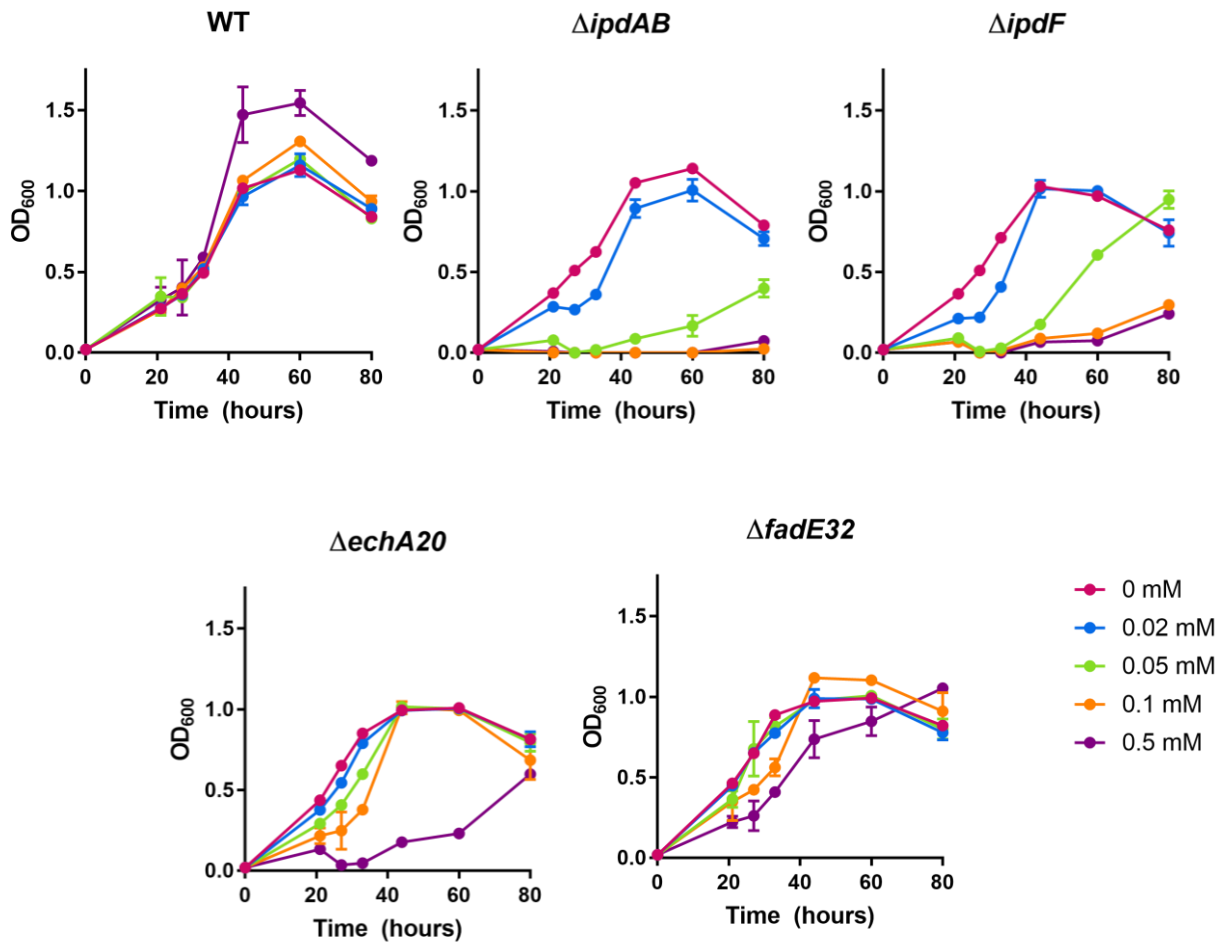

Figure 3.22 Dose-dependent cholesterol-derived toxicity in KstR2 regulon mutants of *M. smegmatis*. Strains were grown in 7H9 medium supplemented with 10 mM acetate, 0.5% tyloxapol and increasing concentrations of cholesterol at 37°C. Data represent the mean of biological triplicates.

3.3.3 Cholesterol-derived metabolite accumulation and CoA depletion

It has been hypothesized that the basis of cholesterol-dependent toxicity in KstR2-regulon mutants is the accumulation of cholesterol-derived CoA thioesters leading to the sequestration of free CoA from other cellular processes (89). Indeed, Crowe *et al*. reported depleted levels of free CoA in the metabolomes of HIP-catabolic mutants (89). However, the metabolomes were prepared from biotransformations of cholesterol: a method in which biomass is concentrated and incubated with a substrate to generate a large amount of a desired metabolite. To verify that CoA depletion was not an artifact of the biotransformation protocol, we analyzed metabolite accumulation and CoA depletion in normally growing cells. We grew WT, Δ*ipdAB*, Δ*ipdF*, and Δ*echA20 M. smegmatis* on 7H9 containing glycerol to mid-log phase, and the cultures were then diluted 1:1 with 7H9 medium containing cholesterol and HIP or glycerol. All strains grew normally when glycerol was added at mid-log phase (Fig. 3.23). When cholesterol and HIP were added to the cultures, the Δ*ipdAB* mutant showed a strong toxic phenotype, while the Δ*ipdF* and Δ*echA20* mutants did not.

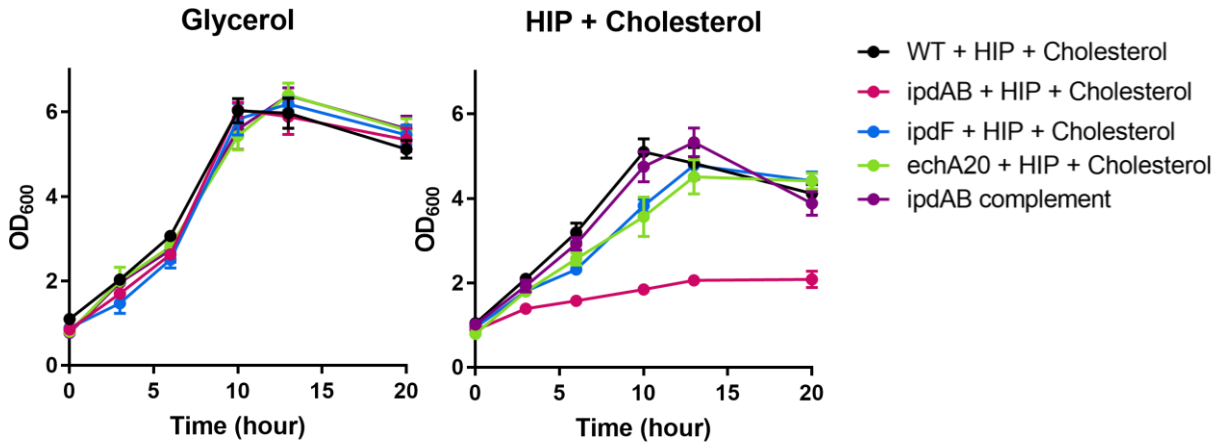

Figure 3.23 Growth of *M. smegmatis* mutant strains following addition of glycerol or HIP + cholesterol at mid-log phase. All strains were grown in 7H9 + 0.2% glycerol to mid-log phase at which point 4.5 mM glycerol (A) or 0.5 mM cholesterol + 0.3 mM HIP (B) were added. The cultures were incubated at 37°C. Data represent the mean of biological triplicates.

At several timepoints following the addition of carbon at mid-log phase, samples were taken for analysis of metabolite accumulation. Intracellular metabolite accumulation was analyzed by HPLC. As expected, the Δ*ipdAB* mutant accumulated COCHEA-CoA, the substrate for IpdAB, while the Δ*ipdF* and Δ*echA20* mutants accumulated 5OH-HIC-CoA (89) (Fig. 3.24A). Interestingly, while all strains showed accumulation of a cholesterol-derived CoA-thioester, the Δ*ipdAB* mutant showed a greater depletion in the levels of free CoA than the Δ*ipdF* and Δ*echA20* mutants (Fig. 3.24B).

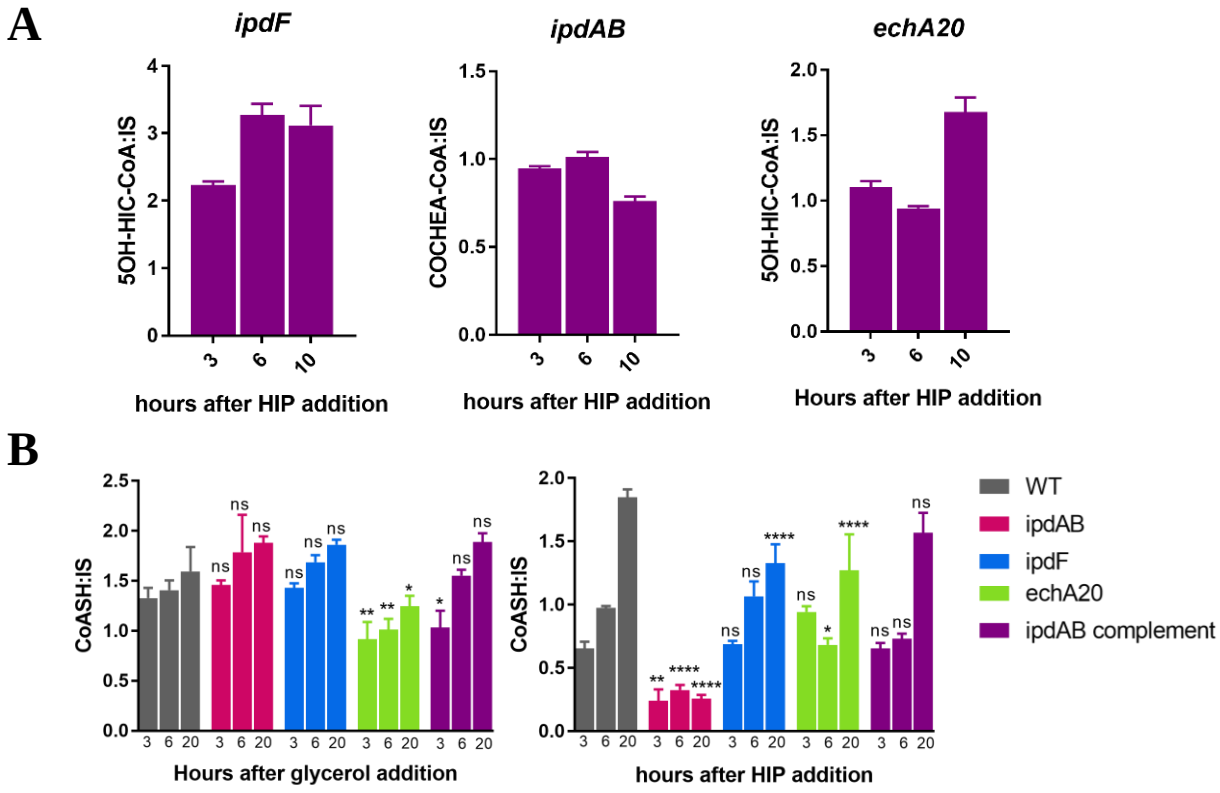

Figure 3.24 Metabolite accumulation and CoA depletion in KstR2-regulon mutants of *M. smegmatis*. Cholesterol-derived metabolite accumulation (A) and levels of free CoA (B) in the Δ*ipdAB*, Δ*ipdF* and Δ*echA20* strains was monitored by HPLC following addition of glycerol or cholesterol + HIP to cultures at mid-log phase. Metabolite abundance was normalized to the internal standard (IS) *p*-coumaroyl-CoA. Data represent the mean of biological triplicates error bars represent the standard error of the mean. Statistical analysis was done using a 2-way ANOVA with Dunnett's multiple comparisons test. *p<0.05, **p<0.005, ****p=0.0001.

In GC-MS analyses of culture supernatants, no extracellular cholesterol-derived metabolites were detected from the WT or the Δ*ipdAB* mutant over time. In contrast, there was a time-dependent accumulation of 5OH-HIC in the culture supernatant of the Δ*ipdF* mutant (Fig. 3.25). These data suggest that the Δ*ipdF* mutant is capable of hydrolyzing 5OH-HIC-CoA and excreting the carboxylate into the culture supernatant. Such hydrolysis may restore intracellular CoASH levels to close to those of the WT strain, leading to diminished toxicity in the presence of cholesterol and HIP. Together, these data suggest a model whereby the inhibition of cholesterol rings C/D catabolizing enzymes leads to the accumulation of CoA-thioester metabolites, depletion of free CoA, and toxicity in the presence of cholesterol.

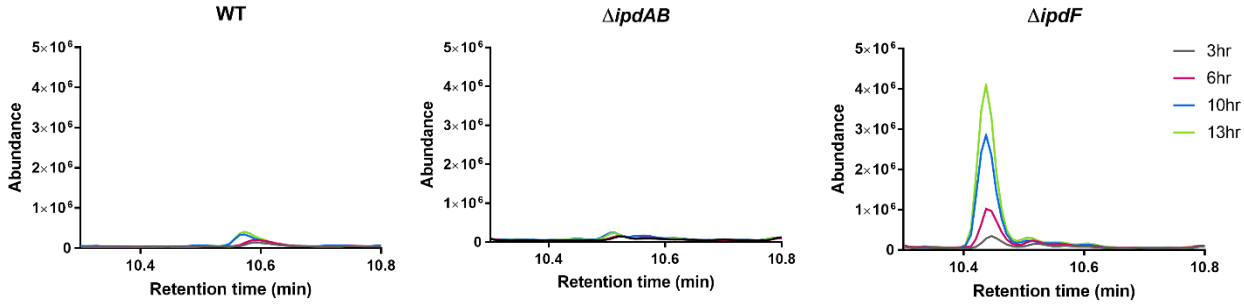

Figure 3.25 Extracellular metabolite accumulation in KstR2-regulon mutants of *M. smegmatis*. Metabolites were extracted from the culture supernatant of strains following addition of cholesterol + HIP at mid-log phase. Extracts were analyzed by GC-MS. Data are representative of three biological replicates.

3.3.4 Metabolic profiling of cholesterol-mediated CoA depletion

The importance of CoA for the survival of Mtb *in vivo* was demonstrated by Evans *et al.* through the conditional knockdown of CoA-biosynthetic genes during infection (181). The authors used LC-MS analysis to characterize the metabolomes of CoA depleted Mtb, establishing a CoA depletion metabolic fingerprint. We used the same approach to characterize the metabolomes of

cholesterol-dependent CoA depletion in *M. smegmatis* mutant strains. For this experiment, WT, Δ*ipdAB*, and Δ*echA20 M. smegmatis* strains were grown in rich medium. Exponentially growing cells were transferred to filters which were placed on 7H10 agar containing glycerol alone or glycerol and HIP. At several timepoints, filters were plunged into solvent in liquid nitrogen for metabolite extraction.

The Δ*ipdAB* mutant showed a growth defect when incubated on plates containing HIP compared to glycerol alone (Fig. 3.26A). Consistent with the liquid growth experiments described in Section 3.3.3, HIP induced less toxicity in the Δ*echA20* mutant as compared to the Δ*ipdAB* mutant. Indeed, for the Δ*echA20* mutant, CFU/ml increased between 5 and 10 hours of incubation. Also consistent with the findings described above, CoA levels were depleted in the Δ*ipdAB* mutant after 5 and 10 hours of incubation in the presence of HIP (Fig. 3.26B). Acetyl-CoA, malonyl-CoA, and succinyl-CoA were also depleted in the Δ*ipdAB* mutant. The WT and Δ*echA20* strains showed similar changes in CoA and CoA thioester levels at both timepoints, with slightly higher amounts of CoA metabolites after 5 hours of incubation with HIP followed by a slight decrease in CoA metabolites after 10 hours. The Δ*ipdAB* strain accumulated the expected cholesterol-derived metabolite COCHEA-CoA, the substrate for IpdAB, while the Δ*echA20* strain accumulated the EchA20 substrate HIEC-CoA along with the upstream metabolites 5OH-HIEC-CoA and 5OH-HIC-CoA. 5OH-HIC-CoA was also found in the metabolome of WT *M. smegmatis*, although in much lower amounts compared to the Δ*echA20* strain. The accumulation of cholesterol-derived CoA thioesters in the Δ*echA20* strain is not consistent with its lack of CoA depletion. However as described above, the CoA thioesters that accumulate appear to be more easily hydrolyzed and export compared to those accumulating in the Δ*ipdAB* mutant. Consistent with this, the absolute amount of the cholesterol-derived CoA thioesters decreased in the Δ*echA20* mutant between 5 and

10 hours of incubation, with the most abundant metabolite, 5OH-HIC-CoA, decreasing by ~43% (Fig. 3.27). In contrast, the amount of COCHEA-CoA in the Δ*ipdAB* strain increased by ~50% between 5 and 10 hours of incubation in the presence of HIP.

As shown in Figure 3.26C, the metabolic profile of the Δ*ipdAB* mutant was distinct from the other two strains. Metabolites that were more abundant in the Δ*ipdAB* mutant in the presence of HIP at both timepoints included citrate, valine, phenylalanine, proline, lysine, and histidine, while α-ketoglutarate, glucose, and methionine were depleted.

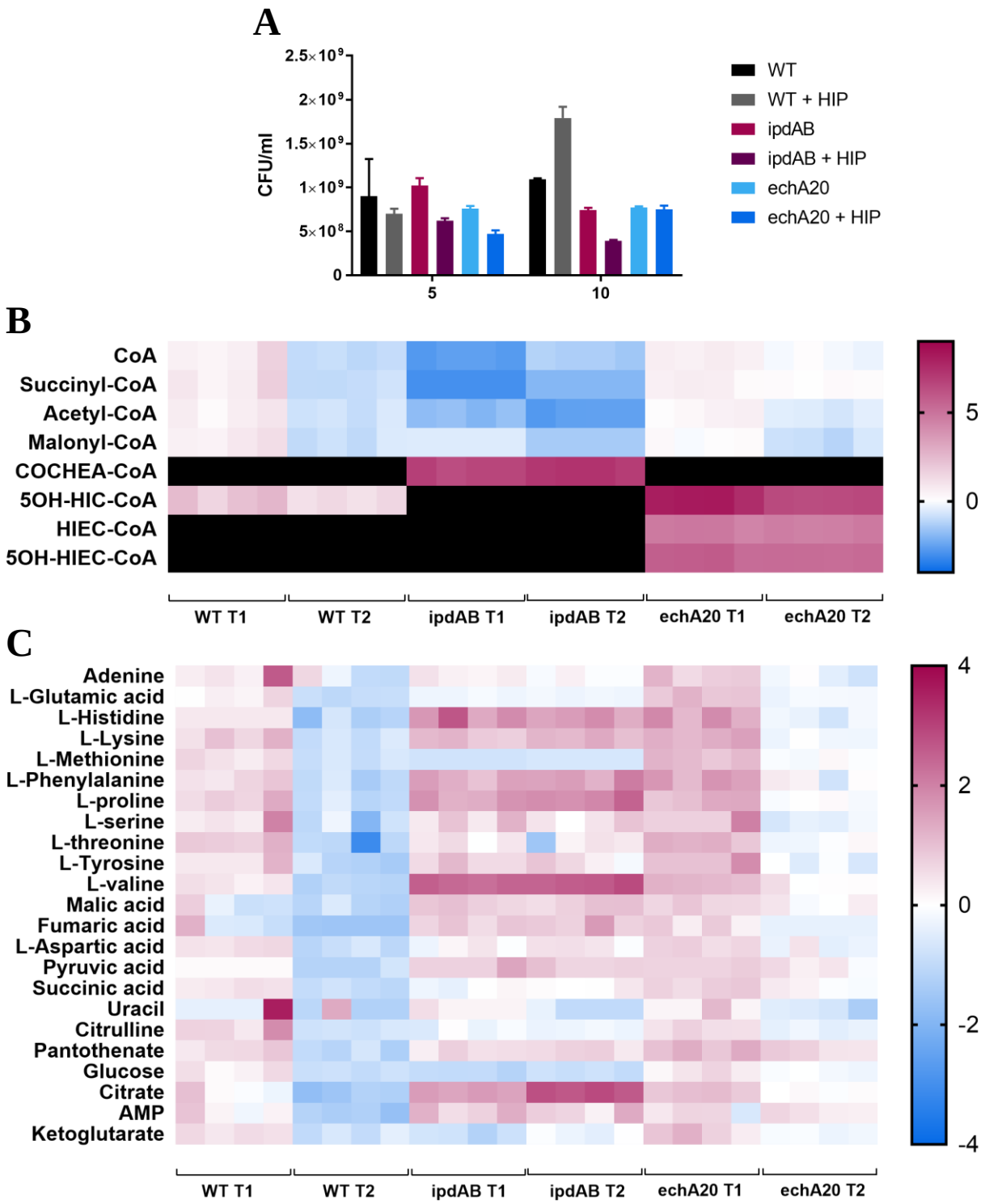

Figure 3.26 Metabolic dysregulation upon cholesterol-mediated CoA depletion. WT and mutant strains were grown on filters placed on 7H10 agar containing 4.5 mM glycerol alone or in combination with 0.3 mM HIP. At 5 hours (T1) and 10 hours (T2), CFU were enumerated (A) and LC-MS analysis was conducted for CoA metabolites (B) and other metabolites (C). Heat maps depict the Log_2 fold change in the presence of HIP of the peak intensities normalized to CFU/ml. Data represent four biological replicates for each strain under each condition.

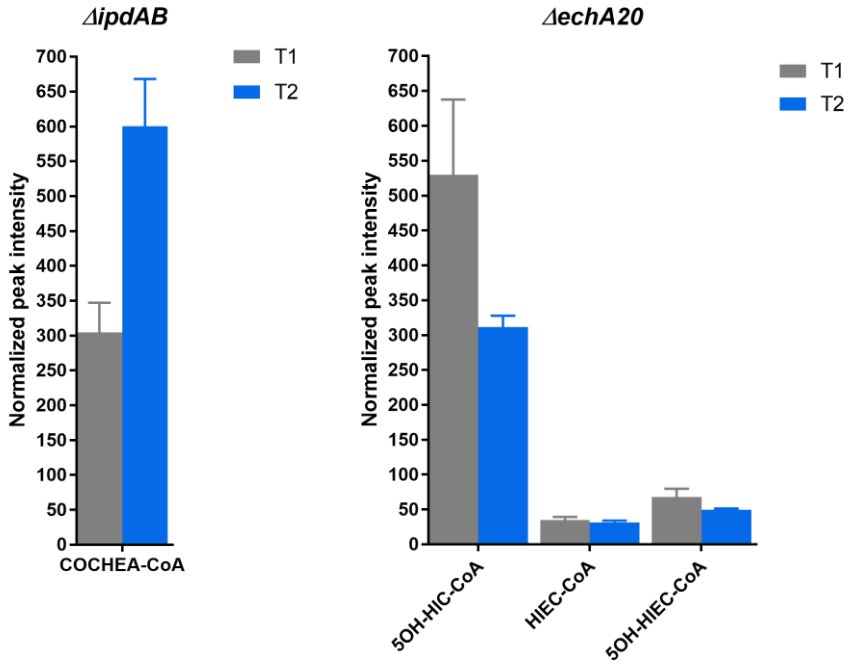

Figure 3.27 Cholesterol-derived CoA thioester accumulation in the metabolomes of *M. smegmatis* Δ*ipdAB* and Δ*echA20*. Strains were grown on filters placed on 7H10 agar containing 4.5 mM glycerol alone or in combination with 0.3 mM HIP. At 5 hours (T1) and 10 hours (T2), LC-MS analysis was conducted for CoA metabolites. Peak intensities were normalized to CFU/ml. Data represent four biological replicates for each strain under each condition, error bars are the standard error of the mean.

3.3.5 Pantothenate supplementation

In prokaryotes, CoA is synthesized in two stages: the biosynthesis of pantothenate, which then feeds into the biosynthesis of CoA. Sambandamurthy *et al.* demonstrated the essentiality of pantothenate biosynthesis *in vitro* and in infection models through the deletion of genes involved in pantothenate biosynthesis (173). Pantothenate supplementation rescued growth of strains lacking *panC* and *panD*, establishing that Mtb is able to assimilate exogenous pantothenate (173). Similarly, conditional knockdowns of genes involved in pantothenate and CoA biosynthesis were rescued through supplementation with pantothenate and pantetheine, respectively (181). Pantothenate supplementation has also been shown to antagonize the activity of pyrazinamide, a TB drug that decreases intracellular concentrations of pantothenate and CoA (200-202). Due to

the nature of cholesterol-dependent toxicity, we hypothesized that cholesterol-mediated CoA depletion could be eliminated by supplementing with pantothenate.

To determine if increasing intracellular CoA levels rescues the growth of KstR2-regulon mutants in the presence of cholesterol, we supplemented with pantothenate, a precursor for CoA biosynthesis. When the Δ*ipdAB* mutant was incubated with cholesterol, pantothenate supplementation increased CoA levels by 56% (Fig. 3.28A). However, growth in the presence of cholesterol was only slightly increased upon pantothenate supplementation (Fig. 3.28B). While supplementing with pantothenate did increase CoA levels in the Δ*ipdAB* mutant grown in the presence of cholesterol, it also led to a 25% increase in the accumulation of the cholesterol-derived CoA-thioester COCHEA-CoA (Fig. 3.28C). These data suggest that pantothenate supplementation can increase intracellular concentrations of CoA, but that the CoA is likely being sequestered by the cholesterol-derived CoA-thioester accumulation and therefore cannot rescue growth in the presence of cholesterol.

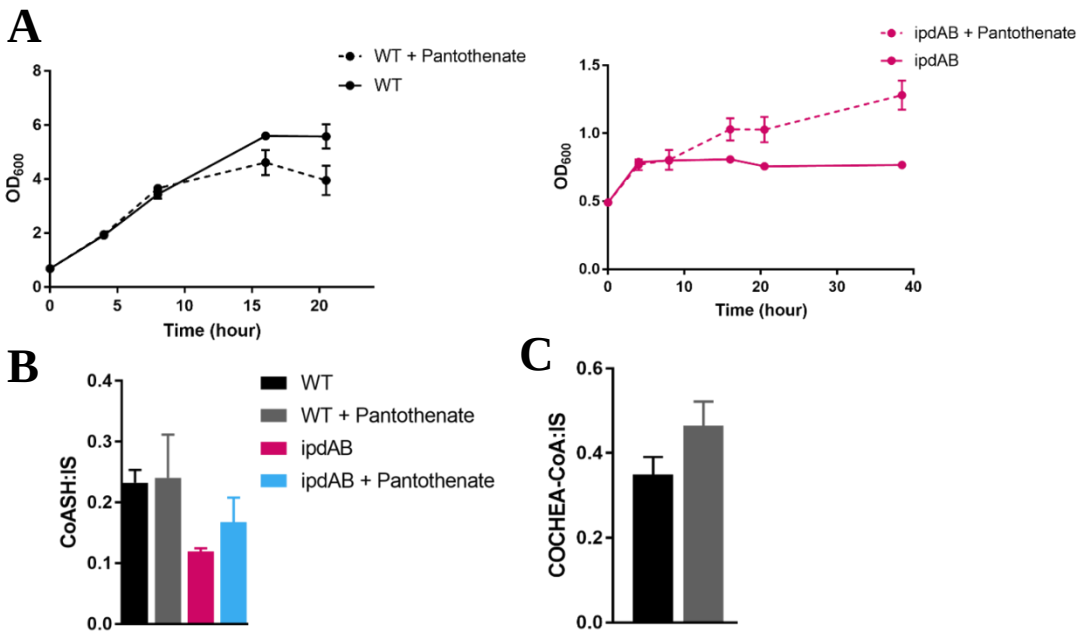

Figure 3.28 Pantothenate supplementation of the Δ*ipdAB* mutant of *M. smegmatis*. Strains were grown in 7H9 media containing 0.2% glycerol to mid-log phase and 0.5 mM cholesterol and 0.3 mM HIP were then added ± 1 mM pantothenate (A). CoA (B) and COCHEA-CoA (C) levels were measured by HPLC 20 hours after the addition of cholesterol and HIP. Metabolite abundance was normalized to the internal standard (IS) *p*-coumaroyl-CoA. Data represent the means of biological triplicates, error bars are the standard error of the mean.

Although pantothenate supplementation increased intracellular CoA levels in the Δ*ipdAB* *M. smegmatis* mutant grown in the presence of cholesterol, this supplementation was unable to abolish the toxic phenotype. Similar findings were reported by Parke *et al*: pantothenate supplementation was unable to rescue growth of the Δ*hcaC* mutant of ADP1 grown in the presence of *p*-coumarate (195). A possible explanation for the lack of rescue in strains that accumulate CoA-thioester metabolites is that while it is possible to increase CoA levels, the CoA is being utilized to generate more CoA-thioester rather than feeding into other essential cellular processes. Consistent with this hypothesis, the Δ*ipdAB M. smegmatis* mutant accumulated more COCHEA-CoA in the presence of cholesterol when supplemented with pantothenate. This contrasts with the rescue of mutants lacking pantothenate and CoA biosynthetic enzymes as the CoA produced as a result of supplementation should be readily available for cellular functions.

3.3.6 Overexpression of CoaA and CoaX

Based on the metabolic profiling of cholesterol-mediated CoA depletion, pantothenate is present in excess amounts in mutant strains incubated in the presence of cholesterol. The accumulation of pantothenate provides another explanation for the lack of rescue when the Δ*ipdAB* mutant was supplemented with pantothenate. To investigate if the excess amounts of pantothenate can be converted into CoA, we overexpressed *coaA* and *coaX* in the Δ*ipdAB M. smegmatis* mutant under tetracycline-inducible promoters. CoaA and CoaX are both pantothenate kinases which catalyze the first step in the production of CoA from pantothenate. The genes were cloned into a tetracycline-inducible expression vector and transformed into the unmarked Δ*ipdAB* and WT *M. smegmatis* strains. Neither enzyme rescued growth of the mutant strain in the presence of cholesterol (Fig. 3.29).

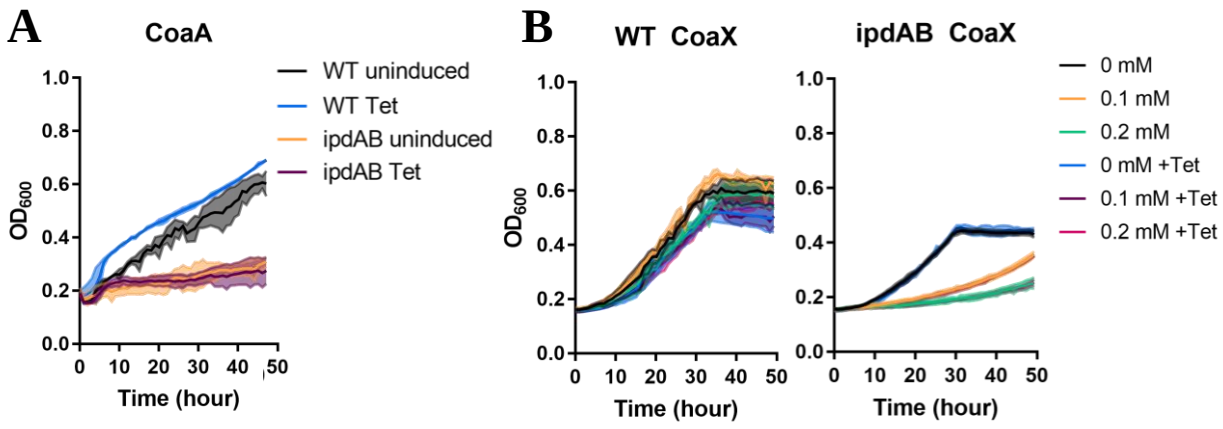

Figure 3.29 Expression of CoaA and CoaX does not rescue growth of Δ*ipdAB M. smegmatis* in the presence of cholesterol. (A) WT and Δ*ipdAB* Mtb harbouring pKWCoaA were grown in 7H9 medium supplemented with 10 mM acetate and 0.5 mM cholesterol with or without 10 ng/ml tetracycline. (B) WT and Δ*ipdAB* Mtb harbouring pKWCoaX were grown in 7H9 medium supplemented with 10 mM acetate with 0, 0.1, or 0.2 mM cholesterol with or without 10 ng/ml tetracycline. Cells were grown in 96-well plates and incubated at 37°C, shaking with am amplitude of 2.0 in a TECAN spark microplate reader. Data represent the mean of biological triplicates, error bars are the standard error of the mean.

3.3.7 *p*-coumarate-dependent toxicity in catabolic mutants of *R. jostii* RHA1

To investigate if CoA-thioester accumulation and subsequent CoA depletion occurs in other catabolic pathways, we used knockout strains in the soil actinobacterium *Rhodococcus jostii* RHA1, a species that is capable of degrading cholesterol as well as the aromatic compound *p*-coumarate (185). Catabolism of *p*-coumarate involves the production of CoA-thioester intermediates (Fig. 3.30A). Deletion of *couL*, which encodes the first enzyme in the pathway, did not lead to toxicity when the strain was grown on acetate in the presence of *p*-coumarate. Consistent with the inability to catabolize *p*-coumarate, the mutant strain grew to the same final OD_{600} as it did on acetate alone, while WT RHA1 catabolized both carbon sources leading to a higher growth yield (Fig. 3.30B). In contrast, deletion of *couO* abrogated the ability to grow on acetate in the presence of *p*-coumarate, consistent with the accumulation of a CoA-thioester metabolite and subsequent CoA depletion.

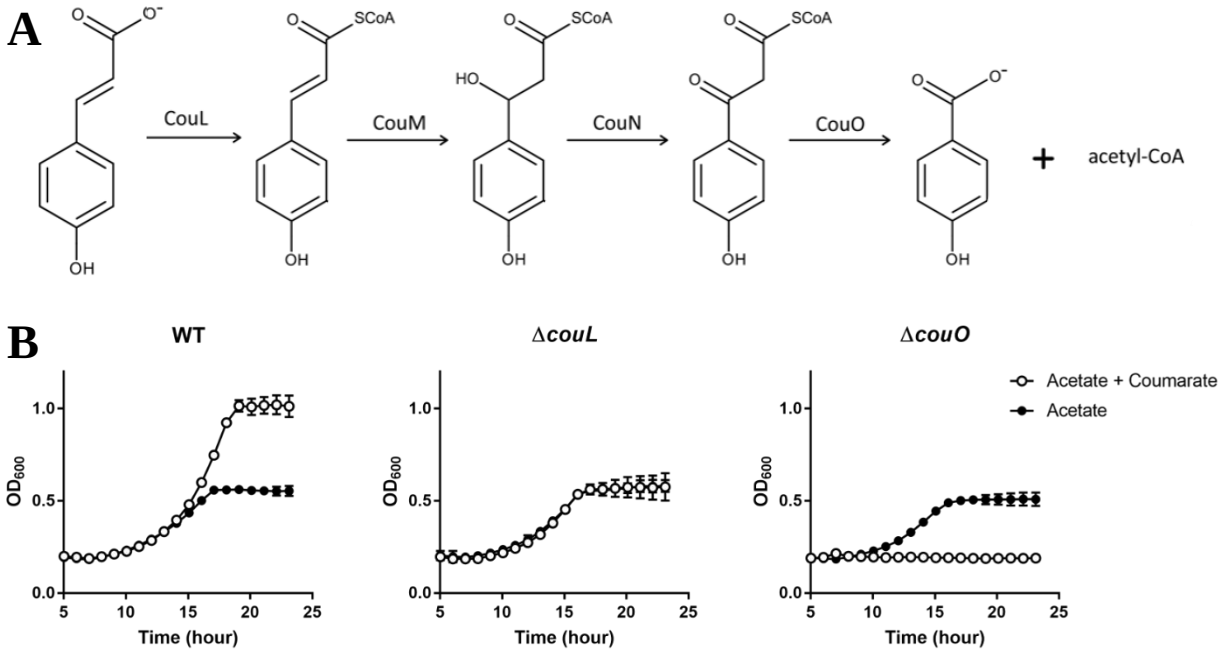

Figure 3.30 Catabolism of *p*-coumarate by *R. jostii* RHA1. The *p*-coumarate catabolic pathway in *R. jostii* RHA1 (A). WT, Δ*couO*, and Δ*couL* strains were grown in M9 medium supplemented with 10 mM acetate with or without 2.5 mM *p*-coumarate (B). Data represent the mean of biological triplicates, error bars are the standard error of the mean.

3.3.8 Catabolite repression of the *p*-coumarate catabolic pathway of *R. jostii* RHA1

Interestingly, the Δ*couO* strain did not show a toxic phenotype when grown on propionate in the presence of *p*-coumarate (Fig. 3.31A). To investigate the possibility of catabolite repression in which propionate inhibits *p*-coumarate catabolism, WT RHA1 was grown on *p*-coumarate alone or in combination with propionate, and substrate depletion was monitored by GC-MS. When grown on *p*-coumarate alone, the growth substrate was completely depleted from the culture supernatant by 20 hours (Fig. 3.31B). When grown on both carbon sources, *p*-coumarate was not catabolized until the 27-hour timepoint. These data demonstrate that the inhibition of *p*-coumarate catabolism by propionate rescues growth of the Δ*couO* mutant on propionate in the presence of *p*-coumarate.

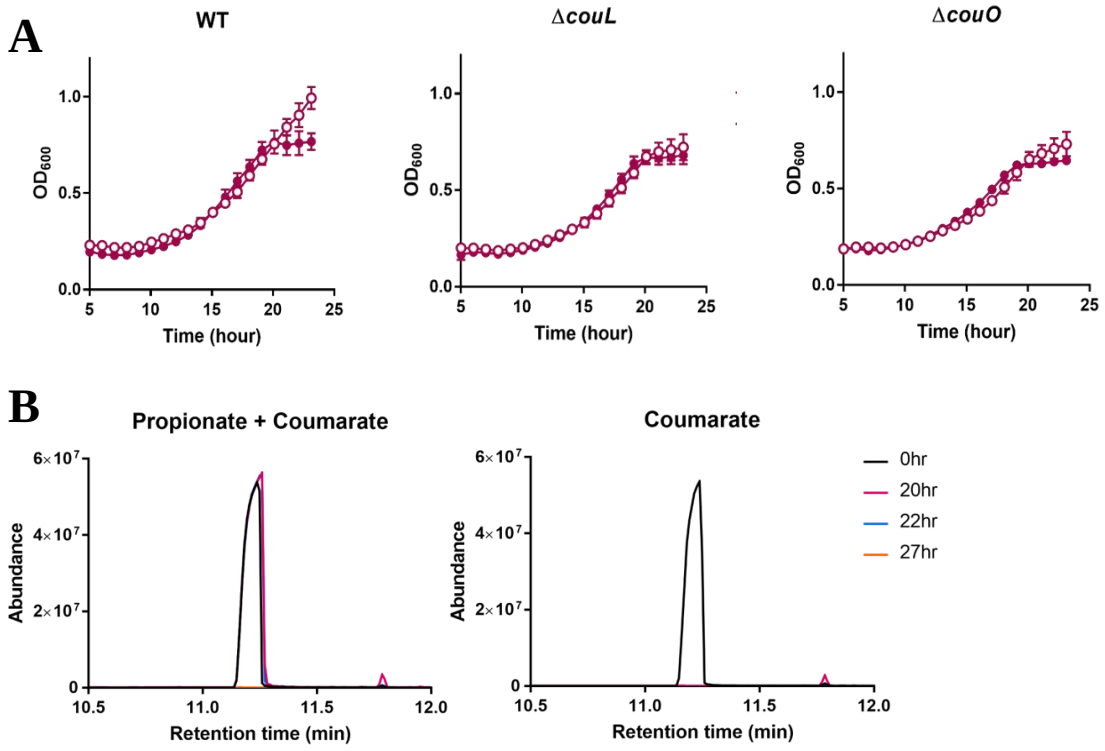

Figure 3.31 Catabolism of *p*-coumarate by *Rhodococcus jostii* RHA1. WT, Δ*couO*, and Δ*couL* strains were grown in M9 medium supplemented with 6.5 mM propionate with or without 2.5 mM *p*-coumarate (A). Depletion of *p*-coumarate from the supernatant of WT Mtb was measured by GC-MS (B). Data represent the mean of biological triplicates, error bars are the standard error of the mean.

Chapter 4: Discussion

The findings presented in this thesis provide insights into cholesterol catabolism in Mtb. These studies: (A) establish that catabolism of cholesterol rings C and D is important for the intracellular survival of Mtb and demonstrate that an inhibitor of intracellular Mtb growth specifically targets cholesterol catabolism (Chapter 3.1); (B) elucidate a post-translational regulatory mechanism controlling catabolism of cholesterol rings C and D (Chapter 3.2); and (D) characterize the mechanism of cholesterol-derived toxicity in catabolic mutants (Chapter 3.3).

4.1 The role of cholesterol catabolism in Mtb virulence

Cholesterol uptake and the catabolism of the sidechain and rings A and B have been shown to be important for the pathogenesis of Mtb (94, 95, 98, 99, 102, 138, 139, 157). With respect to the catabolism of rings C and D, a strain of the horse pathogen *R. equi* lacking the *ipdAB* genes is avirulent and is patented as a live vaccine (140). Further, transposon mutagenesis and transcriptomic studies implicate catabolism of cholesterol rings C and D in the pathogenesis of Mtb. However, this had not yet been explicitly demonstrated. The data presented in Chapter 3.1 builds on these studies and establishes that catabolism of cholesterol rings C and D is important for the intracellular survival of Mtb. Disruption of the genes encoding the rings C and D catabolizing enzyme IpdAB in Mtb inhibited growth on cholesterol and led to attenuated growth in THP-1 derived MΦs.

4.1.1 IpdAB as a drug target

Deletion of certain genes within the KstR2 regulon led to cholesterol-dependent toxicity, with the Δ*ipdAB* mutant showing the strongest phenotype as described in Chapter 3.3. The inability of the Δ*ipdAB* mutant to grow on alternative carbon sources in the presence of cholesterol makes

IpdAB an intriguing drug target. Cholesterol is abundant in infected macrophages and within the TB granuloma (13, 64). The findings described in this thesis suggest that while cholesterol normally represents a source of carbon and energy for Mtb during infection, the pathway can be exploited for the development of novel therapeutics which inhibit key enzymatic steps leading to toxicity. This novel strategy would therefore inhibit growth of the bacterium on other available carbon sources due to the depletion of free CoA and the resulting metabolic toxicity.

While IpdAB is an intriguing drug target for the treatment of TB, there are several potential caveats. FadD3 is the enzyme that initiates cholesterol rings C and D catabolism by producing the inducer for the KstR2 regulon (116, 136). Disruption of *fadD3* in the Δ*ipdAB* background in RHA1 has been shown to rescue growth in the presence of cholesterol and restore free CoA levels to that of WT, at least in a biotransformation approach (89). These findings suggest that there may be strong selection for suppressor mutations to occur in *fadD3* upon inhibition of IpdAB, thereby preventing the accumulation of cholesterol-derived CoA thioesters.

The findings described in Chapter 3.2 represent another potential caveat. Acetylation of FadD3 by MtPat inhibits enzymatic activity, and this presumably occurs under hypoxic conditions which are associated with cAMP production and MtPat activity. These findings suggest that under hypoxia, a condition the bacterium encounters during infection, the KstR2 regulon may not be completely active due to the acetylation of FadD3 and lack of production the inducer for the regulon. Under these circumstances, an inhibitor of IpdAB may be inactive. However, the Δ*ipdAB* mutant is extremely sensitive to cholesterol, showing toxicity at concentrations as low as 0.02 mM. It is therefore possible that small amounts of active FadD3 may be enough to generate COCHEA-CoA in concentrations high enough to cause CoA depletion. Furthermore, growth of the Δ*ipdAB*

mutant in THP-1 derived MΦs is impaired, which suggests that the KstR2 regulon is active during infection.

Multiple screens have been conducted to identify cholesterol-specific inhibitors of intracellular Mtb growth (139). Inhibitors of cholesterol rings C and D catabolism have yet to be identified, which is surprising given the strong toxic phenotypes in deletion mutants and the predicted essentiality of KstR2-regulated genes for virulence in infection models (97, 98). This represents a third challenge: a target-based approach may be necessary to develop inhibitors of IpdAB. Target-based approaches are met with confounding factors including compound permeation, efflux, metabolism and inactivation, and host cell toxicity and off-target effects. However, the enzyme has been well characterized and a crystal structure has been described (203). These data would aid in the design of IpdAB inhibitors.

While it is unclear if IpdAB is an ideal candidate for drug development, the ability to replicate the mechanism of toxicity in bacteria utilizing a different metabolic pathway as described in Chapter 3.3 suggests that the accumulation of CoA thioesters and subsequent CoA depletion is a therapeutic strategy that could be employed for the treatment of other bacterial infections. To determine if IpdAB is a strong candidate for TB drug development, further studies are needed including the evaluation of mutant strains in animal models of infection. Due to the potential of hypoxic conditions to interfere with rings C and D catabolism through post-translational regulation of FadD3, a model that more closely mimics the human granuloma such as the guinea pig or the Kramnik mouse would be ideal (204).

4.1.2 Rv1625c as a drug target

In contrast to rings C and D catabolizing enzymes, Rv1625c has been identified in multiple TB drug screens including the one described in Chapter 3.1 (139). The identification of several

compounds targeting this enzyme suggests that it is a promising target for the development of TB therapeutics. Compounds targeting Rv1625c appear to inhibit cholesterol catabolism indirectly. Rather than binding and inhibiting cholesterol catabolic enzymes, compounds like GSK286A described in Chapter 3.1 stimulate Rv1625c adenylyl cyclase activity leading to excessive production of cAMP. The lack of obvious cholesterol-derived metabolite accumulation in Mtb upon treatment with GSK286A suggests that cAMP does not inhibit a specific cholesterol catabolic enzyme, but that it may downregulate the pathway as a whole. Compounds with a similar mode of action were identified by VanderVen *et al* (2015) and were further characterized by Johnson *et al* (139, 205). Based on their molecular modeling experiments, compounds are predicted to act in a similar mechanism to the plant-derived diterpene forskolin, which is commonly used to stimulate mammalian ACs in cAMP signaling studies, by binding to the cytoplasmic catalytic domain (205). Further studies are therefore needed to elucidate the interaction between GSK286A and Rv1625c.

The mechanisms of regulation of cholesterol catabolism by cAMP has not yet been elucidated and may be governed at the transcriptional or post-transcriptional level. As described in Chapter 3.2, the cAMP-dependent *N*-acetyltransferase MtPat negatively regulates FadD3. These findings suggest that Rv1625c-mediated cAMP production following treatment with GSK286A may lead to acetylation and inactivation of FadD3 by MtPat. However, the lack of suppressor mutations occurring in the *rv0998*, the gene encoding MtPat, as well as the sensitivity of the Δ*mtpat* strain to GSK286A suggests that acetylation is not the mechanism of action of the compound.

The inhibitory effect of Rv1625c stimulation and cAMP production appears to contradict some previously reported findings. Shleeva *et al* demonstrated that overexpression of the Mtb adenylyl cyclase encoded by *rv2212* led to increased intracellular cAMP concentrations, and that

this led to enhanced virulence in a mouse model of infection (206). The authors postulated that the increased pathogenicity was due to the cAMP-mediated survival and recovery from dormancy. Furthermore, cAMP levels have been shown to increase ~50-fold in Mtb upon infection of MΦs, and this increase in cAMP does not correspond to bacterial cell death (166). Finally, Mtb is capable of excreting cAMP and has been shown to do so into the culture medium and into infected MΦs, possibly as a mechanism of immune modulation (23, 166). Whether Mtb is able to mitigate the effects of Rv1625c stimulation through cAMP secretion remains to be determined.

While several compounds targeting Rv1625c have been found to inhibit intracellular growth of Mtb, one potential caveat is that the enzyme itself is not essential for pathogenesis in infection models. This may increase the likelihood of mutations that inhibit enzymatic activity of Rv1625c, rendering compounds that stimulate the enzyme inactive. Studies using animal models are therefore necessary to confirm the potential of Rv1625c as a drug target for the development of novel antimycobacterial agents.

4.2 Post-translational regulation of cholesterol catabolism in Mtb

4.2.1 Post-translational regulation of FadD3

The findings presented in Chapter 3.2 reveal a previously undescribed mechanism of regulating cholesterol catabolism in Mtb. We demonstrated that the cAMP-dependent *N*-acetyltransferase MtPat acetylates and inactivates the acyl-CoA synthetase FadD3, and that the NAD^+-dependent deacetylase Rv1151c restores FadD3 activity. FadD3 catalyzes the first committed step in cholesterol Rings C and D degradation as the product of the reaction, HIP-CoA, is the inducer for the KstR2 regulon (116, 136). Once produced, HIP-CoA binds to KstR2 allowing for the expression of cholesterol Rings C and D degrading enzymes. As described in Chapter 3.3,

the reactions in this part of the pathway involve CoA thioesters and Mtb may use this mechanism to prevent the buildup of these metabolites, and thus the sequestration of CoASH, *in vivo*.

In addition to potentially preventing the buildup of CoA thioesters, FadD3 acetylation by MtPat may act to regulate central carbon metabolism under hypoxic conditions. Deletion of *mtpat* resulted in decreased survival under hypoxic conditions when incubated in the presence of cholesterol. This phenotype was also observed by Rittershaus *et al*. when the Δ*mtpat* strain was incubated under hypoxic conditions in the presence of fatty acids (152). Under hypoxia, Mtb shifts its central carbon metabolism and preferentially shunts carbon through the reductive TCA branch that converts malate to succinate, instead of the oxidative branch which converts citrate to α-ketoglutarate (42, 43, 152). Deletion of *mtpat* led to the continuous use of the oxidative branch of the TCA cycle, suggesting its importance in mediating this metabolic adaptation to hypoxia (152). It has been proposed that MtPat regulates fatty acid β-oxidation under hypoxic conditions to prevent the formation of acetyl-CoA which would feed the oxidative TCA cycle (152). Our findings suggest that Mtb regulates cholesterol catabolism using the same mechanism.

The preferential use of the reductive TCA by the WT strain has been proposed to be important for maintaining redox balance by regenerating NAD^+ (152). Consistent with this, Rittershaus *et al*. demonstrated a redox imbalance in the Δ*mtpat* mutant strain during hypoxia suggesting that deletion of *mtpat* leads to a buildup of NADH (152). Catabolism of fatty acids and cholesterol Rings C and D produces NADH, and in the absence of a terminal electron acceptor for the ETC under hypoxic conditions NAD^+ cannot be efficiently regenerated. Regulation of fatty acid and cholesterol catabolism by MtPat may function to prevent NADH buildup. Furthermore, preferential use of the reductive branch of the TCA cycle allows for NAD^+ regeneration and maintenance of the NADH/NAD^+ ratio.

We hypothesized that the inactivation of FadD3 by MtPat would lead to the production of HIP in the culture supernatant. However, when grown under hypoxic conditions in the presence of cholesterol, no HIP was detected by GC-MS (data not shown). These findings suggest that FadD3 may not be the only regulatory step. FadD19 is an acyl-CoA synthetase that is involved in the β-oxidation of the cholesterol sidechain. FadD19 does contain most of the conserved residues in the motifs identified among FadD enzymes known to be regulated by MtPat. However, it has a lysine instead of a glutamine in the GGXNX4EXE/D motif and a proline instead of a lysine in the PX4GK motif. While we did not detect acetylation of FadD19 *in vitro* (data not shown), it is possible FadD19 and other enzymes in the cholesterol catabolic pathway are subject to post-translational regulation.

4.3 Cholesterol-derived toxicity and Mtb pathogenesis

The current study establishes a model in which the inhibition of cholesterol rings C/D catabolizing enzymes leads to the accumulation of CoA-thioester metabolites, depletion of free CoA, and toxicity in the presence of cholesterol. Deletion of *ipdAB*, *ipdF*, and *echA20* led to varying degrees of cholesterol-dependent toxicity which correlated with the amount of CoA depletion. More specifically, deletion of *ipdAB* resulted in the strongest toxic phenotype. Growth of the Δ*ipdAB M. smegmatis* strain on alternative carbon sources was inhibited when cholesterol and the rings C/D-containing metabolite HIP were added at mid-log phase. The inhibition of growth corresponded with CoA depletion. In contrast, the Δ*ipdF* and Δ*echA20 M. smegmatis* strains were less susceptible when metabolite accumulation was induced at mid-log phase. The lack of toxicity was likely due to the hydrolysis of the accumulating CoA-thioesters and export of the carboxylate, thereby restoring intracellular CoA levels to that of the WT strain. Consistent with

this, 5-OH-HIC was detected in the culture supernatant of the Δ*ipdF* and Δ*echA20* strains. Interestingly, the Δ*ipdF* and Δ*echA20 M. smegmatis* strains were unable to grow on acetate or propionate when cholesterol was included in the culture media from the time of inoculation. These data suggest that exponentially dividing cells may have increased tolerance to perturbations in CoA levels compared to cells in lag phase. Parke *et al* described a similar cell density-dependent toxicity due to CoA-thioester accumulation in *Acinetobacter sp.* strain ADP1 (ADP1) (195). The authors demonstrated that deletion of *hcaC* in ADP1 accumulates *p*-coumaroyl-CoA in the presence of *p*-coumarate, leading to a toxic phenotype which is strongest when cultures are initiated at a lower cell density (195).

In contrast to the Δ*ipdAB*, Δ*ipdF*, and Δ*echA20* mutants, deletion of *fadD3* and *fadE32* in Mtb and *M. smegmatis*, respectively, did not cause cholesterol-dependent toxicity. In the case of Δ*fadD3* Mtb, the strain accumulated HIP, the substrate for FadD3, and was able to grow on the cholesterol sidechain and rings A/B. These data are consistent with the deletion of *fadD3* in *R. jostii* RHA1 (136). The lack of CoA-thioester accumulation and the absence of cholesterol-derived toxicity in Δ*fadD3* mutants is consistent with CoA-thioester accumulation mediating toxicity. The lack of toxicity in the Δ*fadE32 M. smegmatis* mutant was unexpected as FadE32 acts on a CoA-thioester substrate (89). The Δ*fadE32* mutant exports the carboxylate of the CoA-thioester substrate MOODA-CoA into the culture supernatant during growth in the presence of cholesterol. This is similar to the export of 5-OH-HIC by the Δ*ipdF* and Δ*echA20* strains, which rescues growth when cholesterol is added at mid-log phase. It is unclear why some cholesterol-derived CoA-thioesters are more readily hydrolyzed and exported over others. It is also unclear why the Δ*ipdF* and Δ*echA20* strains were able to export the carboxylate only when cholesterol was added at mid-log phase, while the Δ*fadE32* strain hydrolyzed MOODA-CoA and exported MOODA when

cholesterol was present in the media from the time of inoculation. Nevertheless, the hydrolysis and export of CoA-thioesters correlates with reduced toxicity and lack of CoA depletion.

Cholesterol-derived CoA-thioester accumulation led to the dysregulation of metabolic pathways, some of which are consistent with depletion of free CoA. Consistent with the findings of Evans *et al*., cholesterol-mediated CoA depletion resulted in depleted levels of succinyl-CoA, acetyl-CoA, and malonyl-CoA (181). Also consistent with the metabolic adaptations of CoA depletion described by Evans *et al*. was the depletion of α-ketoglutarate and methionine, and the accumulation of AMP (181). The accumulation of pyruvate and valine was consistent with a knockdown of *panB* and *panC*. In contrast to Evans *et al.*, our data demonstrated an increase in TCA cycle metabolites including citrate, fumarate, and malate, all of which were depleted upon knockdown of CoA biosynthetic genes. These differences may be attributed to the carbon sources used: glucose was used by Evans *et al.* while we used glycerol and the cholesterol metabolite HIP. Variation in the metabolomes of independent experiments was also observed by us and Evans *et al.*, which may also explain some of the discrepancies between the two data sets (181).

In prokaryotes, CoA is synthesized in two stages: the biosynthesis of pantothenate, which then feeds into the biosynthesis of CoA. Sambandamurthy *et al.* demonstrated the essentiality of pantothenate biosynthesis *in vitro* and in infection models through the deletion of genes involved in pantothenate biosynthesis (173). Pantothenate supplementation was found to rescue growth of strains lacking *panC* and *panD*, establishing that Mtb is able to assimilate exogenous pantothenate (173). Similarly, conditional knockdowns of genes involved in pantothenate and CoA biosynthesis were rescued through supplementation with pantothenate and pantetheine, respectively (181). Pantothenate supplementation has also been shown to antagonize the activity of pyrazinamide, a TB drug that decreases intracellular concentrations of pantothenate and CoA (200-202). Due to

the nature of cholesterol-dependent toxicity, we hypothesized that cholesterol-mediated CoA depletion could be eliminated by supplementing with pantothenate. While supplementation with pantothenate did increase intracellular CoA levels in the Δ*ipdAB M. smegmatis* mutant grown in the presence of cholesterol, it did not abolish the toxic phenotype. Similar findings were reported by Parke *et al*: pantothenate supplementation did not rescue growth of the Δ*hcaC* mutant of ADP1 grown in the presence of *p*-coumarate (195). A possible explanation for the lack of rescue in strains that accumulate CoA-thioester metabolites is that while it is possible to increase CoA levels, the CoA is being utilized to generate more CoA-thioester rather than feeding into other essential cellular processes. Consistent with this hypothesis, the Δ*ipdAB M. smegmatis* mutant accumulated more COCHEA-CoA in the presence of cholesterol when supplemented with pantothenate. This contrasts with the rescue of mutants lacking pantothenate and CoA biosynthetic enzymes as the CoA produced as a result of supplementation should be readily available for cellular functions.

The inability to rescue the growth of the Δ*ipdAB* mutant by restoring CoA levels makes it difficult to definitively confirm that CoA depletion is the mechanism of toxicity. Other mechanisms of toxicity remain a possibility. For example, HIP-derived CoA thioesters may have some innate toxicity. The restoration of growth seen upon the hydrolysis of the CoA thioesters and export of the carboxylate moieties is consistent with this mechanism of toxicity. Furthermore, certain enzymes are known to be regulated by CoA and its thioesters. For example, CoaA is negatively regulated by free CoA and acetyl-CoA (174, 175). It is therefore possible that the accumulation of cholesterol-derived CoA thioesters, and depletion of free CoA, acetyl-CoA, succinyl-CoA, and malonyl-CoA leads to the dysregulation of enzymes required for survival of Mtb. Finally, free CoA is a low-molecular-weight (LMW) thiol which may be involved in maintaining the redox state of the cell. Mycobacteria use LMW thiols ergothioneine, cysteine, and

mycothiol to serve as redox buffers, helping to maintain a reducing intracellular environment. Free CoA has recently been implicated in redox regulation through protein CoAlation, a post-translational modification involving disulfide bonds between CoA and cysteine residues (207). Extensive protein CoAlation has been observed in Gram-positive and Gram-negative bacteria and occurs in response to oxidative stress and starvation (208). In addition to sequestering free CoA from metabolic processes, cholesterol-mediated CoA depletion may also lead to redox imbalance.

The cholesterol catabolic pathway has been described as a promising target for the development of novel TB drugs (96, 103, 209, 210). Genes encoding cholesterol catabolic enzymes have been shown to be essential for pathogenesis in transposon mutagenesis studies in macrophages (98). These include the rings A/B degrading enzymes KstD, HsaD, and HsaA. Interestingly, cholesterol sidechain and rings A/B degradation have been shown to occur concurrently and the Rings A and B degrading enzyme KshAB shows higher specificity for substrates with partially degraded, CoA-thioesterified sidechains (130). These data suggest that KstD, HsaD, and HsaA may also have a preference for CoA thioester substrates and that mutant strains deficient in these enzymes may accumulate cholesterol-derived CoA thioesters. The Rings C and D catabolizing enzymes IpdA, IpdB, FadE31, and FadE32, all of which act on CoA thioester substrates, were also found to be essential for intracellular survival (98). The essentiality of FadE32 is inconsistent with our findings which show that deletion of *fadE32* in *M. smegmatis* does not result in cholesterol-dependent toxicity. A possible explanation for these inconsistencies is that *Mtb* may not have the capacity to hydrolyze the CoA thioester metabolite and export the carboxylate during infection like the *M. smegmatis* Δ*fadE32* strain does *in vitro*.

The results presented here establish a mechanism for cholesterol-derived toxicity in catabolic mutants. These data suggest that the inhibition of cholesterol catabolic enzymes may

prevent the utilization of an essential carbon source during infection while simultaneously depleting the essential cofactor CoA. The ability to replicate these findings in another catabolic pathway in another bacterium further suggests that targeting enzymes that act on CoA thioester substrates may have broader applicability to the development of novel therapeutics for the treatment of various bacterial pathogens.

4.4 Future directions

The findings presented in Chapter 3.1 demonstrate that production of cAMP inhibits growth of Mtb on cholesterol, however, the effect of cAMP on the cholesterol catabolic pathway remains to be elucidated. A carbon flux analysis using ^{13}C-labeled cholesterol may be useful in determining how cAMP dysregulates cholesterol catabolism, while a transcriptomics experiment would help determine if cAMP-mediated transcriptional dysregulation is involved.

This study focused on CoA depletion resulting from the deletion of genes within the KstR2 regulon. However, catabolism of the cholesterol sidechain and Rings A and B also involve CoA thioester metabolites. It has been demonstrated that sidechain and Rings A and B occurs concurrently, though to what extent remains to be determined. Metabolic profiles of mutant strains deficient in sidechain and Rings A and B degrading enzymes would provide insight into the extent that the two processes occur concurrently, and may also identify other steps that lead to CoA depletion when inhibited. Evaluation of cholesterol catabolic mutants that display varying degrees of CoA depletion in infection models would also provide insight into the importance of CoA depletion during infection.

The essentiality of cholesterol catabolizing enzymes for the virulence of Mtb indicate that the pathway is active during infection. However, it remains to be determined when during infection

the pathway is activated. Constructs in which fluorescent reporters are controlled by KstR- and KstR2-regulated promoters would help determine when the different parts of the cholesterol molecule are catabolized in infection models, and would also be a useful tool in the characterization of cholesterol-specific inhibitors.

Overall, this thesis describes the importance of cholesterol catabolism for the pathogenesis of Mtb, the regulation of cholesterol rings C and D catabolism through reversible lysine acetylation of FadD3, and the mechanism of cholesterol-derived toxicity in cholesterol catabolic mutants. The work in this thesis contributes to the understanding of cholesterol catabolism in Mtb and identifies a novel mechanism for the inhibition of Mtb growth during infection.

Bibliography

1. WHO, Global Tuberculosis Report. (2018).
2. S. Chakraborty, K. Y. Rhee, Tuberculosis Drug Development: History and Evolution of the Mechanism-Based Paradigm. *Cold Spring Harb Perspect Med* **5**, a021147 (2015).
3. K. Andries *et al.*, A diarylquinoline drug active on the ATP synthase of Mycobacterium tuberculosis. *Science* **307**, 223-227 (2005).
4. A. H. Diacon *et al.*, Randomized pilot trial of eight weeks of bedaquiline (TMC207) treatment for multidrug-resistant tuberculosis: long-term outcome, tolerability, and effect on emergence of drug resistance. *Antimicrob Agents Chemother* **56**, 3271-3276 (2012).
5. C. S. Hirsch, J. J. Ellner, D. G. Russell, E. A. Rich, Complement receptor-mediated uptake and tumor necrosis factor-alpha-mediated growth inhibition of Mycobacterium tuberculosis by human alveolar macrophages. *J Immunol* **152**, 743-753 (1994).
6. S. Sturgill-Koszycki *et al.*, Lack of acidification in Mycobacterium phagosomes produced by exclusion of the vesicular proton-ATPase. *Science* **263**, 678-681 (1994).
7. T. Ulrichs, S. H. Kaufmann, New insights into the function of granulomas in human tuberculosis. *J Pathol* **208**, 261-269 (2006).
8. J. L. Flynn, J. Chan, What's good for the host is good for the bug. *Trends Microbiol* **13**, 98-102 (2005).
9. H. M. Algood, P. L. Lin, J. L. Flynn, Tumor necrosis factor and chemokine interactions in the formation and maintenance of granulomas in tuberculosis. *Clin Infect Dis* **41 Suppl 3**, S189-193 (2005).
10. D. G. Russell, Who puts the tubercle in tuberculosis? *Nat Rev Microbiol* **5**, 39-47 (2007).
11. H. M. Algood, J. Chan, J. L. Flynn, Chemokines and tuberculosis. *Cytokine Growth Factor Rev* **14**, 467-477 (2003).
12. E. Guirado, L. S. Schlesinger, Modeling the Mycobacterium tuberculosis Granuloma - the Critical Battlefield in Host Immunity and Disease. *Front Immunol* **4**, 98 (2013).
13. M. J. Kim *et al.*, Caseation of human tuberculosis granulomas correlates with elevated host lipid metabolism. *EMBO Mol Med* **2**, 258-274 (2010).
14. M. C. Chao, E. J. Rubin, Letting sleeping dos lie: does dormancy play a role in tuberculosis? *Annu Rev Microbiol* **64**, 293-311 (2010).
15. R. A. Rienksma *et al.*, Comprehensive insights into transcriptional adaptation of intracellular mycobacteria by microbe-enriched dual RNA sequencing. *BMC Genomics* **16**, 34 (2015).
16. M. I. Voskuil, K. C. Visconti, G. K. Schoolnik, Mycobacterium tuberculosis gene expression during adaptation to stationary phase and low-oxygen dormancy. *Tuberculosis (Edinb)* **84**, 218-227 (2004).
17. L. G. Wayne, K. Y. Lin, Glyoxylate metabolism and adaptation of Mycobacterium tuberculosis to survival under anaerobic conditions. *Infect Immun* **37**, 1042-1049 (1982).
18. T. Lillebaek *et al.*, Molecular evidence of endogenous reactivation of Mycobacterium tuberculosis after 33 years of latent infection. *J Infect Dis* **185**, 401-404 (2002).
19. R. S. Wallis *et al.*, Drug tolerance in Mycobacterium tuberculosis. *Antimicrob Agents Chemother* **43**, 2600-2606 (1999).
20. K. Lewis, Persister cells, dormancy and infectious disease. *Nat Rev Microbiol* **5**, 48-56 (2007).

21. N. H. Smith, R. G. Hewinson, K. Kremer, R. Brosch, S. V. Gordon, Myths and misconceptions: the origin and evolution of Mycobacterium tuberculosis. *Nat Rev Microbiol* **7**, 537-544 (2009).
22. E. C. Hett, E. J. Rubin, Bacterial growth and cell division: a mycobacterial perspective. *Microbiol Mol Biol Rev* **72**, 126-156, table of contents (2008).
23. N. Agarwal, G. Lamichhane, R. Gupta, S. Nolan, W. R. Bishai, Cyclic AMP intoxication of macrophages by a Mycobacterium tuberculosis adenylate cyclase. *Nature* **460**, 98-102 (2009).
24. J. G. Holt, N. R. Krieg, P. H. A. Sneath, J. T. Staley, S. T. Williams, *Bergey's manual of determinative bacteriology* (William & Wilkins, Baltimore, MD, ed. 9th, 1994).
25. C. Goffin, J. M. Ghuysen, Multimodular penicillin-binding proteins: an enigmatic family of orthologs and paralogs. *Microbiol Mol Biol Rev* **62**, 1079-1093 (1998).
26. A. Quémard *et al.*, Enzymatic characterization of the target for isoniazid in Mycobacterium tuberculosis. *Biochemistry* **34**, 8235-8241 (1995).
27. C. E. Barry *et al.*, Mycolic acids: structure, biosynthesis and physiological functions. *Prog Lipid Res* **37**, 143-179 (1998).
28. M. L. Schaeffer *et al.*, Purification and biochemical characterization of the Mycobacterium tuberculosis beta-ketoacyl-acyl carrier protein synthases KasA and KasB. *J Biol Chem* **276**, 47029-47037 (2001).
29. L. Kremer *et al.*, Mycolic acid biosynthesis and enzymic characterization of the beta-ketoacyl-ACP synthase A-condensing enzyme from Mycobacterium tuberculosis. *Biochem J* **364**, 423-430 (2002).
30. H. Marrakchi, M. A. Lanéelle, M. Daffé, Mycolic acids: structures, biosynthesis, and beyond. *Chem Biol* **21**, 67-85 (2014).
31. P. J. Brennan, G. S. Besra, Structure, function and biogenesis of the mycobacterial cell wall. *Biochem Soc Trans* **25**, 188-194 (1997).
32. R. B. S. T. Cole , J. Parkhill , T. Garnier , C. Churcher , D. Harris , S. V. Gordon , K. Eiglmeier , S. Gas , C. E. Barry III , F. Tekaia , K. Badcock , D. Basham , D. Brown , T. Chillingworth , R. Connor , R. Davies , K. Devlin , T. Feltwell , S. Gentles , N. Hamlin , S. Holroyd , T. Hornsby , K. Jagels , A. Krogh , J. McLean , S. Moule , L. Murphy , K. Oliver , J. Osborne , M. A. Quail , M.-A. Rajandream , J. Rogers , S. Rutter , K. Seeger , J. Skelton , R. Squares , S. Squares , J. E. Sulston , K. Taylor , S. Whitehead & B. G. Barrell, Deciphering the biology of *Mycobacterium tuberculosis* from the complete genome sequence. *Nature* **393**, 537-544 (1998).
33. G. JE, M. JD., M. tuberculosis persistence, latency, and drug tolerance. *Tuberculosis (Edinb)* **84**, 29-44 (2004).
34. H. I. Boshoff, C. E. Barry, Tuberculosis - metabolism and respiration in the absence of growth. *Nat Rev Microbiol* **3**, 70-80 (2005).
35. S. Rao, S. Alonso, L. Rand, T. Dick, K. Pethe, The protonmotive force is required for maintaining ATP homeostasis and viability of hypoxic, nonreplicating Mycobacterium tuberculosis. *Proc Natl Acad Sci USA* **105**, 11945–11950 (2008).
36. L. E. Via *et al.*, Tuberculous granulomas are hypoxic in guinea pigs, rabbits, and nonhuman primates. *Infect Immun* **76**, 2333–2340 (2008).
37. D. R. Sherman *et al.*, Regulation of the Mycobacterium tuberculosis hypoxic response gene encoding alpha -crystallin. *Proc Natl Acad Sci USA* **98**, 7534–7539 (2001).

38. D. M. Roberts, R. P. Liao, G. Wisedchaisri, W. G. Hol, D. R. Sherman, Two sensor kinases contribute to the hypoxic response of Mycobacterium tuberculosis. *J Biol Chem* **279**, 23082-23087 (2004).
39. R. L. Leistikow *et al.*, The Mycobacterium tuberculosis DosR regulon assists in metabolic homeostasis and enables rapid recovery from nonrespiring dormancy. *J Bacteriol* **192**, 1662-1670 (2010).
40. H. D. Park *et al.*, Rv3133c/dosR is a transcription factor that mediates the hypoxic response of Mycobacterium tuberculosis. *Mol Microbiol* **48**, 833-843 (2003).
41. T. R. Rustad, M. I. Harrell, R. Liao, D. R. Sherman, The enduring hypoxic response of Mycobacterium tuberculosis. *PLoS One* **3**, e1502 (2008).
42. S. Watanabe *et al.*, Fumarate reductase activity maintains an energized membrane in anaerobic Mycobacterium tuberculosis. *PLoS Pathog* **7**, e1002287 (2011).
43. H. Eoh, K. Y. Rhee, Multifunctional essentiality of succinate metabolism in adaptation to hypoxia in Mycobacterium tuberculosis. *Proc Natl Acad Sci U S A* **110**, 6554-6559 (2013).
44. J. J. De Voss, K. Rutter, B. G. Schroeder, C. E. Barry, 3rd, Iron acquisition and metabolism by mycobacteria. *J Bacteriol* **181**, 4443-4451 (1999).
45. G. M. Rodriguez, I. Smith, Identification of an ABC transporter required for iron acquisition and virulence in Mycobacterium tuberculosis. *J Bacteriol* **188**, 424-430 (2006).
46. C. M. Sassetti, E. J. Rubin, Genetic requirements for mycobacterial survival during infection. *Proc Natl Acad Sci U S A* **100**, 12989-12994 (2003).
47. P. V. Reddy *et al.*, Disruption of mycobactin biosynthesis leads to attenuation of Mycobacterium tuberculosis for growth and virulence. *J Infect Dis* **208**, 1255-1265 (2013).
48. G. M. Rodriguez, I. Smith, Mechanisms of iron regulation in mycobacteria: role in physiology and virulence. *Mol Microbiol* **47**, 1485-1494 (2003).
49. P. A. Lazaridis, A. P. Fotopoulos, S. A. Karakoulia, K. S. Triantafyllidis, Catalytic Fast Pyrolysis of Kraft Lignin With Conventional, Mesoporous and Nanosized ZSM-5 Zeolite for the Production of Alkyl-Phenols and Aromatics. *Frontiers in Chemistry* **6** (2018).
50. V. H. Ng, J. S. Cox, A. O. Sousa, J. D. MacMicking, J. D. McKinney, Role of KatG catalase-peroxidase in mycobacterial pathogenesis: countering the phagocyte oxidative burst. *Mol Microbiol* **52**, 1291-1302 (2004).
51. K. D. Green *et al.*, Acetylation by Eis and Deacetylation by Rv1151c of Mycobacterium tuberculosis HupB: Biochemical and Structural Insight. *Biochemistry* **57**, 781-790 (2018).
52. D. L. Piddington *et al.*, Cu,Zn superoxide dismutase of Mycobacterium tuberculosis contributes to survival in activated macrophages that are generating an oxidative burst. *Infect Immun* **69**, 4980-4987 (2001).
53. K. M. Edwards *et al.*, Iron-cofactored superoxide dismutase inhibits host responses to Mycobacterium tuberculosis. *Am J Respir Crit Care Med* **164**, 2213-2219 (2001).
54. N. Buchmeier, R. C. Fahey, The mshA gene encoding the glycosyltransferase of mycothiol biosynthesis is essential in Mycobacterium tuberculosis Erdman. *FEMS Microbiol Lett* **264**, 74-79 (2006).
55. C. J. Queval *et al.*, Mycobacterium tuberculosis Controls Phagosomal Acidification by Targeting CISH-Mediated Signaling. *Cell Rep* **20**, 3188-3198 (2017).

56. D. Wong, H. Bach, J. Sun, Z. Hmama, Y. Av-Gay, Mycobacterium tuberculosis protein tyrosine phosphatase (PtpA) excludes host vacuolar-H+-ATPase to inhibit phagosome acidification. *Proc Natl Acad Sci U S A* **108**, 19371-19376 (2011).
57. K. Pethe *et al.*, Isolation of Mycobacterium tuberculosis mutants defective in the arrest of phagosome maturation. *Proc Natl Acad Sci U S A* **101**, 13642-13647 (2004).
58. J. A. Philips, J. D. Ernst, Tuberculosis pathogenesis and immunity. *Annu Rev Pathol* **7**, 353-384 (2012).
59. O. H. Vandal, L. M. Pierini, D. Schnappinger, C. F. Nathan, S. Ehrt, A membrane protein preserves intrabacterial pH in intraphagosomal Mycobacterium tuberculosis. *Nat Med* **14**, 849-854 (2008).
60. O. H. Vandal, C. F. Nathan, S. Ehrt, Acid resistance in Mycobacterium tuberculosis. *J Bacteriol* **191**, 4714-4721 (2009).
61. S. B. Walters *et al.*, The Mycobacterium tuberculosis PhoPR two-component system regulates genes essential for virulence and complex lipid biosynthesis. *Mol Microbiol* **60**, 312-330 (2006).
62. J. J. Baker, B. K. Johnson, R. B. Abramovitch, Slow growth of Mycobacterium tuberculosis at acidic pH is regulated by phoPR and host-associated carbon sources. *Mol Microbiol* **94**, 56-69 (2014).
63. L. Shi *et al.*, Carbon flux rerouting during Mycobacterium tuberculosis growth arrest. *Mol Microbiol* **78**, 1199-1215 (2010).
64. E. V. Nazarova *et al.*, Rv3723/LucA coordinates fatty acid and cholesterol uptake in Mycobacterium tuberculosis. *Elife* **6** (2017).
65. D. Schnappinger *et al.*, Transcriptional Adaptation of Mycobacterium tuberculosis within Macrophages: Insights into the Phagosomal Environment. *J Exp Med* **198**, 693-704 (2003).
66. E. J. Munoz-Elias, A. M. Upton, J. Cherian, J. D. McKinney, Role of the methylcitrate cycle in Mycobacterium tuberculosis metabolism, intracellular growth, and virulence. *Mol Microbiol* **60**, 1109-1122 (2006).
67. S. Savvi *et al.*, Functional characterization of a vitamin B12-dependent methylmalonyl pathway in Mycobacterium tuberculosis: implications for propionate metabolism during growth on fatty acids. *J Bacteriol* **190**, 3886-3895 (2008).
68. A. M. Upton, J. D. McKinney, Role of the methylcitrate cycle in propionate metabolism and detoxification in Mycobacterium smegmatis. *Microbiology* **153**, 3973-3982 (2007).
69. M. Jain *et al.*, Lipidomics reveals control of Mycobacterium tuberculosis virulence lipids via metabolic coupling. *Proc Natl Acad Sci U S A* **104**, 5133-5138 (2007).
70. D. G. Russell *et al.*, Mycobacterium tuberculosis wears what it eats. *Cell Host Microbe* **8**, 68-76 (2010).
71. K. H. Rohde, D. F. Veiga, S. Caldwell, G. Balazsi, D. G. Russell, Linking the transcriptional profiles and the physiological states of Mycobacterium tuberculosis during an extended intracellular infection. *PLoS Pathog* **8**, e1002769 (2012).
72. W. Lee, B. C. VanderVen, R. J. Fahey, D. G. Russell, Intracellular Mycobacterium tuberculosis exploits host-derived fatty acids to limit metabolic stress. *J Biol Chem* **288**, 6788-6800 (2013).

73. L. S. Schlesinger, Macrophage phagocytosis of virulent but not attenuated strains of Mycobacterium tuberculosis is mediated by mannose receptors in addition to complement receptors. *J Immunol* **150**, 2920-2930 (1993).
74. K. E. Killick *et al.*, Receptor-mediated recognition of mycobacterial pathogens. *Cell Microbiol* **15**, 1484-1495 (2013).
75. B. J. Appelmelk *et al.*, The mannose cap of mycobacterial lipoarabinomannan does not dominate the Mycobacterium-host interaction. *Cell Microbiol* **10**, 930-944 (2008).
76. K. V. Sawant, D. N. McMurray, Guinea pig neutrophils infected with Mycobacterium tuberculosis produce cytokines which activate alveolar macrophages in noncontact cultures. *Infect Immun* **75**, 1870-1877 (2007).
77. A. Gupta, A. Kaul, A. G. Tsolaki, U. Kishore, S. Bhakta, Mycobacterium tuberculosis: immune evasion, latency and reactivation. *Immunobiology* **217**, 363-374 (2012).
78. M. V. Carroll, N. Lack, E. Sim, A. Krarup, R. B. Sim, Multiple routes of complement activation by Mycobacterium bovis BCG. *Mol Immunol* **46**, 3367-3378 (2009).
79. E. Torrado, A. M. Cooper, IL-17 and Th17 cells in tuberculosis. *Cytokine Growth Factor Rev* **21**, 455-462 (2010).
80. A. M. Caruso *et al.*, Mice deficient in CD4 T cells have only transiently diminished levels of IFN-gamma, yet succumb to tuberculosis. *J Immunol* **162**, 5407-5416 (1999).
81. M. Sester, C. Giehl, U. Sester, A. Meyerhans, "Management of tuberculosis in HIV infection: where T-cells matter" in Eur Respir J. (England, 2010), vol. 35, pp. 475-476.
82. J. M. Tufariello, J. Chan, J. L. Flynn, Latent tuberculosis: mechanisms of host and bacillus that contribute to persistent infection. *Lancet Infect Dis* **3**, 578-590 (2003).
83. J. M. Achkar, J. Chan, A. Casadevall, Role of B cells and antibodies in acquired immunity against Mycobacterium tuberculosis. *Cold Spring Harb Perspect Med* **5**, a018432 (2014).
84. D. F. Warner, Mycobacterium tuberculosis metabolism. *Cold Spring Harb Perspect Med* **5** (2014).
85. N. J. Garton *et al.*, Cytological and transcript analyses reveal fat and lazy persister-like bacilli in tuberculous sputum. *PLoS Med* **5**, e75 (2008).
86. D. A. Aguilar-Ayala *et al.*, The transcriptome of Mycobacterium tuberculosis in a lipid-rich dormancy model through RNAseq analysis. *Sci Rep* **7**, 17665 (2017).
87. M. F. Wipperman, N. S. Sampson, S. T. Thomas, Pathogen roid rage: cholesterol utilization by Mycobacterium tuberculosis. *Crit Rev Biochem Mol Biol* **49**, 269-293 (2014).
88. P. Fontán, V. Aris, S. Ghanny, P. Soteropoulos, I. Smith, Global transcriptional profile of Mycobacterium tuberculosis during THP-1 human macrophage infection. *Infect Immun* **76**, 717-725 (2008).
89. A. M. Crowe *et al.*, Catabolism of the Last Two Steroid Rings in. *MBio* **8** (2017).
90. J. PaweŁczyk, L. Kremer, The Molecular Genetics of Mycolic Acid Biosynthesis. *Microbiol Spectr* **2**, MGM2-0003-2013 (2014).
91. D. E. Minnikin, L. Kremer, L. G. Dover, G. S. Besra, The methyl-branched fortifications of Mycobacterium tuberculosis. *Chem Biol* **9**, 545-553 (2002).
92. V. Jarlier, H. Nikaido, Mycobacterial cell wall: structure and role in natural resistance to antibiotics. *FEMS Microbiol Lett* **123**, 11-18 (1994).

93. L. Nguyen, J. Pieters, Mycobacterial subversion of chemotherapeutic reagents and host defense tactics: challenges in tuberculosis drug development. *Annu Rev Pharmacol Toxicol* **49**, 427-453 (2009).
94. A. K. Pandey, C. M. Sassetti, Mycobacterial persistence requires the utilization of host cholesterol. *Proc Natl Acad Sci U S A* **105**, 4376-4380 (2008).
95. K. C. Yam *et al.*, Studies of a ring-cleaving dioxygenase illuminate the role of cholesterol metabolism in the pathogenesis of Mycobacterium tuberculosis. *PLoS Pathog* **5**, e1000344 (2009).
96. H. Ouellet, J. B. Johnston, P. R. de Montellano, Cholesterol catabolism as a therapeutic target in Mycobacterium tuberculosis. *Trends Microbiol* **19**, 530-539 (2011).
97. J. E. Griffin *et al.*, High-resolution phenotypic profiling defines genes essential for mycobacterial growth and cholesterol catabolism. *PLoS Pathog* **7**, e1002251 (2011).
98. J. Rengarajan, B. R. Bloom, E. J. Rubin, Genome-wide requirements for Mycobacterium tuberculosis adaptation and survival in macrophages. *Proc Natl Acad Sci U S A* **102**, 8327-8332 (2005).
99. N. M. Nesbitt *et al.*, A thiolase of Mycobacterium tuberculosis is required for virulence and production of androstenedione and androstadienedione from cholesterol. *Infect Immun* **78**, 275-282 (2010).
100. J. E. Griffin *et al.*, Cholesterol catabolism by Mycobacterium tuberculosis requires transcriptional and metabolic adaptations. *Chem Biol* **19**, 218-227 (2012).
101. A. Brzostek, B. Dziadek, A. Rumijowska-Galewicz, J. Pawelczyk, J. Dziadek, Cholesterol oxidase is required for virulence of Mycobacterium tuberculosis. *FEMS Microbiol Lett* **275**, 106-112 (2007).
102. Y. Hu *et al.*, 3-Ketosteroid 9alpha-hydroxylase is an essential factor in the pathogenesis of Mycobacterium tuberculosis. *Mol Microbiol* **75**, 107-121 (2010).
103. A. Ryan *et al.*, Investigation of the mycobacterial enzyme HsaD as a potential novel target for anti-tubercular agents using a fragment-based drug design approach. *Br J Pharmacol* **174**, 2209-2224 (2017).
104. A. M. Crowe (2018) The catabolism of the last two rings of cholesterol by *Mycobacterium tuberculosis*. (University of British Columbia).
105. S. Raffy, J. Teissie, Control of lipid membrane stability by cholesterol content. *Biophys J* **76**, 2072-2080 (1999).
106. E. Ikonen, Cellular cholesterol trafficking and compartmentalization. *Nat Rev Mol Cell Biol* **9**, 125-138 (2008).
107. A. Birkenmaier *et al.*, Biochemical and genetic investigation of initial reactions in aerobic degradation of the bile acid cholate in Pseudomonas sp. strain Chol1. *J Bacteriol* **189**, 7165-7173 (2007).
108. A. Hartlova, L. Cerveny, M. Hubalek, Z. Krocova, J. Stulik, Membrane rafts: a potential gateway for bacterial entry into host cells. *Microbiol Immunol* **54**, 237-245 (2010).
109. J. M. Ridlon, D. J. Kang, P. B. Hylemon, J. S. Bajaj, Bile acids and the gut microbiome. *Curr Opin Gastroenterol* **30**, 332-338 (2014).
110. K. Kieslich, Microbial side-chain degradation of sterols. *J Basic Microbiol* **25**, 461-474 (1985).
111. X. Zhang, Z. Rao, L. Zhang, M. Xu, T. Yang, Efficient 9alpha-hydroxy-4-androstene-3,17-dione production by engineered Bacillus subtilis co-expressing Mycobacterium

neoaurum 3-ketosteroid 9alpha-hydroxylase and B. subtilis glucose 1-dehydrogenase with NADH regeneration. *Springerplus* **5**, 1207 (2016).
112. R. Van der Geize *et al.*, A gene cluster encoding cholesterol catabolism in a soil actinomycete provides insight into Mycobacterium tuberculosis survival in macrophages. *Proc Natl Acad Sci U S A* **104**, 1947-1952 (2007).
113. S. L. Kendall *et al.*, Cholesterol utilization in mycobacteria is controlled by two TetR-type transcriptional regulators: kstR and kstR2. *Microbiology* **156**, 1362-1371 (2010).
114. S. L. Kendall *et al.*, A highly conserved transcriptional repressor controls a large regulon involved in lipid degradation in Mycobacterium smegmatis and Mycobacterium tuberculosis. *Mol Microbiol* **65**, 684-699 (2007).
115. N. A. Ho *et al.*, The Structure of the Transcriptional Repressor KstR in Complex with CoA Thioester Cholesterol Metabolites Sheds Light on the Regulation of Cholesterol Catabolism in Mycobacterium tuberculosis. *J Biol Chem* **291**, 7256-7266 (2016).
116. I. Casabon *et al.*, Regulation of the KstR2 regulon of Mycobacterium tuberculosis by a cholesterol catabolite. *Mol Microbiol* **89**, 1201-1212 (2013).
117. D. C. Ekiert *et al.*, Architectures of Lipid Transport Systems for the Bacterial Outer Membrane. *Cell* **169**, 273-285.e217 (2017).
118. S. Arruda, G. Bomfim, R. Knights, T. Huima-Byron, L. W. Riley, Cloning of an M. tuberculosis DNA fragment associated with entry and survival inside cells. *Science* **261**, 1454-1457 (1993).
119. N. Casali, L. W. Riley, A phylogenomic analysis of the Actinomycetales mce operons. *BMC Genomics* **8**, 60 (2007).
120. L. I. Klepp *et al.*, Impact of the deletion of the six mce operons in Mycobacterium smegmatis. *Microbes Infect* **14**, 590-599 (2012).
121. R. H. Senaratne *et al.*, Mycobacterium tuberculosis strains disrupted in mce3 and mce4 operons are attenuated in mice. *J Med Microbiol* **57**, 164-170 (2008).
122. J. Capyk (2012) Iron-containing monooxygenases in Mycobacterium tuberculosis cholesterol degradation: biochemical and phylogenetic perspectives. (University of British Columbia).
123. J. K. Capyk, I. D'Angelo, N. C. Strynadka, L. D. Eltis, Characterization of 3-ketosteroid 9{alpha}-hydroxylase, a Rieske oxygenase in the cholesterol degradation pathway of Mycobacterium tuberculosis. *J Biol Chem* **284**, 9937-9946 (2009).
124. M. D. Driscoll *et al.*, Structural and biochemical characterization of Mycobacterium tuberculosis CYP142: evidence for multiple cholesterol 27-hydroxylase activities in a human pathogen. *J Biol Chem* **285**, 38270-38282 (2010).
125. J. K. Capyk *et al.*, Mycobacterial cytochrome p450 125 (cyp125) catalyzes the terminal hydroxylation of c27 steroids. *J Biol Chem* **284**, 35534-35542 (2009).
126. I. Casabon, K. Swain, A. M. Crowe, L. D. Eltis, W. W. Mohn, Actinobacterial acyl coenzyme A synthetases involved in steroid side-chain catabolism. *J Bacteriol* **196**, 579-587 (2014).
127. M. F. Wipperman, M. Yang, S. T. Thomas, N. S. Sampson, Shrinking the FadE proteome of Mycobacterium tuberculosis: insights into cholesterol metabolism through identification of an alpha2beta2 heterotetrameric acyl coenzyme A dehydrogenase family. *J Bacteriol* **195**, 4331-4341 (2013).

128. M. Yang *et al.*, Unraveling Cholesterol Catabolism in Mycobacterium tuberculosis: ChsE4-ChsE5 alpha2beta2 Acyl-CoA Dehydrogenase Initiates beta-Oxidation of 3-Oxo-cholest-4-en-26-oyl CoA. *ACS Infect Dis* **1**, 110-125 (2015).
129. S. Gilbert, L. Hood, S. Y. K. Seah, Characterization of an Aldolase Involved in Cholesterol Side Chain Degradation in Mycobacterium tuberculosis. *J Bacteriol* **200** (2018).
130. J. K. Capyk, I. Casabon, R. Gruninger, N. C. Strynadka, L. D. Eltis, Activity of 3-ketosteroid 9α-hydroxylase (KshAB) indicates cholesterol side chain and ring degradation occur simultaneously in Mycobacterium tuberculosis. *J Biol Chem* **286**, 40717-40724 (2011).
131. X. Yang, J. Gao, I. Smith, E. Dubnau, N. S. Sampson, Cholesterol is not an essential source of nutrition for Mycobacterium tuberculosis during infection. *J Bacteriol* **193**, 1473-1476 (2011).
132. J. Knol, K. Bodewits, G. I. Hessels, L. Dijkhuizen, R. van der Geize, 3-Keto-5alpha-steroid Delta(1)-dehydrogenase from Rhodococcus erythropolis SQ1 and its orthologue in Mycobacterium tuberculosis H37Rv are highly specific enzymes that function in cholesterol catabolism. *Biochem J* **410**, 339-346 (2008).
133. C. Dresen *et al.*, A flavin-dependent monooxygenase from Mycobacterium tuberculosis involved in cholesterol catabolism. *J Biol Chem* **285**, 22264-22275 (2010).
134. N. A. Lack *et al.*, Characterization of a carbon-carbon hydrolase from Mycobacterium tuberculosis involved in cholesterol metabolism. *J Biol Chem* **285**, 434-443 (2010).
135. J. Carere, S. E. McKenna, M. S. Kimber, S. Y. Seah, Characterization of an aldolase-dehydrogenase complex from the cholesterol degradation pathway of Mycobacterium tuberculosis. *Biochemistry* **52**, 3502-3511 (2013).
136. I. Casabon, A. M. Crowe, J. Liu, L. D. Eltis, FadD3 is an acyl-CoA synthetase that initiates catabolism of cholesterol rings C and D in actinobacteria. *Mol Microbiol* **87**, 269-283 (2013).
137. C. S. Harwood, R. E. Parales, The beta-ketoadipate pathway and the biology of self-identity. *Annu Rev Microbiol* **50**, 553-590 (1996).
138. J. C. Chang *et al.*, igr Genes and Mycobacterium tuberculosis cholesterol metabolism. *J Bacteriol* **191**, 5232-5239 (2009).
139. B. C. VanderVen *et al.*, Novel inhibitors of cholesterol degradation in Mycobacterium tuberculosis reveal how the bacterium's metabolism is constrained by the intracellular environment. *PLoS Pathog* **11**, e1004679 (2015).
140. R. van der Geize, A. W. Grommen, G. I. Hessels, A. A. Jacobs, L. Dijkhuizen, The steroid catabolic pathway of the intracellular pathogen Rhodococcus equi is important for pathogenesis and a target for vaccine development. *PLoS Pathog* **7**, e1002181 (2011).
141. A. Feklistov, B. D. Sharon, S. A. Darst, C. A. Gross, Bacterial sigma factors: a historical, structural, and genomic perspective. *Annu Rev Microbiol* **68**, 357-376 (2014).
142. M. M. Meyer, The role of mRNA structure in bacterial translational regulation. *Wiley Interdiscip Rev RNA* **8** (2017).
143. T. Pisithkul, N. M. Patel, D. Amador-Noguez, Post-translational modifications as key regulators of bacterial metabolic fluxes. *Curr Opin Microbiol* **24**, 29-37 (2015).

144. S. Prisic *et al.*, Extensive phosphorylation with overlapping specificity by Mycobacterium tuberculosis serine/threonine protein kinases. *Proc Natl Acad Sci U S A* **107**, 7521-7526 (2010).
145. A. M. Hansen *et al.*, The Escherichia coli phosphotyrosine proteome relates to core pathways and virulence. *PLoS Pathog* **9**, e1003403 (2013).
146. H. M. O'Hare *et al.*, Regulation of glutamate metabolism by protein kinases in mycobacteria. *Mol Microbiol* **70**, 1408-1423 (2008).
147. J. A. Cain, N. Solis, S. J. Cordwell, Beyond gene expression: the impact of protein post-translational modifications in bacteria. *J Proteomics* **97**, 265-286 (2014).
148. S. Nambi, N. Basu, S. S. Visweswariah, cAMP-regulated protein lysine acetylases in mycobacteria. *J Biol Chem* **285**, 24313-24323 (2010).
149. H. Xu, S. S. Hegde, J. S. Blanchard, Reversible acetylation and inactivation of Mycobacterium tuberculosis acetyl-CoA synthetase is dependent on cAMP. *Biochemistry* **50**, 5883-5892 (2011).
150. S. Nambi *et al.*, Cyclic AMP-dependent protein lysine acylation in mycobacteria regulates fatty acid and propionate metabolism. *J Biol Chem* **288**, 14114-14124 (2013).
151. J. Bi *et al.*, Modulation of Central Carbon Metabolism by Acetylation of Isocitrate Lyase in Mycobacterium tuberculosis. *Sci Rep* **7**, 44826 (2017).
152. E. S. C. Rittershaus *et al.*, A Lysine Acetyltransferase Contributes to the Metabolic Adaptation to Hypoxia in Mycobacterium tuberculosis. *Cell Chem Biol* **25**, 1495-1505.e1493 (2018).
153. O. Vergnolle *et al.*, Post-translational Acetylation of MbtA Modulates Mycobacterial Siderophore Biosynthesis. *J Biol Chem* **291**, 22315-22326 (2016).
154. F. Liu *et al.*, Acetylome analysis reveals diverse functions of lysine acetylation in Mycobacterium tuberculosis. *Mol Cell Proteomics* **13**, 3352-3366 (2014).
155. J. Bi *et al.*, Acetylation of lysine 182 inhibits the ability of Mycobacterium tuberculosis DosR to bind DNA and regulate gene expression during hypoxia. *Emerg Microbes Infect* **7**, 108 (2018).
156. H. J. Lee, P. T. Lang, S. M. Fortune, C. M. Sassetti, T. Alber, Cyclic AMP regulation of protein lysine acetylation in Mycobacterium tuberculosis. *Nat Struct Mol Biol* **19**, 811-818 (2012).
157. W. Lee, B. C. VanderVen, S. Walker, D. G. Russell, Novel protein acetyltransferase, Rv2170, modulates carbon and energy metabolism in Mycobacterium tuberculosis. *Sci Rep* **7**, 72 (2017).
158. O. Barzu, A. Danchin, Adenylyl cyclases: a heterogeneous class of ATP-utilizing enzymes. *Prog Nucleic Acid Res Mol Biol* **49**, 241-283 (1994).
159. W. J. Tang, Q. Guo, The adenylyl cyclase activity of anthrax edema factor. *Mol Aspects Med* **30**, 423-430 (2009).
160. T. L. Yahr, A. J. Vallis, M. K. Hancock, J. T. Barbieri, D. W. Frank, ExoY, an adenylate cyclase secreted by the Pseudomonas aeruginosa type III system. *Proc Natl Acad Sci U S A* **95**, 13899-13904 (1998).
161. A. Lee *et al.*, Vibrio vulnificus RtxA Is a Major Factor Driving Inflammatory T Helper Type 17 Cell Responses in vitro and in vivo. *Front Immunol* **9**, 2095 (2018).
162. J. U. Linder, J. E. Schultz, The class III adenylyl cyclases: multi-purpose signalling modules. *Cell Signal* **15**, 1081-1089 (2003).

163. A. R. Shenoy, S. S. Visweswariah, Mycobacterial adenylyl cyclases: biochemical diversity and structural plasticity. *FEBS Lett* **580**, 3344-3352 (2006).
164. N. Smith, S. K. Kim, P. T. Reddy, D. T. Gallagher, Crystallization of the class IV adenylyl cyclase from Yersinia pestis. *Acta Crystallogr Sect F Struct Biol Cryst Commun* **62**, 200-204 (2006).
165. A. R. Shenoy, S. S. Visweswariah, New messages from old messengers: cAMP and mycobacteria. *Trends Microbiol* **14**, 543-550 (2006).
166. G. Bai, D. D. Schaak, K. A. McDonough, cAMP levels within Mycobacterium tuberculosis and Mycobacterium bovis BCG increase upon infection of macrophages. *FEMS Immunol Med Microbiol* **55**, 68-73 (2009).
167. G. S. Knapp, K. A. McDonough, Cyclic AMP Signaling in Mycobacteria. *Microbiol Spectr* **2** (2014).
168. L. Rickman *et al.*, A member of the cAMP receptor protein family of transcription regulators in Mycobacterium tuberculosis is required for virulence in mice and controls transcription of the rpfA gene coding for a resuscitation promoting factor. *Mol Microbiol* **56**, 1274-1286 (2005).
169. N. Ahuja, P. Kumar, R. Bhatnagar, The adenylate cyclase toxins. *Crit Rev Microbiol* **30**, 187-196 (2004).
170. K. M. Krueger, J. T. Barbieri, The family of bacterial ADP-ribosylating exotoxins. *Clin Microbiol Rev* **8**, 34-47 (1995).
171. S. Lory, M. Wolfgang, V. Lee, R. Smith, The multi-talented bacterial adenylate cyclases. *Int J Med Microbiol* **293**, 479-482 (2004).
172. C. Spry, K. Kirk, K. J. Saliba, Coenzyme A biosynthesis: an antimicrobial drug target. *FEMS Microbiol Rev* **32**, 56-106 (2008).
173. V. K. Sambandamurthy *et al.*, A pantothenate auxotroph of Mycobacterium tuberculosis is highly attenuated and protects mice against tuberculosis. *Nat Med* **8**, 1171-1174 (2002).
174. D. S. Vallari, S. Jackowski, C. O. Rock, Regulation of pantothenate kinase by coenzyme A and its thioesters. *J Biol Chem* **262**, 2468-2471 (1987).
175. C. O. Rock, H. W. Park, S. Jackowski, Role of feedback regulation of pantothenate kinase (CoaA) in control of coenzyme A levels in Escherichia coli. *J Bacteriol* **185**, 3410-3415 (2003).
176. Y. M. Zhang, C. O. Rock, S. Jackowski, Feedback regulation of murine pantothenate kinase 3 by coenzyme A and coenzyme A thioesters. *J Biol Chem* **280**, 32594-32601 (2005).
177. M. Yun *et al.*, Structural basis for the feedback regulation of Escherichia coli pantothenate kinase by coenzyme A. *J Biol Chem* **275**, 28093-28099 (2000).
178. S. Das, P. Kumar, V. Bhor, A. Surolia, M. Vijayan, Expression, purification, crystallization and preliminary X-ray crystallographic analysis of pantothenate kinase from Mycobacterium tuberculosis. *Acta Crystallogr Sect F Struct Biol Cryst Commun* **61**, 65-67 (2005).
179. S. Das, P. Kumar, V. Bhor, A. Surolia, M. Vijayan, Invariance and variability in bacterial PanK: a study based on the crystal structure of Mycobacterium tuberculosis PanK. *Acta Crystallogr D Biol Crystallogr* **62**, 628-638 (2006).

180. K. Yang *et al.*, Crystal structure of a type III pantothenate kinase: insight into the mechanism of an essential coenzyme A biosynthetic enzyme universally distributed in bacteria. *J Bacteriol* **188**, 5532-5540 (2006).
181. J. C. Evans *et al.*, Validation of CoaBC as a Bactericidal Target in the Coenzyme A Pathway of Mycobacterium tuberculosis. *ACS Infect Dis* **2**, 958-968 (2016).
182. A. Geerlof, A. Lewendon, W. V. Shaw, Purification and characterization of phosphopantetheine adenylyltransferase from Escherichia coli. *J Biol Chem* **274**, 27105-27111 (1999).
183. T. Izard, A novel adenylate binding site confers phosphopantetheine adenylyltransferase interactions with coenzyme A. *J Bacteriol* **185**, 4074-4080 (2003).
184. S. Jackowski, C. O. Rock, Consequences of reduced intracellular coenzyme A content in Escherichia coli. *J Bacteriol* **166**, 866-871 (1986).
185. H. Otani, Y. E. Lee, I. Casabon, L. D. Eltis, Characterization of p-hydroxycinnamate catabolism in a soil Actinobacterium. *J Bacteriol* **196**, 4293-4303 (2014).
186. J. C. van Kessel, L. J. Marinelli, G. F. Hatfull, Recombineering mycobacteria and their phages. *Nat Rev Microbiol* **6**, 851-857 (2008).
187. J. Burian *et al.*, The mycobacterial transcriptional regulator whiB7 gene links redox homeostasis and intrinsic antibiotic resistance. *J Biol Chem* **287**, 299-310 (2012).
188. N. Nakashima, T. Tamura, Isolation and characterization of a rolling-circle-type plasmid from Rhodococcus erythropolis and application of the plasmid to multiple-recombinant-protein expression. *Appl Environ Microbiol* **70**, 5557-5568 (2004).
189. M. Nandakumar, G. A. Prosser, L. P. de Carvalho, K. Rhee, Metabolomics of Mycobacterium tuberculosis. *Methods Mol Biol* **1285**, 105-115 (2015).
190. J. Sambrook, D. W. Russell, *Molecular cloning : a laboratory manual* (Cold Spring Harbor Laboratory Press, Cold Spring Harbor, NY, 2001).
191. P. Domenech, M. B. Reed, Rapid and spontaneous loss of phthiocerol dimycocerosate (PDIM) from Mycobacterium tuberculosis grown in vitro: implications for virulence studies. *Microbiology* **155**, 3532-3543 (2009).
192. L. R. Camacho, D. Ensergueix, E. Perez, B. Gicquel, C. Guilhot, Identification of a virulence gene cluster of Mycobacterium tuberculosis by signature-tagged transposon mutagenesis. *Mol Microbiol* **34**, 257-267 (1999).
193. J. S. Cox, B. Chen, M. McNeil, W. R. Jacobs, Jr., Complex lipid determines tissue-specific replication of Mycobacterium tuberculosis in mice. *Nature* **402**, 79-83 (1999).
194. P. Domenech, M. B. Reed, C. E. Barry, 3rd, Contribution of the Mycobacterium tuberculosis MmpL protein family to virulence and drug resistance. *Infect Immun* **73**, 3492-3501 (2005).
195. D. Parke, L. N. Ornston, Toxicity caused by hydroxycinnamoyl-coenzyme A thioester accumulation in mutants of Acinetobacter sp. strain ADP1. *Appl Environ Microbiol* **70**, 2974-2983 (2004).
196. A. R. Horswill, J. C. Escalante-Semerena, Characterization of the propionyl-CoA synthetase (PrpE) enzyme of Salmonella enterica: residue Lys592 is required for propionyl-AMP synthesis. *Biochemistry* **41**, 2379-2387 (2002).
197. Z. Chen *et al.*, Acetylome Profiling Reveals Extensive Lysine Acetylation of the Fatty Acid Metabolism Pathway in the Diatom. *Mol Cell Proteomics* **17**, 399-412 (2018).

198. T. Noy, H. Xu, J. S. Blanchard, Acetylation of acetyl-CoA synthetase from Mycobacterium tuberculosis leads to specific inactivation of the adenylation reaction. *Arch Biochem Biophys* **550-551**, 42-49 (2014).
199. H. A. Crosby, E. K. Heiniger, C. S. Harwood, J. C. Escalante-Semerena, Reversible N epsilon-lysine acetylation regulates the activity of acyl-CoA synthetases involved in anaerobic benzoate catabolism in Rhodopseudomonas palustris. *Mol Microbiol* **76**, 874-888 (2010).
200. P. Gopal *et al.*, Pyrazinamide Resistance Is Caused by Two Distinct Mechanisms: Prevention of Coenzyme A Depletion and Loss of Virulence Factor Synthesis. *ACS Infect Dis* **2**, 616-626 (2016).
201. P. Gopal *et al.*, Pyrazinoic Acid Inhibits Mycobacterial Coenzyme A Biosynthesis by Binding to Aspartate Decarboxylase PanD. *ACS Infect Dis* **3**, 807-819 (2017).
202. N. A. Dillon, N. D. Peterson, B. C. Rosen, A. D. Baughn, Pantothenate and pantetheine antagonize the antitubercular activity of pyrazinamide. *Antimicrob Agents Chemother* **58**, 7258-7263 (2014).
203. A. M. Crowe *et al.*, IpdAB, a virulence factor in Mycobacterium tuberculosis, is a cholesterol ring-cleaving hydrolase. *Proc Natl Acad Sci U S A* **115**, E3378-e3387 (2018).
204. I. Kramnik, G. Beamer, Mouse models of human TB pathology: roles in the analysis of necrosis and the development of host-directed therapies. *Semin Immunopathol* **38**, 221-237 (2016).
205. R. M. Johnson *et al.*, Chemical activation of adenylyl cyclase Rv1625c inhibits growth of Mycobacterium tuberculosis on cholesterol and modulates intramacrophage signaling. *Mol Microbiol* **105**, 294-308 (2017).
206. M. O. Shleeva *et al.*, Overexpression of Adenylyl Cyclase Encoded by the Mycobacterium tuberculosis Rv2212 Gene Confers Improved Fitness, Accelerated Recovery from Dormancy and Enhanced Virulence in Mice. *Front Cell Infect Microbiol* **7**, 370 (2017).
207. I. Gout, Coenzyme A, protein CoAlation and redox regulation in mammalian cells. *Biochem Soc Trans* **46**, 721-728 (2018).
208. I. Gout, Coenzyme A: a protective thiol in bacterial antioxidant defence. *Biochem Soc Trans* **47**, 469-476 (2019).
209. A. Abuhammad, Cholesterol metabolism: a potential therapeutic target in Mycobacteria. *Br J Pharmacol* **174**, 2194-2208 (2017).
210. C. M. Schaefer *et al.*, FadA5 a thiolase from Mycobacterium tuberculosis: a steroid-binding pocket reveals the potential for drug development against tuberculosis. *Structure* **23**, 21-33 (2015).